UNIVERSITÀ DEL PIEMONTE ORIENTALE

UNIVERSITY OF PIEMONTE ORIENTALE "AMEDEO AVOGADRO"

DEPARTMENT OF HEALTH SCIENCES

Ph.D. Program in Food, Health and Longevity

XXXVII Cycle

MICROBIAL CELL FACTORIES FOR THE SYNTHESIS OF SUSTAINABLE BIOMATERIALS LATEX-BASED

SSD BIOS-10/A

Supervisor
Prof. Diego Cotella

PhD candidate
Chiara Mocchetti

Coordinator
Prof. Antonia Follenzi

Firmato digitalmente da Diego Cotella
Data: 19.06.2025 09:31:51 CEST
Organizzazione: UNIVERSITA' DEGLI STUDI DEL PIEMONTE ORIENTALE/01943490027

La borsa di dottorato è stata cofinanziata con risorse del
Programma Operativo Nazionale Ricerca e Innovazione 2014-2020 (CCI 2014IT16M2OP005),
Fondo Sociale Europeo, Azione I.1 "Dottorati Innovativi con caratterizzazione Industriale"

UNIONE EUROPEA
Fondo Sociale Europeo

Ministero dell'Università e della Ricerca

PON RICERCA E INNOVAZIONE 2014 - 2020

STUDENT DECLARATION

I declare that the PhD thesis titled “Microbial cell factories for the synthesis of sustainable biomaterials latex-based” represents my own work and that it has not been submitted previously, either in whole or in part, for any degree. The work has not yet been submitted for publication, and it should be considered confidential.

The following results were obtained in collaboration with the Department of Pharmaceutical Sciences at the University of Eastern Piedmont, specifically with Prof. Ivana Miletto and Prof. Giovanni Battista Giovenzana for the chemical characterization, and with TissueGraft Srl for the electrospinning process, where I spent six months.

The work presented in this thesis represents a substantial portion of my doctoral research, but it does not represent the entirety. The following publications have been part of my work:

- Lecchi G, **Mocchetti C**, Tunesi D, Berto A, Balasubramanian HB, Biswas S, Bagchi A, Pollastro F, Fresu LG, Talmon M (2024). Single-Nucleotide Polymorphisms of TAS2R46 Affect the Receptor Downstream Calcium Regulation in Histamine-Challenged Cells. *Cells*,13(14):1204.doi: 10.3390/cells13141204.
- Morra M, Marradi D, Gandini L, Ivagnes V, Ottolini G, Bovio A, Jabali G, Maraschi L, Dada IA, Chawanda VT, Gorla M, Tarasiuk O, **Mocchetti C**, Soluri MF, Boccafoschi F, Sblattero D and Cotella D (2025). A Non-Hypothesis-Driven Practical Laboratory Activity on Functional Metagenomics: "Fishing" Protein-Coding DNA Sequences from Microbiomes. Front Bioeng Biotechnol. 2025 May 20;13:1602982. doi: 10.3389/fbioe.2025.1602982.

TABLE OF CONTENTS

SUMMARY - ENGLISH

Hevea brasiliensis is the main source of natural rubber (NR), a critical material for many industrial and biomedical applications due to its excellent mechanical properties. However, NR production presents several challenges, including environmental impacts, allergenic proteins, and vulnerabilities in its supply chain, emphasizing the need for sustainable alternatives. A dual strategy will be used in this project to overcome these limitations: developing an electrospinning procedure that can be reproduced for biomaterials based on NR, and examining the microbial biosynthesis of polyisoprene as an eco-friendly latex substitute. NR/PVA nanofibrous biomaterials were successfully produced in the first step through the electrospinning process with optimized conditions. The addition of Triton X-100 and the thermal treatment enhanced the stability and uniformity of the fibers. The resulting materials were tested on Normal Human Dermal Fibroblasts (NHDF) cells that indicated good biocompatibility, indicating their potential for application in regenerative medicine. In the second step, the cis-1,4-polysoprene biosynthetic pathway was reconstructed in *Escherichia coli* through heterologous expression of the key proteins, HRT2 and SRPP. Despite successful expression, the proteins were mainly insoluble, in inclusion bodies, probably due to the absence of lipid structures essential for biosynthesis in bacterial systems. Solubility was partially improved by expression in Arctic Express strains, but polymer production remained insufficient for definitive characterization. Results of this study highlight the limitations in replicating the complex machinery of NR biosynthesis using microbial hosts, indicating the need to use eukaryotic or cell-free systems as more viable approaches. In conclusion, this study highlights the advantages and limitations of electrospinning and microbial biosynthesis approaches for the development of sustainable biomaterials. NR/PVA electrospun scaffolds are biocompatible and making them potential candidates for biomedical applications. However, further interdisciplinary work is needed to overcome critical issues in microbial engineering as an alternative source for polymer synthesis.

SUMMARY - ITALIANO

La gomma naturale (NR), derivata principalmente dalla pianta *Hevea brasiliensis*, è un materiale fondamentale per le applicazioni biomediche e industriali grazie alle sue proprietà meccaniche uniche e alla sua biocompatibilità. Tuttavia, la produzione di NR presenta sfide legate all'impatto ambientale, al contenuto di proteine allergeniche e alla vulnerabilità della catena di approvvigionamento, sottolineando la necessità di alternative sostenibili. Questo lavoro mira ad affrontare queste limitazioni attraverso una duplice strategia: stabilire un protocollo riproducibile di elettrofilatura per biomateriali a base di NR ed esplorare la biosintesi microbica di cis-1,4-poliisoprene come sostituto sostenibile del lattice. Nella prima fase, sono stati prodotti con successo biomateriali nanofibrosi composti da NR/PVA utilizzando la tecnica dell'elettrofilatura e ottimizzandone le condizioni. L'utilizzo di Triton X-100 e il trattamento termico hanno permesso di migliorare l'omogeneità e la stabilità delle fibre. I materiali ottenuti sono stati testati su una linea cellulare di fibroblasti della pelle (*Normal Human Dermal Fibroblasts*, NHDF) e hanno dimostrato una buona biocompatibilità, rendendoli potenzialmente adatti ad applicazioni in medicina rigenerativa. Nella seconda fase, la via biosintetica del cis-1,4-polisoprene è stata ricostruita in *Escherichia coli* attraverso l'espressione eterologa delle proteine chiave, HRT2 e SRPP. Nonostante la riuscita nell'espressione, le proteine sono risultate principalmente insolubili, in corpi di inclusione, probabilmente a causa dell'assenza di strutture lipidiche essenziali per la biosintesi nei sistemi batterici. La solubilità è stata parzialmente migliorata grazie all'espressione in ceppi Artic Express, ma la produzione di polimeri è rimasta insufficiente per una caratterizzazione definitiva. Questi risultati evidenziano i limiti nell'utilizzo di ospiti microbici per replicare il complesso macchinario della biosintesi di NR, suggerendo la necessità di sistemi eucariotici o di sistemi *cell-free* come alternative più valide. In conclusione, questo studio evidenzia i vantaggi e i limiti degli approcci di elettrofilatura e biosintesi microbica per lo sviluppo di biomateriali sostenibili. La biocompatibilità degli scaffold NR/PVA elettrofilati li rendono candidati promettenti per le applicazioni biomediche, ma ulteriori sforzi interdisciplinari saranno necessari per superare le criticità nell'ingegnerizzazione microbica come fonte alternativa per la sintesi di polimeri.

ABBREVIATIONS

NR: natural rubber

IPP: isopentenyl pyrophosphate

MVA: mevalonate

MEP: 2-C-methyl-d-erythritol-4-phosphate

FPP: Farnesyl pyrophosphate

RPs: rubber particles

BF: bottom fraction

LRPs: large rubber particles

SRPs: small rubber particles

SEM: Scanning electron microscopy

DMAPP: dimethylallyl pyrophosphate

PTs: prenyltransferases

G3P: glyceraldehyde 3-phosphate

cPTs: cis-prenyltransferases

HRT1: Hevea rubber transferase 1

HRT2: Hevea rubber transferase 2

REF: rubber elongation factor

SRPP: small rubber particle protein

HRBP: HRT1-REF bridging protein

ACAT: acetyl-CoA acetyltransferase

HMGS: 3-hydroxy-3-methyl-glutaryl-coenzyme A synthase

HMGR: HMG-CoA reductase

MVK: mevalonate kinase

PMK: phosphomevalonate kinase

MVD: mevalonate diphosphate decarboxylase

DXS: 1-deoxy-D-xylulose 5-phosphate synthase

DXP: 1-deoxy-D-xylulose 5-phosphate

GPP: geranyl pyrophosphate

RBS: ribosome binding site

ECM: extracellular matrix

PLDLA: poly(L-co-D,L-lactic acid)

PVA: polyvinyl alcohol

1. INTRODUCTION

Natural rubber (NR) is a hydrocarbon polymer extracted from the *Hevea brasiliensis* tree and it is chemically identified as cis-1,4-polyisoprene. Due to its unique physical properties, such as high tensile strength and elasticity, NR is an important raw material for the manufacture of medical (e.g., gloves and catheters) and transport equipment (e.g., tires) (Cornish, 2017).

There are more than 2500 plant species that produce NR, but the *H. brasiliensis* tree, commonly known as the para rubber tree, produces most of the commercial latex. This specie is favoured because its latex contains a higher percentage (30-50%) of high molecular weight rubber ($MW>1\times10^6$) than other species, and this characteristic gives the final product superior mechanical properties (Mooibroek & Cornish, 2000; van Beilen & Poirier, 2007a). Even though scientific advances have improved understanding of the enzymes involved in cis-1,4-polysoprene synthesis, the molecular mechanisms of NR biosynthesis are still unknown (Yamashita & Takahashi, 2020).

Global NR production has significantly increased, growing about 75% in the last decades; however, this expansion is associated with a wide range of environmental and sustainability issues (Andler, 2020). Large-scale cultivation of *H. brasiliensis* fosters deforestation and land exploitation. The effect is thus both the destruction of native ecosystems and the loss of land for other agricultural production. Rubber plantations are also more prone to plant infections and climatic changes, factors that could be detrimental to their health and productivity (Cornish, 2017).

Due to the recent COVID-19 pandemic, the demand for personal protective equipment has surged. This global increase in demand has led the European Union to classify this polymer as a critical raw material, highlighting the need to identify sustainable alternatives for its supply (European Commission, 2020). One significant concern with NR is its potential to cause allergic reactions. Latex contains proteins that can trigger responses in sensitive individuals, ranging from mild skin irritation to severe respiratory complications (van Beilen & Poirier, 2007a, 2007b). This has made the use of synthetic alternatives such as nitrile or vinyl. Unfortunately, these synthetic rubbers (SR) are derived from petroleum, which is unsustainable.

Relying predominantly on a single plant species, *H. brasiliensis*, for the global supply of NR introduces vulnerability into the supply chain. To address this fragility and meet growing demand, various research strategies are underway. Among them is

metabolic engineering, which involves introducing key genes from NR biosynthetic pathways into alternative species to enable rubber production beyond *H. brasiliensis* (Yamashita & Takahashi, 2020).

1.1 NR production in plant

NR, primarily composed of cis-1,4-polyisoprene, is synthetise in plants from isopentenyl pyrophosphate (IPP) via two distinct biosynthetic pathways: the mevalonate (MVA) pathway and the 2-C-methyl-D-erythritol 4-phosphate (MEP) pathway. There are three main steps in the reaction catalysed by rubber transferase: initiation, polymerization, and termination. In vivo, the initiating molecule is primarily farnesyl pyrophosphate (FPP), with divalent metal ions such as Mg^{2+} or Mn^{2+} as cofactors (Cornish, 2001; da Costa et al., 2005). Despite efforts to understand the mechanism of NR synthesis, the termination mechanism has yet to be understood. Nevertheless, it has been determined that increased IPP concentrations produce NR of higher molecular weight, while elevated concentrations of FPP do the opposite. Moreover, a ubiquitin-proteasome degradation pathway would be implicated in the termination regulation of polymerization (Cornish et al., 2000; Wang et al., 2018).

NR is mainly accumulated in the lactiferous cells, vessel-like structures containing latex, a cytoplasm rich in specialised metabolites that protect plants from herbivores. More specifically, NR is stored in specialised spherical organelles known as rubber particles (RPs) (Figure 1a). RPs composition is a hydrophobic rubber core (>90% of the particle's weight) enveloped by a lipid monolayer containing membrane-bound proteins (Figure 1b) (Cornish et al., 1999). The diameters of RPs in *H. brasiliensis* range from 0.08 to 3 µm, with an average diameter of 1 µm (Wood & Cornish, 2000).

H. brasiliensis fresh latex can be fractionated by ultracentrifugation into four principal subcellular fractions: the top fraction of rubber which contain RPs, an aqueous cytosolic fraction named C-serum, a plastid-enriched yellow complex termed Frey–Wyssling particles, and a sediment bottom fraction (BF) containing membrane-bound polydisperse particles known as lutoids (Figure 1c). The rubber portion can further be stratified into two sub-areas according to the size of the RPs in a white rubber cream zone with large RPs (LRPs; ~0.3–3 µm diameter), and an zone containing small RPs (SRPs; ~0.01–0.2 µm diameter) (Wood & Cornish, 2000; Yamashita et al., 2018).

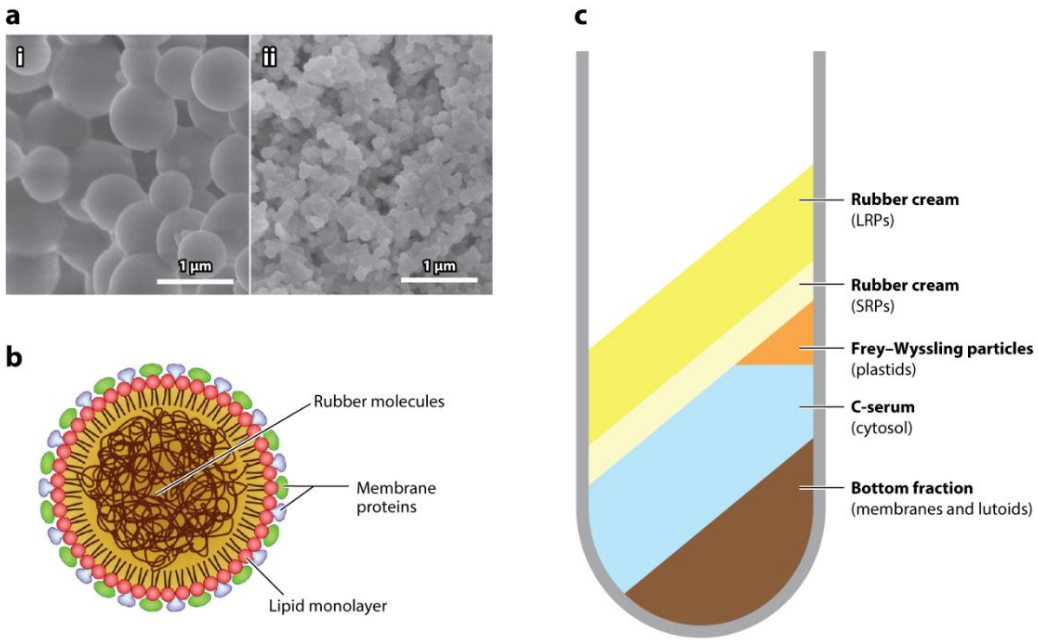

Figure 1*: Scanning electron microscopy (SEM) images of RPs, showing: (a-i) large rubber particles and (a-ii) small rubber particles, with distinct differences in size and morphology. (b) A schematic illustration of an RP, depicting the lipid monolayer, associated membrane proteins, and the rubber-containing core. (c) Latex components separated via ultracentrifugation of Hevea brasiliensis, including the rubber cream layer (containing LRPs and SRPs), Frey-Wyssling bodies (originating from plastids), and the C-serum, which corresponds to the cytosolic fraction* (Yamashita & Takahashi, 2020).

1.2 NR biosynthetic pathway

Three steps are involved in the isoprenoid biosynthesis pathway. In the initial step, IPP, the basic isoprenoid unit, is generated, which is subsequently isomerized to dimethylallyl pyrophosphate (DMAPP). Linear isoprenoids are synthesised following sequential condensation of IPP (non-allyl) with DMAPP (allyl). This process generates longer allylic pyrophosphates through the action of prenyltransferases (PT), enzymes responsible for transferring allylic prenyl groups to acceptor molecules such as IPP, aromatic intermediates involved in quinone biosynthesis, or other specific proteins. Linear isoprenoids contain carbon chains ranging from C10 for geranyl and neryl pyrophosphates to C45 for solanesyl pyrophosphates. Longer molecules like dolichol phosphate are more variable in size, ranging from C55 to C100. Rubber is highly heterogeneous in length, usually higher than C100,000 (Ducluzeau et al., 2012; Hirooka, K. et al., 2003).

The cis-prenyltransferases (cPTs) are members of the PT family involved in the elongation of polyprenyl chains. In *H. brasiliensis* two cPTs, Hevea rubber transferase HRT1 and HRT2, contribute to rubber biosynthesis (Asawatreratanakul et al., 2003; Kharel & Koyama, 2003). Other proteins are also involved in the NR synthesis process,

including rubber elongation factor (REF) and small rubber particle protein (SRPP), which are members of the stress-related protein family, are extremely abundant on rubber particles and play a role in rubber stability (figure 2) (Berthelot et al., 2014). These proteins interact and may regulate rubber particle aggregation, elongation and stabilization. Their role in NR synthesis has not been precisely identified, but studies show that RNAi silencing of REF/SRPP genes causes altered NR content and altered NR molecular weight in some species (Collins-Silva et al., 2012; Hillebrand et al., 2012; Priya et al., 2007). Additionally, during the past decade, an additional protein, HRBP has also been discovered. This protein interacts with cPT and REF, facilitating the assembly of the rubber biosynthetic machinery on rubber particles (Yamashita et al., 2016).

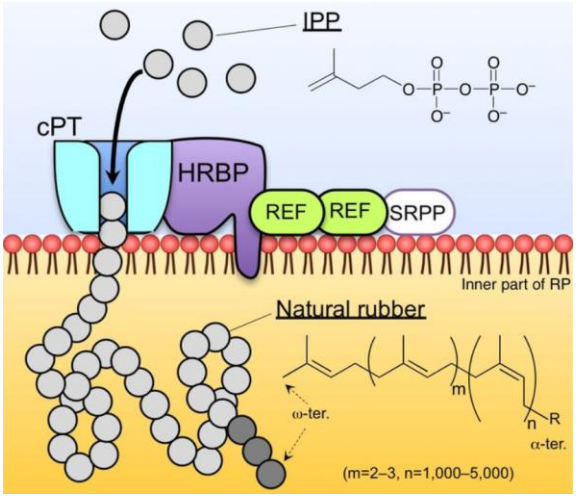

***Figure 2**: Model of the H. brasiliensis rubber biosynthetic machinery. The figure illustrates the key molecular components and enzymatic complexes involved in the biosynthesis of NR within the RP. IPP is the repeating unit for polymer elongation, catalyzed by the coordinated action of cPT. REF and SRPP are also implicated in NR biosynthesis, stabilizing the growing polymer. The resulting cis-1,4-polyisoprene chains are accumulated within the hydrophobic core. Modified from* (Yamashita et al., 2016).

1.2.1 Mevalonate (MVA) and 2-C-methyl-d-erythritol-4-phosphate (MEP) pathways

The MVA pathway and the MEP pathway are the pathways through which IPP is produced in plants in the cytosol and plastid, respectively. Sugar carbon metabolism supplies substrates for the two isoprenoid biosynthetic pathways in plants: the MEP pathway uses pyruvate and glyceraldehyde 3-phosphate (G3P), while the MVA pathway begins with acetyl-CoA as the primary precursor (Figure 3). IPP and its isomer DMAPP are produced by both pathways, but their regulation, localization, and metabolic flux differ significantly across plant species (Whited et al., 2010).

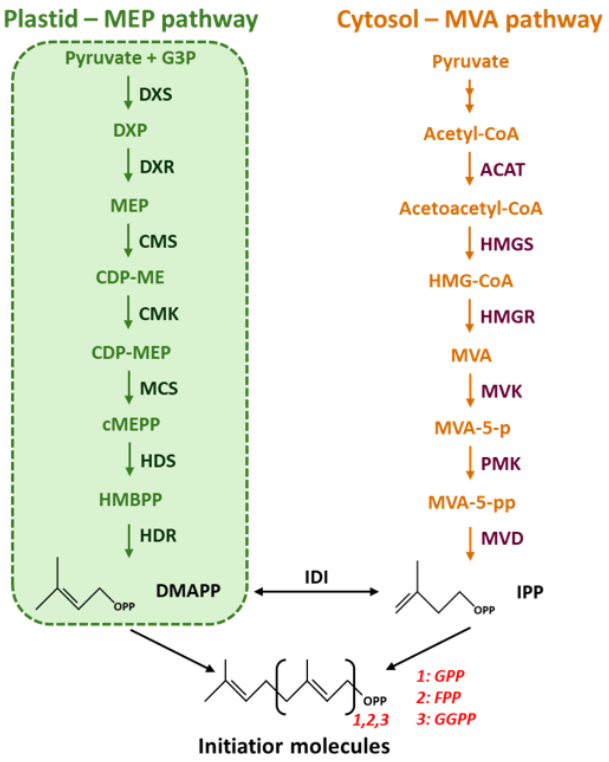

***Figure 3**: Biosynthetic pathways leading to the production of isoprenoid precursors for NR biosynthesis. The plastidial MEP pathway (green) and the cytosolic MVA pathway (orange) contribute to the synthesis of DMAPP and IPP, which are interconverted by isopentenyl diphosphate isomerase (IDI). These precursor molecules serve as initiator molecules for the synthesis of geranyl diphosphate (GPP), farnesyl diphosphate (FPP), and geranylgeranyl diphosphate (GGPP), intermediates in the biosynthesis of polyisoprenoids, including NR.*

In the cytoplasmic MVA pathway, acetyl-CoA derived from sucrose, glucose, or fructose is the predominant substrate. This pathway includes six enzymatic reactions catalysed by acetyl-CoA acetyltransferase (ACAT), 3-hydroxy-3-methyl-glutaryl-coenzyme A synthase (HMGS), HMG-CoA reductase (HMGR), mevalonate kinase (MVK), phosphomevalonate kinase (PMK), and mevalonate diphosphate decarboxylase (MVD) (Bouvier et al., 2005). The HMGR is considered a bottleneck in the MVA pathway (Chappell et al., 1995) and the HMGS is a rate-limiting step in plants (Meng et al., 2017).

The MEP pathway, localised in plastids, involves a sequence of eight enzymatic steps through which pyruvate and G3P are converted into the isoprenoid precursors IPP and DMAPP. The pathway begins with the enzyme 1-deoxy-D-xylulose 5-phosphate synthase (DXS), which mediates the condensation of the two carbon substrates to generate 1-deoxy-D-xylulose 5-phosphate (DXP). This first step is considered rate-limiting. DXS activity is highly regulated, with evidence suggesting its involvement in flux control within the MEP pathway of Arabidopsis thaliana MEP

pathway, reinforcing its role as a key regulatory step. In the end, IPP is formed as a result of downstream enzyme reactions (Cordoba et al., 2009; Wright et al., 2014).

In the cytosol, IPP undergoes isomerisation to DMAPP through the catalytic activity of IPP isomerase. Subsequently, PTs facilitate the sequential head-to-tail condensation of DMAPP with additional IPP units, leading to the formation of short-chain prenyl diphosphates. These include geranyl diphosphate (GPP), C10, a precursor for monoterpenoids, and FPP, C15, which serves as an intermediate in the biosynthesis of sesquiterpenoids and triterpenoids (van Beilen & Poirier, 2007a). These intermediates are allylic primer substrates for following IPP condensation and subsequent polymerization reactions for rubber molecule and other isoprenoids formation.

1.3 Isoprene synthesis in microorganisms

Isoprene (2-methyl-1,3-butadiene) is a crucial diolefin used as a precursor for some terpenoids. Currently, industrial isoprene production relies primarily on petroleum-based chemical synthesis (Whited et al., 2010). Isoprene biosynthesis naturally occurs in green plants, fungi, bacteria, and algae (Sharkey et al., 2005). *Escherichia coli*, cyanobacteria and *Saccharomyces cerevisiae* are among the microbial hosts that have been explored for alternative isoprene production. Two main biosynthetic pathways are responsible for the production of isoprene: the MVA pathway, occurring in the cytosol in eukaryotes and archaea, and the MEP pathway, of bacterial origin but also present in plant plastids (Lichtenthaler, 2000; L. Zhao et al., 2013). Since no canonical isoprene synthase gene has been identified in bacteria, microbial isoprene biosynthesis relies on the heterologous expression of plant-derived PTs genes.

Metabolic engineering of microbial systems has been seen as a possible alternative for sustainable isoprene production, responding to the growing need for research into environmentally sustainable industrial methods (Martin et al., 2003). *E. coli* has been studied for isoprene biosynthesis for this purpose and is one of the most widely used model organisms for alternative isoprene biosynthesis. However, integrating MVA or MEP pathways into microbial hosts can lead to the accumulation of IPP and DMAPP, which are toxic to bacterial growth (George et al., 2018; Kim et al., 2016). Evidence suggests that metabolic engineering in cell factories holds great

potential for isoprene production. In fact, Zhao Y., et al successfully optimised the MEP pathway in *E. coli* by introducing heterologous PTs and overexpressing key enzymes of the pathway. Their study demonstrated that over-expressing DXS genes significantly enhanced isoprene production, achieving a 2.3-fold increase (Y. Zhao et al., 2011). In general the increase in isoprene production was observed following the introduction of the complete plant-derived isoprene biosynthetic pathway, removal of genes to reduce byproduct formation, over-expression of limiting enzymes, and expression of both pathways simultaneously (Kim et al., 2016; Kim, S. W. & Keasling, J. D., 2001; H. Liu et al., 2014).

Since the MEP pathway is native to *E. coli*, most studies have targeted this route to enhance precursor availability. However, due to the limited activity of key enzymes, flux through the MEP pathway remains suboptimal (L. Zhao et al., 2013), but one strategy to improve precursor flux involves balancing the availability of pyruvate and G3P (Chang & Keasling, 2006).

Further enhancement of isoprene production has been achieved through the heterologous expression of the MVA pathway alongside the native MEP pathway, demonstrating a synergistic effect in precursor accumulation. Co-expression of these pathways led to a 20-fold increase in isoprene titers compared to MEP pathway expression alone (Yang et al., 2016).

Additional metabolic optimizations include ribosome binding site (RBS) modifications to fine-tune gene expression (Kim et al., 2016) and elimination of competing pathways. For instance, deletion of acetate-producing genes in E. coli reduced acetate accumulation by 89% and increased isoprene production by 39% (C. L. Liu et al., 2019)

While significant progress has been made in microbial isoprene production, the conversion of isoprene into polyisoprene remains an emerging area of metabolic engineering (H. Liu et al., 2022). Different studies have demonstrated that E. coli can be engineered to produce short chain polypentenol by expressing heterologous cPT genes. Oh et al. successfully synthesized C120 polypentenol using *Arabidopsis thaliana*-derived cPT expression in E. coli (Oh et al., 2000). Further modifications, including the introduction of cPT from guayule (Parthenium argentatum) and the

endogenous undecaprenyl pyrophosphate (UDP) synthase, led to the production of a 500 kDa polypentenol, structurally similar to cis-1,4-polyisoprene (Lee & Kim, 2016).

Polyisoprene biosynthesis in yeast has also been explored, with Surmacz et al. reporting the activity of A. thaliana-derived cPT in yeast, confirming its role in short-chain polyisoprene synthesis. However, despite these advances, achieving high-molecular-weight polyisoprene with microbial systems remains challenging due to incomplete understanding of the enzymatic mechanisms and low yield. This has not yet been achieved, but as this strategy has high economic potential and is likely to be pursued (Surmacz et al., 2014).

1.4 NR in biomedical applications

Functional biomaterials with biological characteristics are among the most critical fields of biomedical research in regenerative medicine. Natural biomaterials derived from marine (Silva et al., 2012), animal (Chen & Liu, 2016), and plant (Gervaso et al., 2017), have received extensive attention due to their biocompatibility, bioactivity, and potential for tissue regeneration. A traditional wound dressing like gauze may provide passive mechanical protection, while next-generation dressings actively support tissue repair through controlling the wound healing process by interfering with cell processes (Guerra et al., 2021; Rosa et al., 2019).

Biomaterials derived from plants used in biomedical applications, such as NR latex from *H. brasiliensis*, have shown significant potential to be used in different biomedical areas. Herculano and colleagues successfully developed and characterised a new Aloe vera-loaded NR latex dressing and optimised the formulation for biocompatibility. Their study showed that the dressing sustained the release of Aloe vera up to 96 hours without compromising its antioxidant activity. Moreover, biocompatibility tests showed that it was safe and effective based on high cell viability and no haemolytic effects, suggesting its potential as a therapeutic alternative (Herculano et al., 2023).

Besides, Krupp and colleagues prepared and characterised NR membranes with propolis and demonstrated their efficiency in enhancing wound healing in a second-degree burn model. They revealed that membranes significantly enhanced lesion retraction, collagen synthesis and angiogenesis and reduced inflammation. The histopathological analysis further confirmed that wounds treated with NR membranes

with propolis exhibited higher tissue organization and healing when compared to the control, revealing the potential of NR membranes with propolis as a promising alternative to the treatment of burns (Krupp et al., 2019).

Furthermore, their potential in tissue engineering and regeneration, NR membranes are also being explored for their potential as a drug delivery system. Relating to this, Lima and colleagues successfully developed and characterised an ibuprofen-loaded NR latex membrane for transdermal drug release applications, demonstrating favourable drug release characteristics, good mechanical properties, and low haemolysis, suggesting its potential for localised treatment of inflammatory conditions (Lima et al., 2021). Similarly, Gemeinder and colleagues designed an NR-based gentamicin sulfate release system for the treatment of skin ulcers infected with *Staphylococcus aureus* and *E. coli*, showing that the biomembrane sustained antimicrobial activity, highlighting its potential as an effective wound dressing material (Gemeinder et al., 2021). NR has been shown to be biocompatible in a wide range of biomedical applications. NRL's ability to promote cell proliferation and extracellular matrix production underscores its value as a regenerative medicine biomaterial.

1.5 Electrospinning technique for the synthesis of NR-based biomaterials

Nanotechnology has been extensively studied and has achieved remarkable advancements in the past few decades. The performance of nanomaterials obtained through nanotechnology has attracted considerable attention, and they have had a high impact on various industries, especially the medical field (Yan et al., 2022).

Electrospinning is an innovative and versatile fiber fabrication method that can produce non-woven fibrous structures with diameters between a few micrometers and tens of nanometers (Li & Xia, 2004). It was initially patented in the early 1900s by Cooley, but it became established only later when Formhals used the technology on synthetic fibers in the textile industry (Anton, 1934; Cooley, 1902). In the past few years, electrospinning has gained significant attention because it can create nanoscale scaffolds with controlled surface morphology, thus becoming a tool that can be used in drug delivery and tissue regeneration applications (Hu et al., 2014; Yan et al., 2022).

1.5.1 Electrospinning Process

The electrospinning process, summarized in figure 4, relies on the application of an electrostatic field to create ultrafine fibers from melt or polymer solution. During the process, a polymer solution is continuously driven through a nozzle with a syringe pump at a controlled rate of feed. When a high voltage is applied, the droplet at the nozzle tip becomes electrically charged, forming a conical shape known as the Taylor cone. As soon as the voltage applied is over a critical point, overcoming the surface tension, a charged liquid jet is shot towards a collector. As the jet moves toward the collector, solvent evaporation contributes to the jet's elongation and thinning. At the end of the process, the polymer solidifies upon deposition, forming a network of dry nanofibers with controlled structural properties suitable for biomedical applications (Yarin et al., 2001).

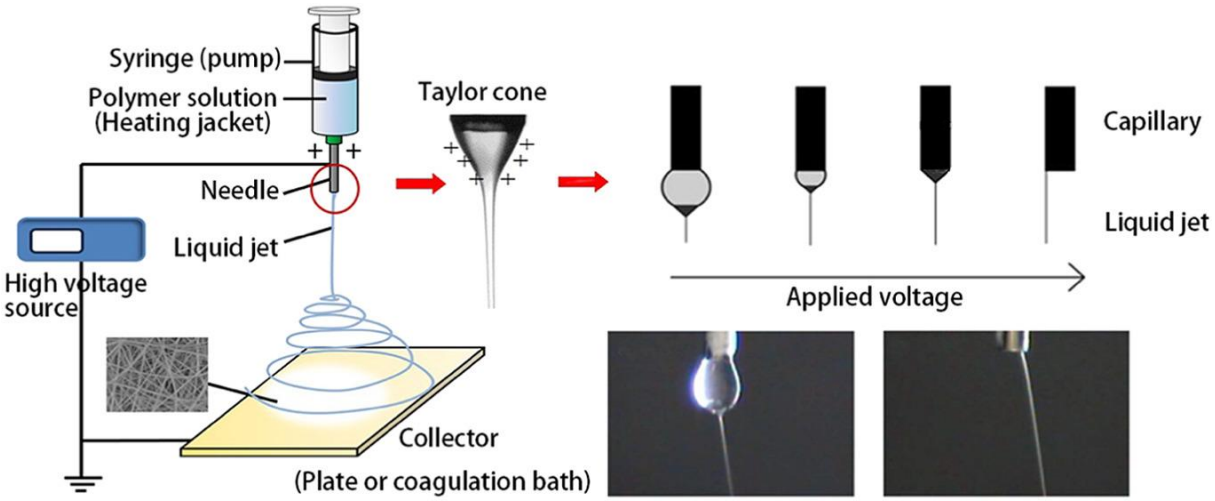

***Figure 4**: Schematic illustration of electrospinning setup (left) and Taylor cone formation (right)*(G. Liu et al., 2017).

1.5.2 Electrospun NR-based biomaterials and biomedical applications

One of the main advantages of electrospinning is its versatility, allowing it to be used with both natural and synthetic materials. This technique can produce highly porous, interconnected scaffolds that closely mimic the extracellular matrix (ECM). Natural polymers like chitosan (Adeli et al., 2019), silk fibroin (Qian et al., 2020), and NR (Panichpakdee et al., 2019a) have been successfully electrospun into nanofibrous biomaterials. Thanks to these properties, electrospun membranes are widely used in applications such as wound healing, tissue regeneration, and drug delivery (Dai et al., 2024).

NR has excellent mechanical properties, elasticity, water resistance, and biocompatibility, making it a promising material for biomedical applications due to its beneficial effects on biological processes (Andrade et al., 2023). For improving mechanical properties and “electrospinnability”, NR has been blended with synthetic polymers such as poly(L-co-D,L-lactic acid) (PLDLA) and polyvinyl alcohol (PVA). Electrospun NR/PLDLA and NR/PVA fibers offer enhanced tensile strength, swelling, and elongation, making them suitable for wound dressings, scaffolds, and controlled drug delivery systems (Panichpakdee et al., 2019b; Pinto et al., 2023). In fact, Pinto et al. successfully developed an electrospun membrane by incorporating copaiba oil into a PLDLA/NR matrix, optimizing its antimicrobial properties (Pinto et al., 2023).

Due to its high molecular weight, low polarity, and limited compatibility with many synthetic polymers, electrospinning NR remains challenging. The selection of an appropriate solvent is one of the key challenges, but selecting a solvent alone is not sufficient, since increasing NR concentration can lead to a change in fiber diameter, which can affect the uniformity of the fibers (Andrade et al., 2023).

In this project, electrospinning has been applied to process NR latex with special focus on overcoming the current limitations in NR electrospinning, focusing on optimizing electrospinning parameters and investigating the formed fiber morphology. This work aims to exploit electrospinning to produce nanofibrous structures for different applications, including biomedicine and biomaterial engineering.

AIM OF THE THESIS

Natural rubber is derived mainly from the *H. brasiliensis* tree and is widely used for biomedical and industrial applications. Despite the industrial importance of this material, problems associated with environmental impact as well as the fact that allergenic proteins are present highlight the need for a sustainable and hypoallergenic alternative. The aim of this work is to synthetize a hypoallergenic recombinant latex biomaterial from metabolically engineered bacteria that can synthesize cis,1-4,polyisoprene which is the main component of natural rubber. In consideration of the dual approach required to achieve this goal, the present work is structured into two main sections:

- **Part 1**: Synthesis of a latex-based matrix using electrospinning technique in collaboration with TissueGraft Srl. In the first part, it was necessary to set up an electrospinning protocol for cis,1-4, polyisoprene and optimize the parameters to form nanofibers. This matrix will be evaluated in vitro, assessing its biocompatibility, cytotoxicity and cell adhesion properties, to determine its potential for biomedical applications.
- **Part 2**: Microbial biosynthesis of polyisoprene as a sustainable latex alternative. The second objective is the reconstruction of the cis-1,4-polyisoprene biosynthetic pathway from *H. brasiliensis* within a microbial host. Optimized key genes from the MEP pathway will be cloned into bacteria. The strategy aims to provide a sustainable and hypoallergenic alternative to polyisoprene, reducing environmental impact and maintaining its properties.

2. PART-1

2. Part 1: Synthesis of a latex-based matrix using electrospinning technique

2.1 Materials and methods

2.1.1 NR\PVA solution preparation

The solutions to be electrospun were prepared following two different protocols. Following the first protocol, a 5% w/v of polyvinyl alcohol (PVA, Sigma-Aldrich, 81365) solution was prepared by dissolving PVA in deionized water in 10 mL final volume with magnetic stirring at room temperature for 2 hours. NR solution was then added at different v/v concentrations (10%, 25%, and 50%) and glycidoxypropyltrimethoxysilane (GPTMS) (Sigma-Aldrich, 440167) was used as a crosslinker.

Following the second protocol (Panichpakdee et al., 2019b), a 15% w/v of PVA solution was prepared by dissolving PVA in deionized water with magnetic stirring at 80 °C for 3 hours. PVA solution and NR at 70:30 weight ratios were then mixed and stirred at room temperature for 3 hours. After that, Triton X-100 (Sigma-Aldrich, T8787) at the final concentration of 1% w/w was added into the mixture solutions and stirred overnight.

In both cases, the final volume of the solution loaded into the electrospinning system was 10 mL.

2.1.2 Electrospinning

Electrospun scaffolds were produced with the NE300 electrospinning system (Inovenso, Turkey). Process parameters were set as follows: cylindrical collector; electric field: 25 kV; needle size: 18 Ga; solution flow rate: 1.5 mL/h; collector rotation speed: 750 rpm; needle-to-collector distance = 22 cm; collector horizontal displacement: 20 mm/s; humidity: 20%; temperature: 40 °C. The fibers obtained with this system exhibited a random orientation. The experiments were conducted at the TissueGraft Srl spin-off.

2.1.3 Heat treatment

The electrospun membrane was heat-treated by placing it 20 minutes in an oven at 180°C and then rehydrated in 1X Phosphate-Buffered Saline (PBS). The membrane was UV-sterilized for 60 minutes before seeding the cells or conditioning the medium.

2.1.4 Conditioned media preparation

Conditioned culture media were prepared by incubating electrospun material (6 mg/mL) in complete cell culture medium at 37 °C for 72 hours. After incubation, the medium was filtered using 0.2 µm filters, collected and used to treat cells at specified time points.

2.1.5 Cell culture

NHDF cells (Primary Normal Human Dermal Fibroblasts) isolated from the dermis of adult skin (Lonza NHDF-Ad CC-2511, Switzerland) were used from passage 8 to passage 12 and tested negative for mycoplasma contamination. Cells were maintained in Dulbecco's Modified Eagle Medium (DMEM) high glucose, GlutaMAX™ Supplement (Thermo Fisher Scientific, 61965059) supplemented with 10% heat-inactivated fetal bovine serum (FBS, Thermo Fisher Scientific, A5256701) and 1% antibiotic–antimycotic (Thermo Fisher Scientific, 15240062) at 37 °C under a 5% CO2 humidified atmosphere.

2.1.6 Cell viability

Cell viability was assessed using the 3-(4,5-dimethylthiazol-2-yl)-2,5-diphenyltetrazolium bromide (MTT) assay (Sigma-Aldrich, M5655). 1×10^4 NHDF cells per well were seeded in a 24-well microplate. After 24 hours of incubation, the culture medium was removed and cells were treated using two different approaches: (1) exposure to conditioned medium for 24 hours, 72 hours, and 6 days; or (2) direct contact with a section of the electrospun material (0.8 cm per side) placed into the well for the same time points. Following treatment, the medium was discarded and 500 µL of MTT solution (1 mg/mL in 1× PBS) was added to each well. Cells were then incubated at 37 °C in a humidified atmosphere containing 5% CO_2 for 4 hours. After incubation, the solution was removed, and the formazan crystals formed were dissolved in dimethyl sulfoxide (DMSO, Sigma-Aldrich, D2650). Absorbance was measured at 570 nm using a VICTOR X Multilabel Plate Reader (Perkin Elmer).

2.1.7 Scanning electron microscopy (SEM)

Cells seeded on the electrospun post heat-treatments were fixed for SEM visualization as follows: cells were washed with 0.2 M Cacodylate buffer (pH 7.4) (C0250**,** Sigma-Aldrich) twice, 5 minutes each. Subsequently, cells were fixed with 2.5% Glutaraldehyde (Sigma-Aldrich, 49626) for 30 minutes at room temperature and

then washed with 0.2 M Cacodylate buffer (pH 7.4) for 5 minutes. After that, the samples were dehydrated with an ethanol scale 50%, 70%, 80%, 95% and 100% for 5 minutes each and then incubated with hexamethyldisilazane (VWR, 999-97-3), until complete evaporation of the solution. Biomaterials were sputtered with a gold layer for 60 seconds (10 nm layer by SmartCoater, Jeol) and then visualized using SEM (JSM-IT500 InTouchScope™ Scanning Electron Microscope, Jeol) at various magnifications. The images at x4000 magnification were then analyzed using ImageJ graphics software to obtain fibers measurement.

2.1.8 Statistical analysis

Statistical analysis was performed using GraphPad Prism 10 (California, USA). Data were expressed as mean ± SEM of *n* independent experiments. Statistical significance was assessed by one-way ANOVA multiple comparisons. Statistical significance was defined as $p < 0.05$.

2.2 Results

2.2.1 Morphological characterization of the NR\PVA nanofiber

The morphological properties of electrospun nanofibers obtained from NR/PVA blends with various volumetric ratios were examined through SEM, as shown in Figure 5. In all the formulations, PVA was kept at a constant value of 5% (w/v), and NR was used at concentrations of 10% (fig. 5a), 25% (fig. 5b), and 50% (fig. 5c) (v/v). In Figure 5a the nanofibers are mostly continuous and randomly oriented. There is, nevertheless, some degree of bead formation and swelling, suggesting phase separation or incomplete miscibility between NR and PVA. This would indicate that although electrospinning was able to produce fibers, the compatibility between hydrophilic PVA and hydrophobic NR may be suboptimal, whereby localized NR-rich domains are created. Figure 5b indicates an increase in morphological irregularities. Fibrous architecture becomes less uniform, and bead-like structures are more prominent. This results in irregular fiber formation and agglomeration of NR within the matrix. To confirm this, figure 5c, where the NR concentration is further increased, the fibrous structure is significantly compromised. The electrospun biomaterial appears to change from a fibrous to a film-like morphology, with fused areas and fewer distinct nanofibers.

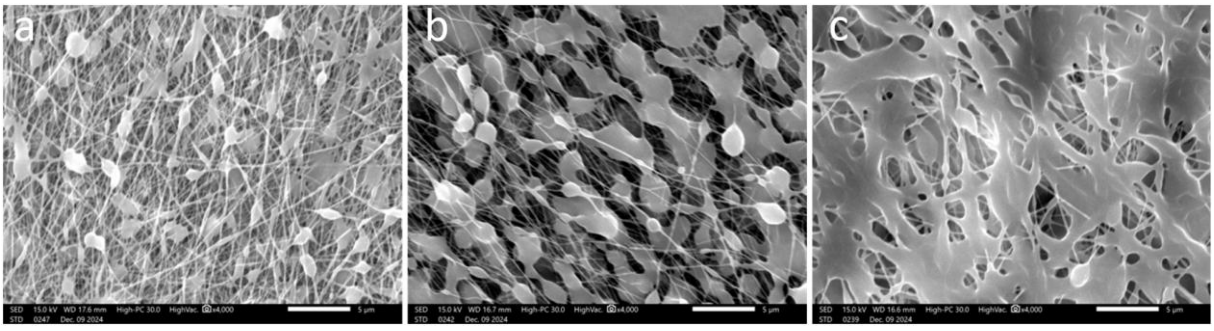

Figure 5*: SEM images of electrospun PVA/NR nanofibers at a constant PVA concentration (5% w/v) and increasing NR contents: (a) 10% v/v, (b) 25% v/v, and (c) 50% v/v. All images were taken at 4000× magnification. The presence of bead-like structures and discontinuous fibers becomes more pronounced with higher NR content, indicating poor miscibility between the two polymers and reduced electrospinnability of the blend at elevated NR ratios.*

In order to improve the homogeneity in the NR/PVA solution, the protocol of Panichpakdee and colleagues (Panichpakdee et al., 2019b) was followed using a PVA:NR weight ratio of 70:30, with Triton X-100 (1% w/w). The resultant nanofibers were characterized using SEM at different magnifications (x500, x4000, and x10000) and from different regions of the electrospun material, as illustrated in Figure 6. The

morphological analysis of the fibers revealed significant enhancement in fiber continuity and homogeneity. At lower magnification (fig. 6a, d, and g), nanofibers are of three-dimensional structure without finding any indication of bead formation and phase-separated domains. This reflects enhanced miscibility between NR and PVA due to the surfactant. The higher magnification images (middle and right panels) confirm the presence of smoother and more defined surfaces. The discontinuity regions are reduced compared to the previous formulation, support higher compatibility due to the addition of Triton X-100. The fibers become more stable, which is a sign of a better electrospinning process and possibly better mechanical properties for the final scaffold.

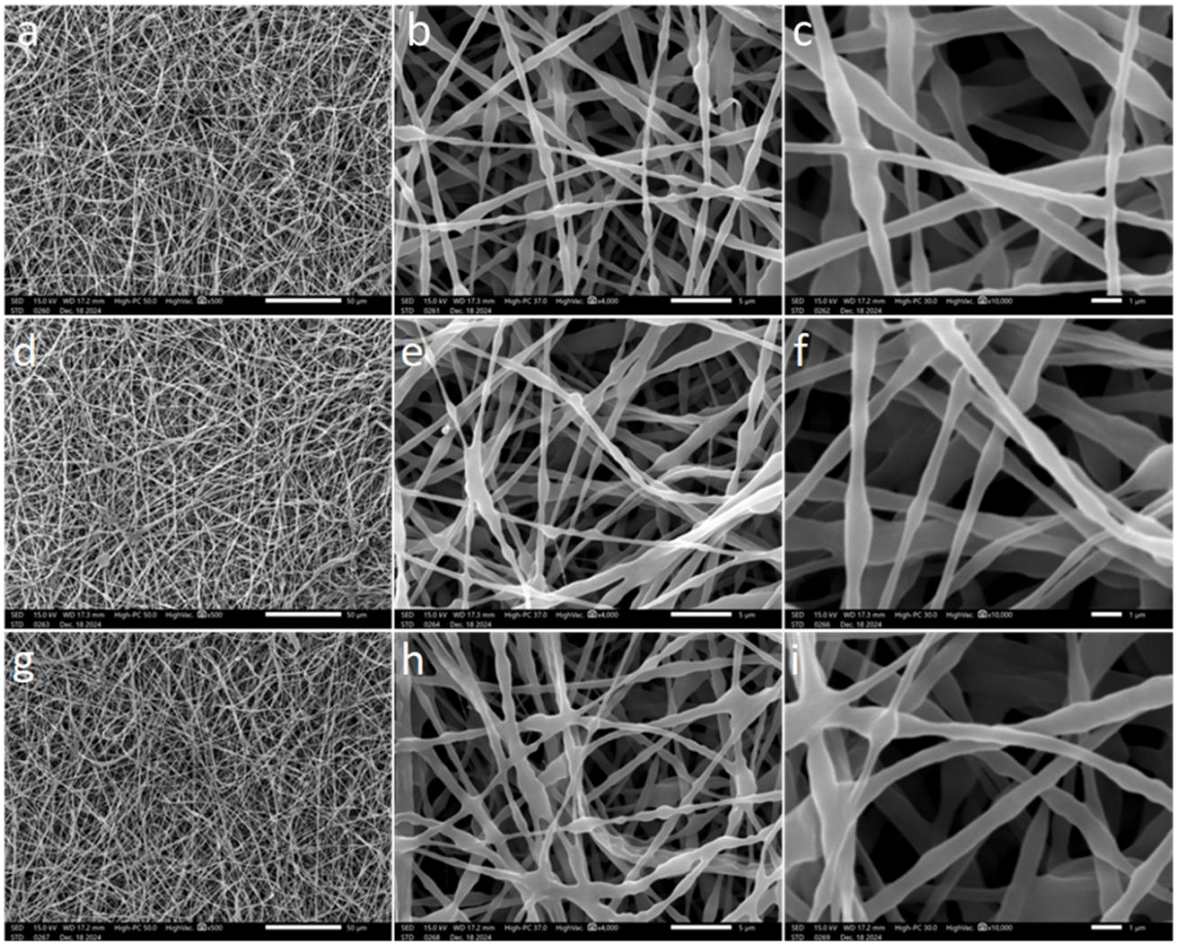

***Figure 6**: SEM images of electrospun PVA/NR nanofibers obtained from a blend of 15% w/v PVA and 30% w/w NR, mixture with 1% w/w Triton X-100 added as surfactant. Images (a–c), (d–f), and (g–i) are three areas of the same sample, recorded at successively higher magnifications: 500× (a, d, g), 4000× (b, e, h), and 10000× (c, f, i). The fibers exhibit uniform morphology and partially smooth surfaces, indicating improved electrospinnability and phase compatibility.*

2.2.2 Quantitative fiber diameter analysis

Diameter of the fibers obtained with the 70:30 ratio was measured to assess the homogeneity of the fibers forming the biomaterial. The resulting distribution is shown in Figure 7. The histogram shows a symmetrical fiber diameter distribution, with most fibers ranging from 0.7 µm to 1.3 µm. The estimated average fiber diameter was around 0.96 µm. The absence of significant outliers supports the observation of homogeneous fibers with minimal bead formation. The diameter profile exhibits improved spinnability when Triton X-100 is present.

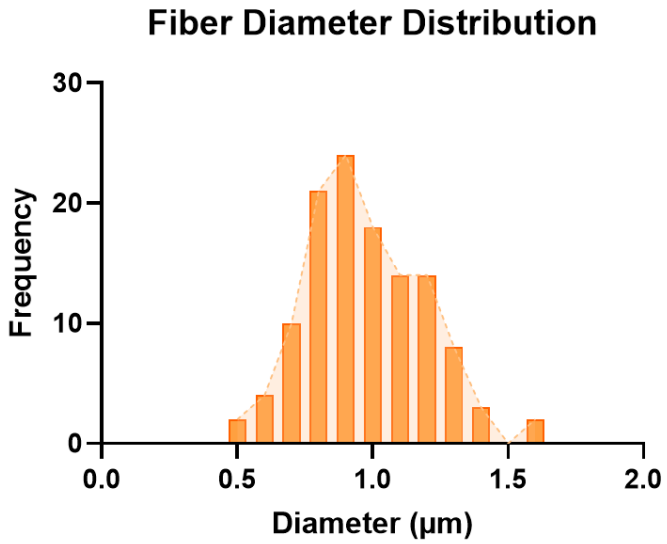

***Figure 7**: Distribution of fiber diameters of electrospun PVA/NR biomaterials (70:30 w/w) from 15% (w/v) PVA and 1% (w/w) Triton X-100. Histogram of frequency of fiber diameters (µm) as obtained from SEM images. The distribution is Gaussian-like, with most fibers in the 0.7–1.3 µm range, which reflects a fairly uniform morphology.*

2.2.3 Cell viability in response to NR/PVA-conditioned medium

To further investigate the potential cytotoxicity of the electrospun NR/PVA scaffolds, an indirect MTT assay was performed using conditioned media. In this approach, the electrospun scaffolds were incubated in complete culture medium. The conditioned media were then collected and applied to cell cultures to assess metabolic activity. As shown in Figure 8, cell viability remained above 80% under all conditions tested, indicating a generally low cytotoxic potential of the biomaterials. Specifically, despite some statistically significant differences, cell viability in response to 10% NR-conditioned media remained above 80% at almost all time points. There was no significant cytotoxicity associated with media conditioned from 25% NR electrospun materials at any time point during testing, with cell viability consistently exceeding 90%. After six days, viability showed a slight increase. Media derived from 50% NR

electrospun materials had slightly lower viability than media derived from lower NR concentrations; however, viability remained above 85% at all time points, suggesting a modest impact without overt cytotoxicity. These results indicate that the materials did not release cytotoxic substances into the culture medium.

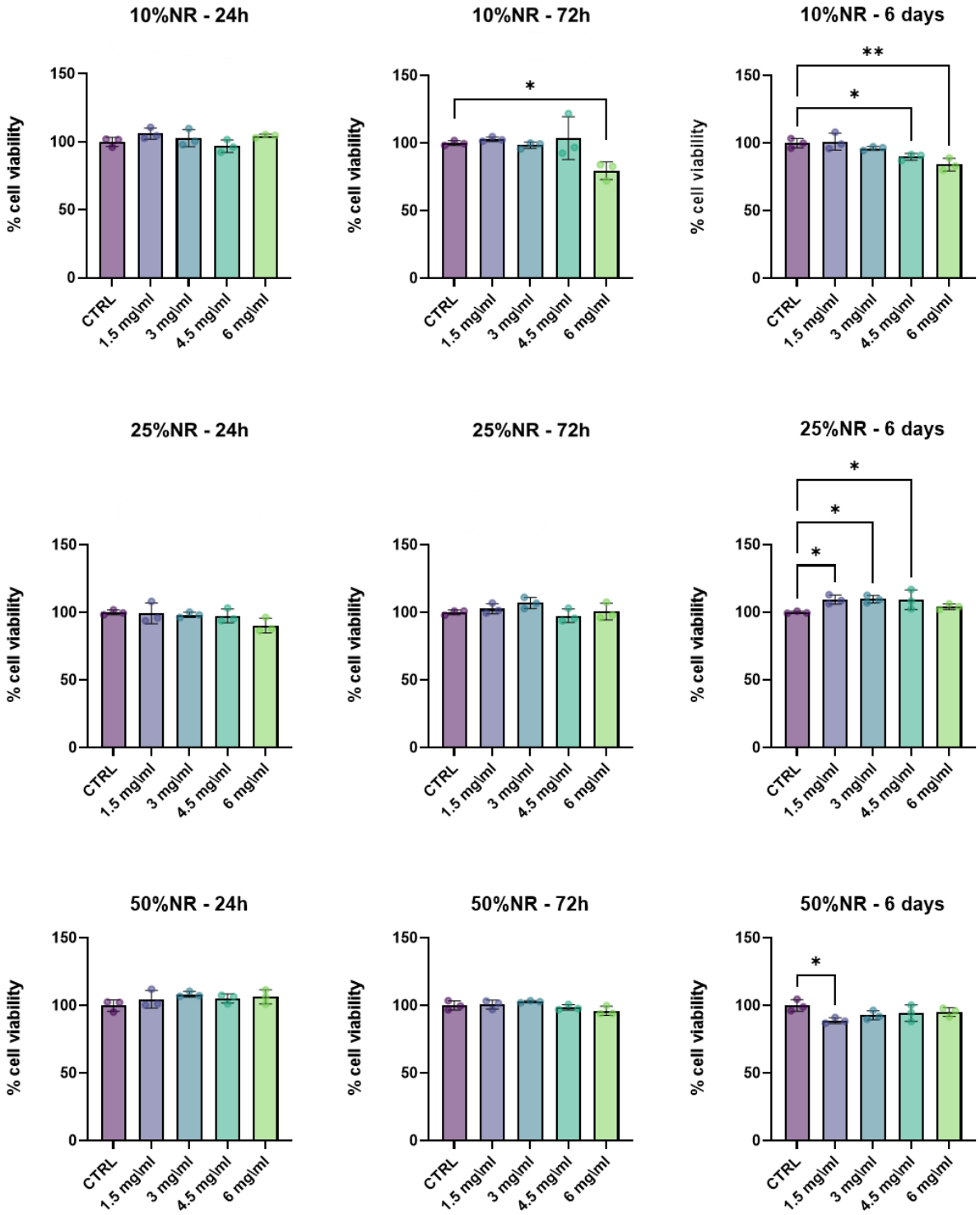

***Figure 8**: MTT assay on cells treated with conditioned media from electrospun NR-based scaffolds. Bar graphs show cell viability following 24 h treatment with media conditioned for 24h (left column), 72 h (middle column), or 6 days (right column) by electrospun materials containing 10% (top row), 25% (middle row), or 50% (bottom row) natural rubber. Cell viability is expressed as percentage relative to untreated control. Bars represent mean ± standard deviation. The experiment was conducted in triplicate and repeated independently three times. Data points represent the mean of each individual experiment (*p < 0.05, **p < 0.01, ***p < 0.001, ****p < 0.0001)*

2.2.4 Cell viability in direct contact with electrospun NR/PVA scaffolds

To determine the biocompatibility of the electrospun NR/PVA scaffold, different NR concentrations (10%, 25%, and 50%) were tested, as well as different incubation times (12 h, 72 h, and 6 days). The results in Figure 9 show a dose- and time-dependent decrease in cell viability, independent of NR content. There was no clear correlation between increasing NR percentage and cytotoxicity, suggesting that NR content is not the only causative factor of the cellular response. The reduction in cell viability could also be explained by the physical dimensions of the biomaterial in the wells. A larger scaffold piece might have caused mechanical stress to the monolayer of cells, compromising their proliferation or viability. The effects of material composition may be decoupled from scaffold mechanical performance with further testing using different sample sizes.

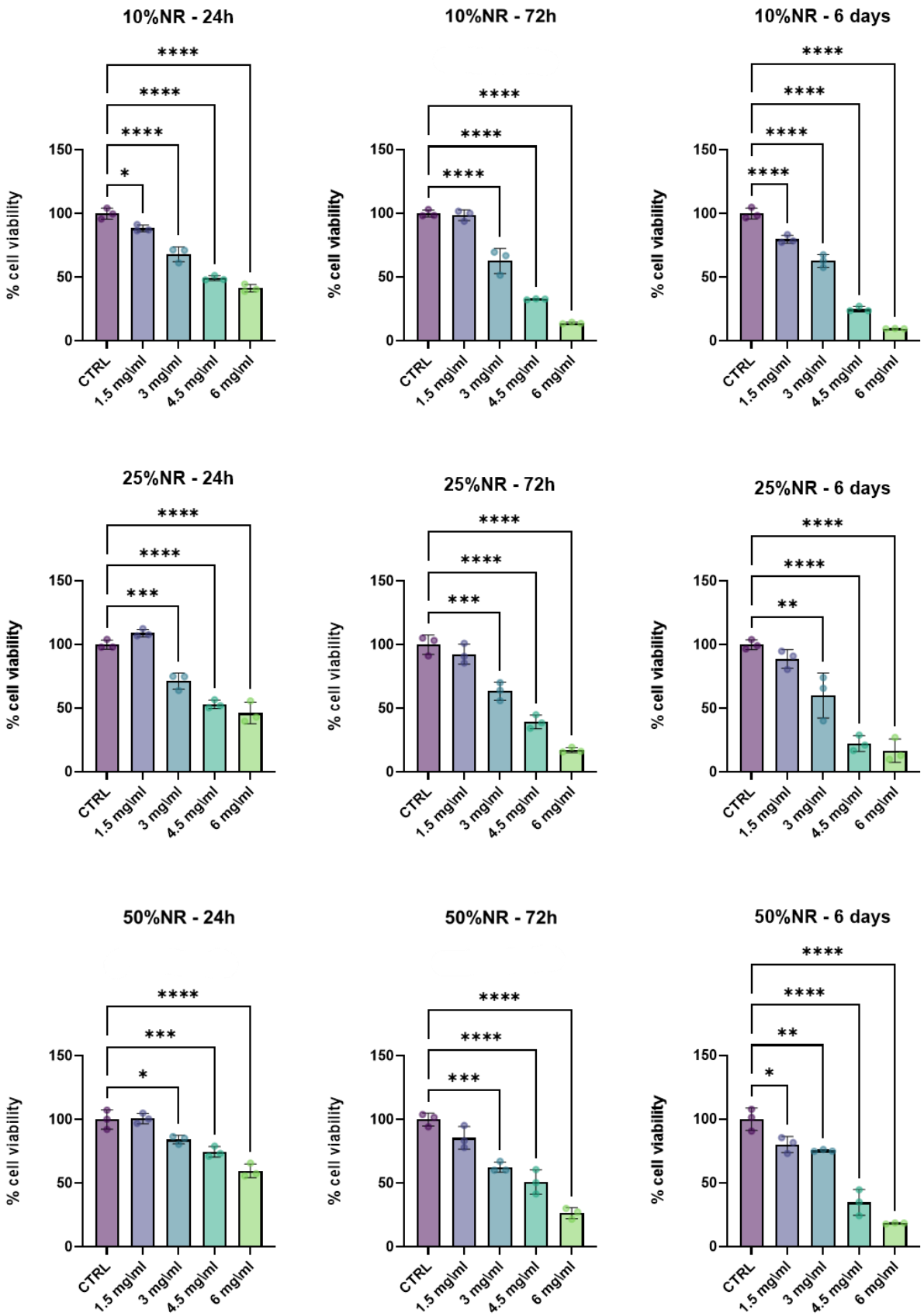

***Figure 9**: MTT assay performed by directly placing electrospun PVA/NR scaffolds into the culture wells. Scaffolds were composed of 10% (top row), 25% (middle row), or 50% (bottom row) natural rubber (NR) and incubated for 24 h (left column), 72 h (middle column), or 6 days (right column). Cell viability is*

*expressed as percentage relative to untreated control. Bars represent mean ± standard deviation. The experiment was conducted in triplicate and repeated independently three times. Data points represent the mean of each individual experiment (*p < 0.05, **p < 0.01, ***p < 0.001, ****p < 0.0001).*

2.2.5 Cell viability using 70:30 biomaterial

Cell viability assays were conducted on electrospun membrane conditioned media before and after thermal treatment to assess the biocompatibility of an optimized NR/PVA scaffold (70:30 weight ratio). As illustrated in Figure 10, at all-time points (24 h, 72 h, and 6 days) the scaffold untreated (non-crosslinked) demonstrated a strong cytotoxic effect as evidenced by a significant decrease in cell viability. This result can be attributed to the structural instability of the non-crosslinked fibers, which disintegrated upon contact with the aqueous culture medium, potentially releasing soluble, cytotoxic degradation products.

In contrast, thermal crosslinking of the electrospun membrane at 180 °C for 20 minutes resulted in a remarkable stabilization of the scaffold. Cell viability remained consistently above 80% in the medium conditioned from the heat-treated biomaterial at all time points, without any cytotoxic effects, except for the highest dose. As a result of the thermal treatment, fibers were able to prevent disintegration and maintain scaffold integrity during incubation in the culture medium, preventing the release of toxic compounds.

Overall, the data demonstrates that the optimized 70:30 NR/PVA electrospun scaffold, when thermally crosslinked, is biocompatible and suitable for applications in tissue engineering or regenerative medicine.

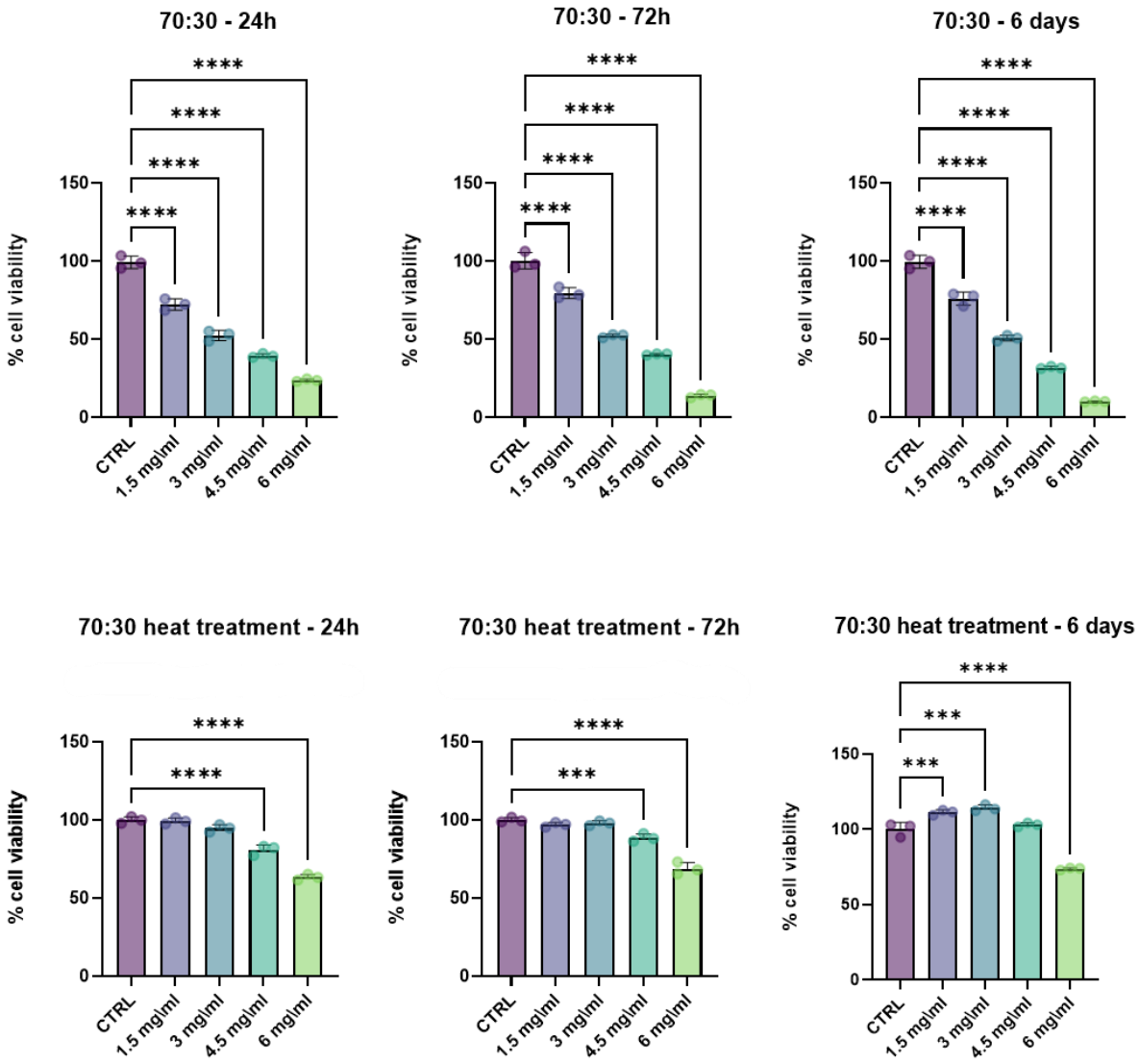

***Figure 10**: **MTT assay on cells treated with conditioned media from 70:30 NR/PVA electrospun scaffolds.** Bar graphs show cell viability following 24 h treatment with media conditioned for 24 h (left column), 72 h (middle column), or 6 days (right column) by electrospun NR/PVA membranes, either non-crosslinked (top row) or thermally crosslinked at 180 °C for 20 min (bottom row). Cell viability is expressed as percentage relative to untreated control. Bars represent mean ± standard deviation. The experiment was conducted in triplicate and repeated independently three times. Data points represent the mean of each individual experiment (*p < 0.05, **p < 0.01, ***p < 0.001, ****p < 0.0001).*

2.2.6 Cell seeding on 70:30 biomaterial

To determine the biocompatibility of the 70:30 NR/PVA thermally crosslinked scaffold, direct cell seeding tests were done. For investigation of cell morphology and adhesion onto the surface of the membrane upon seeding for 48 hours, the samples were fixed and analyzed with SEM (Figure 11). SEM images suggest that the scaffold supports cell attachment, with numerous cells adhering to the surface of the electrospun fibers. The cells appear viable, exhibiting anchoring morphology onto the underlying nanofibrous network. This morphology suggests active cytoskeletal

remodeling and strong interactions with the scaffold, suggesting a good substrate for cell adhesion. Furthermore, the cells are not isolated but often appear in clusters or in proximity, suggesting a possible proliferation. Nanofibrous morphology can still be observed under the cells, determining that the scaffold does not break down under cell culture conditions. Overall, these findings support that the crosslinked 70:30 NR/PVA electrospun membrane provides a supportive environment for cell adhesion and spreading, thus further validating its potential use in tissue engineering applications.

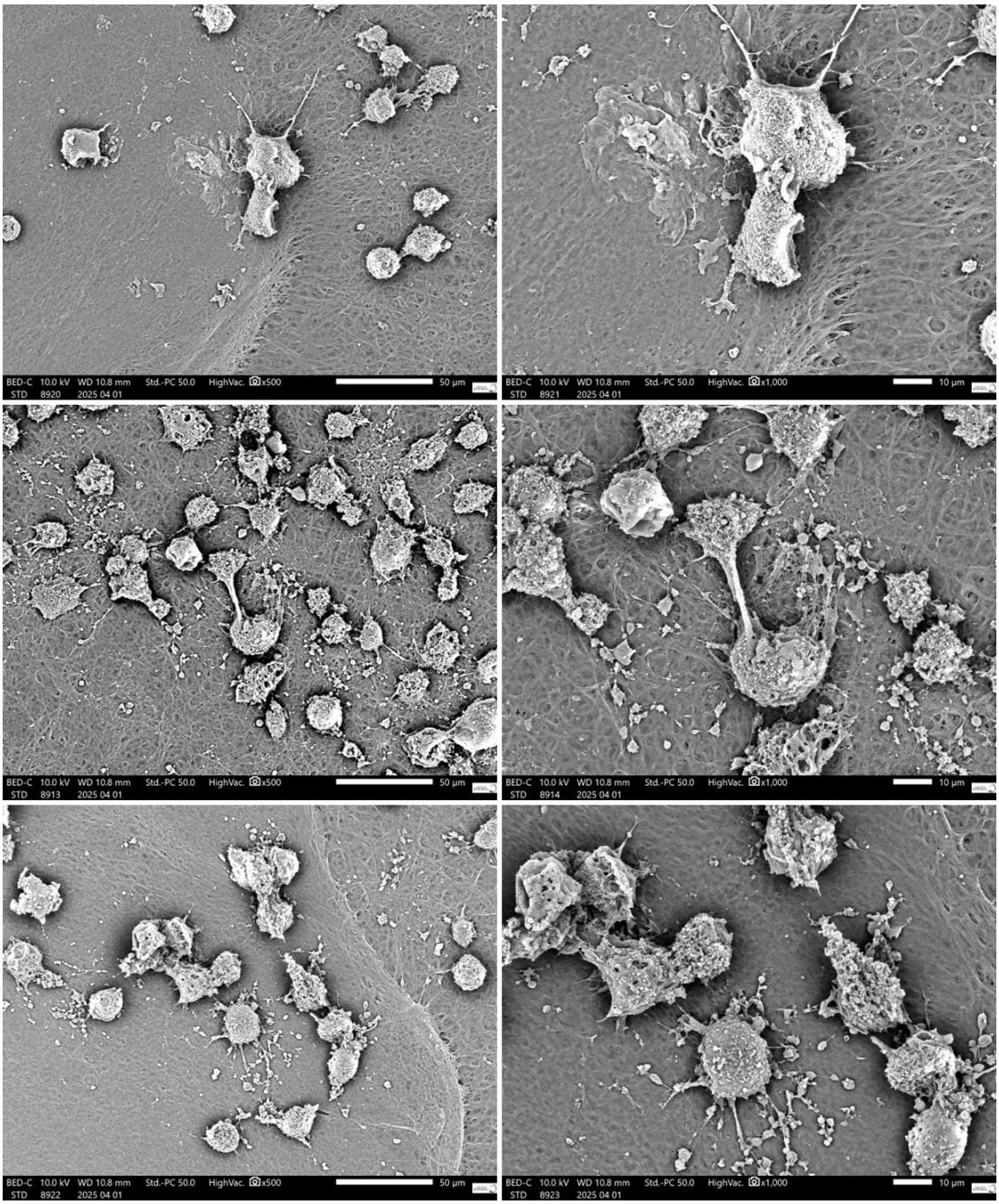

Figure 11*: SEM images of cells seeded on electrospun NR/PVA (70:30) scaffolds. SEM images showing the surface morphology of electrospun NR and PVA scaffolds (70:30 weight ratio) after 24 h of cell*

seeding. Images were acquired at 500× magnification (left column, scale bar = 50 μm) and 1000× magnification (right column, scale bar = 10 μm). Cells are visible on the scaffold surface, displaying varying degrees of adhesion and spreading. The underlying fibrous structure of the scaffold is also discernible, with fibers forming a porous network that supports cellular attachment.

3. PART-2

3. Part 2: Microbial biosynthesis of polyisoprene as a sustainable latex alternative

3.1 Materials and methods

3.1.1 Plasmid design and primers

To engineer the MEP pathway in *E. coli* to cis-1,4-polyisoprene biosynthesis, xenogenic *H. brasiliensis* genes were introduced. Specifically, the HRT2 prenyltransferase gene (GenBank: AB064661.2) was cloned into a pET100 expression vector regulated by an IPTG-inducible promoter, with an N-terminal 6×His tag for detection. The plasmid has an ampicillin resistance gene as a selection marker. Given the requirement of a cofactor for optimal prenyltransferase activity, the SRPP gene (GenBank: AF051317.1) was cloned into another IPTG-inducible pET100 vector, also optimized for bacterial expression and with an N-terminal 6×His tag. To allow co-expression of both proteins, a third construct (pET30_SRPP_HRT2, kanamycin resistance) was generated via standard restriction digestion and ligation techniques. In this plasmid, HRT2 retains the 6×His tag, while SRPP was fused to a V5 tag. Furthermore, for increased solubility, fusion constructs were designed. The plasmids pET32_SRPP and pET30_TrxA_HRT2 were assembled to express SRPP and HRT2, respectively, as thioredoxin fusion proteins. All synthetic genes were codon-optimized for *E. coli* expression. Primer sequences are shown in Table 1.

SRPP_r	AGCTCTCGAGTTAGCTGGCTTCATCACC
SRPP_f	AGCTGAATTCATGGCCGAAGAAGTTGAAG
SRPP+V5_r	CAGTGGATCCTCAATCCAGGCCCAGCAGCGGGTTCGGAATGCTGGCTTCATCACCAAA
SRPP+V5_f	CTCGAGCACCACCACCAC
HRT2\TrxA_r	CAGTCTCGAGTTTCAGATATTCTTTGTG
HRT2\TrxA_f	CAGTGGATCCTTTTGTTTAACTTTAAGAAGGAGATATACATATATGGAACTGTATAATGG

Table 1: Primer sequences used for the amplification and cloning of HRT2 and SRPP into various expression vectors.

3.1.2 Bacterial strains

Three *E. coli* strains were used throughout this study for cloning and recombinant protein expression. *E. coli* DH5α, with the genotype F^- Φ80lacZΔM15 Δ(lacZYA-argF) U169 recA1 endA1 hsdR17 (r_K^-, m_K^+) phoA supE44 λ^- thi-1 gyrA96 relA1, was employed for plasmid propagation and molecular cloning due to its high transformation efficiency and reduced recombination activity. *E. coli* BL21(DE3), with

the genotype F^- ompT gal dcm lon hsdS_B(r_B^-, m_B^-) λ(DE3 [lacI lacUV5-T7p07 ind1 sam7 nin5]) [malB$^+$]K-12(λ$^-$), was utilized for protein expression. *E. coli* ArcticExpress (DE3) (Agilent Technologies) was also used to enhance protein solubility during expression at low temperatures. This strain is derived from BL21(DE3) and co-expresses the cold-adapted chaperonins Cpn10 and Cpn60, facilitating the correct folding of recombinant proteins under cold-shock conditions. This strain is maintained under gentamicin selection. Cultures of all strains were grown under appropriate antibiotic pressure: ampicillin (100 µg/mL), kanamycin (50 µg/mL), and gentamicin (20 µg/mL), depending on the plasmid or strain-specific resistance markers.

3.1.3 Bacterial transformation and culture

Plasmid constructs were first introduced into *E. coli* DH5α chemically competent cells using the heat shock transformation method. Following transformation, cells were recovered in 2xYT medium at 37 °C for 1 hour with agitation and then plated on 2xYT (Sigma-Aldrich, X2377) with agar and containing the appropriate antibiotic for selection. Single colonies were cultured overnight in 2xYT medium under selective conditions, and plasmids were subsequently purified using a commercial miniprep kit (Thermo Fisher, K070). The isolated plasmids were subsequently transformed into chemically competent *E. coli* BL21(DE3) or ArcticExpress (DE3) cells by the heat shock method, and the resulting colonies were screened on 2xTY-agar plates supplemented with antibiotics. For protein expression, positive clones were grown overnight in 2×YT medium containing the appropriate antibiotics. The following day, cultures were diluted 1:100 into fresh 2×YT medium with antibiotics and incubated at 37 °C in orbital shaker (Medline, IS-971R) (200 rpm) until an optical density at 600 nm (OD_{600}) of 0.8–1.0 was reached. Protein expression was induced by the addition of isopropyl β-D-1-thiogalactopyranoside (IPTG) (Sigma-Aldrich, 5810-5GM) to a final concentration of 1 mM. Cultures were then incubated for 4 hours at 37 °C (BL21(DE3)) or at 12–15 °C (ArcticExpress (DE3)). Samples were collected before and after induction for SDS-PAGE and Western blot analysis.

3.1.4 SDS-page and Western blot

Protein expression was evaluated by SDS–polyacrylamide gel electrophoresis (SDS-PAGE) followed by Coomassie Blue staining and Western blot analysis. Culture samples were collected before and after induction, centrifuged, and bacterial pellets were resuspended in Laemmli buffer and lysed by heating at 95 °C for 5 minutes.

Proteins were separated on 12.5% SDS-PAGE gels under denaturing conditions. To visualize the proteins, gels were stained with Coomassie Blue (Sigma-Aldrich, B0149) and then gently destained using a solution of 10% methanol and 10% acetic acid in distilled water until the background was clear and distinct bands appeared. For Western blot analysis, the separated proteins were transferred to nitrocellulose membranes using a semi-dry transfer system (Trans-Blot® SD, Bio-Rad) used at 15 V for 20 minutes. After the transfer, the membranes were blocked for one hour at room temperature in PBS with 0.1% Tween-20 (Sigma, SLBZ6541) (PBS-T), supplemented with 4% bovine serum albumin (BSA, Sigma-Aldrich, A2153-100G) to prevent non-specific binding. After that, membranes were incubated with a mouse monoclonal anti-6xHis tag antibody (Thermo Fisher Scientific, MA1-21315), diluted 1:5000 in PBS-T containing 2% BSA, for one hour at room temperature. After three 5-minute washes in PBS-T, the membranes were incubated for 45 minutes at room temperature with a rabbit anti-mouse IgG secondary antibody conjugated to horseradish peroxidase (HRP) (Novex, A16160), diluted 1:5000 in PBS-T containing 4% BSA. Following incubation, the membranes were washed three more times in PBS-T and developed using the Clarity Western ECL Substrate (Bio-Rad, 1705061) and the chemiluminescent signals were detected using the ChemiDoc Imaging System (Bio-Rad).

To detect V5-tagged proteins, membranes were first incubated with a mouse monoclonal anti-V5 antibody (Thermo Fisher Scientific, MA5-15253), then processed using the same secondary antibody and detection steps as described above. Protein sizes were estimated using the PageRuler™ Unstained Protein Ladder (Thermo Scientific, 26614) for SDS-PAGE, and the PageRuler™ Prestained Protein Ladder (Thermo Scientific, 26616) for accurate molecular weight determination during Western blot analysis.

3.1.5 Solubility test

The bacterial cell pellets were resuspended in a non-denaturing lysis solution (0.1% Triton X-100 in PBS supplemented with 200 µg/ml lysozyme, Sigma-Aldrich, 62971-10G-F). The pellet was mixed in a buffer volume corresponding to 10% of the starting culture. These resuspended pellets were mechanically disrupted using a sonicator (Bandelin Sonopuls). The lysate was centrifuged to remove cellular debris, and each step of the solubility test was evaluated by Western blot.

3.1.6 Polymer extraction

As chloroform was employed in the extraction process, only glassware laboratory equipment was chosen. The bacteria were separated using a centrifuge and discarding the supernatant. The bacteria were lysed, and the polymer produced was solubilized by adding chloroform. The chloroform fraction was recovered, and methanol was added in a 1:1 ratio, resulting in the precipitation of cis-1,4-polyisoprene. Precipitate was recovered, resolubilized with chloroform, and dried on a glass slide prior to analysis.

3.1.7 Infrared spectroscopy

Infrared (IR) analyses were performed at the Department of Pharmaceutical Sciences (DSF), *Università del Piemonte Orientale*, under the supervision of Dr. Ivana Miletto. IR spectra were recorded in ATR (Attenuated Total Reflection) mode, by using a Bruker Alpha II instrument equipped with ATR accessory with monolithic diamond crystal and a DTGS detector, operating in the 4000-450 cm-1 range at a resolution of 4 cm-1. OPUS Software (Release 8.7) was used for processing ATR-FTIR spectra.

3.2 RESULTS

3.2.1 Expression of HRT2 and SRPP proteins in *E. coli* using pET100 vectors

Expression of *H. brasiliensis* SRPP and HRT2 proteins in *E. coli* was examined with pET100-based constructs encoding an N-terminal 6×His tag. Protein expression was induced by the addition of 1 mM IPTG, and samples were collected at three time points: non-induced (NI), and at 2 hours (I-2h) and 4 hours (I-4h) post-induction. The lysates of cell lysates were analyzed by SDS-PAGE and stained with Coomassie Blue staining. Distinct protein bands were observed near 26.5 kDa for SRPP and 37 kDa for HRT2 that matched the recombinant protein estimated molecular weights in figure 12. These bands were absent in non-induced controls and became progressively more intense following IPTG induction, confirming time-dependent accumulation of the target proteins. These results establish successful and IPTG-dependent heterologous expressions of SRPP and HRT2 in *E. coli*.

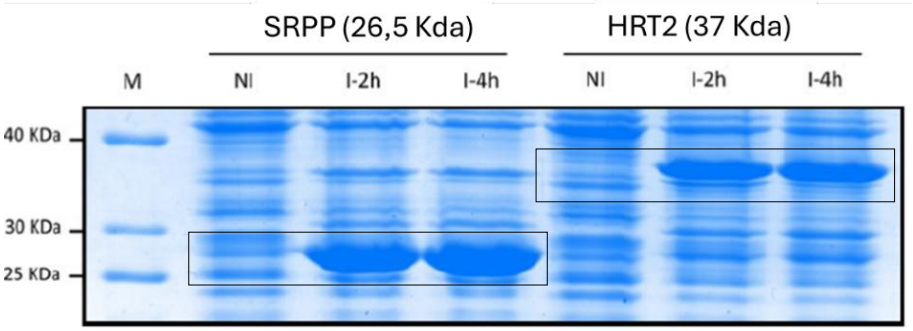

***Figure 12**: SDS-PAGE analysis of total protein extracts from E. coli expressing HRT2 (~37 kDa) and SRPP (~26.5 kDa). Samples were collected before induction (NI), and after 2 h (I 2h) and 4 h (I 4h) of IPTG induction. The presence of distinct bands in induced samples confirms the expression of the target proteins.*

3.2.2 Solubility test of recombinant HRT2 and SRPP proteins

To evaluate the solubility of the heterologously expressed proteins, *E. coli* cells were lysed under non-denaturing conditions following IPTG induction. The lysates were fractionated by differential centrifugation into total (Tot), soluble (Sol), and insoluble (Pellet) fractions. Western blot analysis using an anti-His antibody was performed to selectively detect the recombinant SRPP and HRT2 proteins. As shown in Figure 13, both SRPP (26.5 kDa) and HRT2 (37 kDa) were primarily detected in the insoluble fraction, while only faint signals were observed in the soluble fractions. These results indicate that most of the recombinant proteins are present in an aggregated and insoluble form, likely as inclusion bodies. This suggests that, under the tested

expression conditions, SRPP and HRT2 exhibit poor solubility, which may impair their native folding and functional activity in *E. coli*.

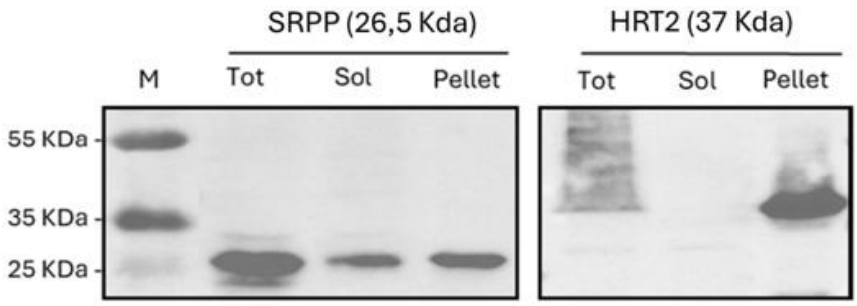

***Figure 13**: Western blot analysis of His-tagged SRPP (26.5 kDa) and HRT2 (37 kDa) expressed in E. coli. Protein samples were separated into total (Tot), soluble (Sol), and insoluble (Pellet) fractions after cell lysis and centrifugation. Detection was performed using an anti-His antibody. most of each protein was detected in the insoluble fraction, particularly for HRT2, which showed exclusive accumulation in this fraction.*

3.2.3 Enhancement of solubility through Thioredoxin fusion protein and temperature optimization

An alternative expression strategy was implemented to overcome the limited solubility of SRPP and HRT2 observed with initial constructs, in which each target protein was fused to thioredoxin (TrxA), a solubility-enhancing tag. Solubility profiles of these fusion proteins were examined in *E. coli* BL21(DE3) upon IPTG induction at two temperatures: 37 °C and 25 °C. SRPP levels of expression and solubility were assessed through SDS-PAGE and Western blot of total, soluble, and insoluble protein fractions. As shown in Figure 14, SRPP expression through the pET32_SRPP construct resulted in a band around ~35–40 kDa in the induced samples, which corresponds to the calculated molecular weight of the SRPP-TrxA fusion protein. Western blotting confirmed the presence of this protein and revealed that SRPP was expressed at both temperatures. However, a difference in solubility was observed. In fact, at 25 °C, protein was present in the soluble fraction, while at 37 °C, SRPP was predominantly in the insoluble pellet, indicating inclusion body formation.

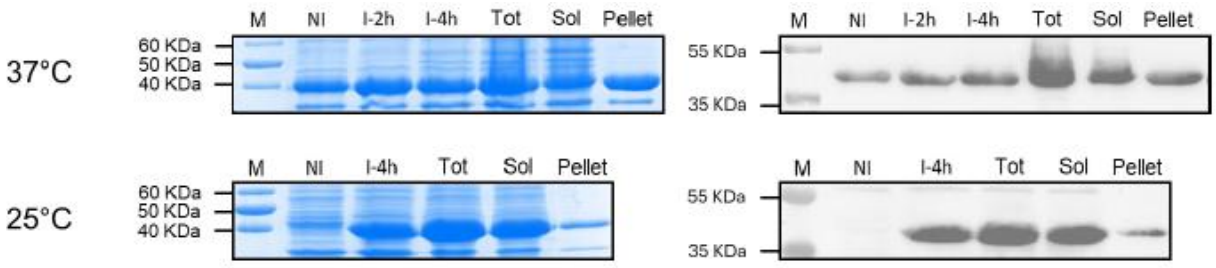

***Figure 14**: Expression and solubility analysis of SRPP-TrxA fusion protein in E. coli at 37 °C and 25 °C. SDS-PAGE (left panels) and Western blot (right panels) analysis of total protein extracts from E. coli*

BL21(DE3) cells transformed with the pET32_SRPP construct, collected before induction (NI), and after 2h or\and 4h (I-4h) of IPTG induction. Protein solubility was assessed by analysing total (Tot), soluble (Sol), and insoluble (Pellet) fractions from bacteria grown at 25 °C and at 37°C.

Similarly, expression of HRT2 from the pET30_TrxA_HRT2 construct is shown in Figure 15. A recombinant fusion protein of predicted molecular weight of approximately 60–65 kDa was expressed well under both temperature conditions. As observed through Western blot, HRT2 was more soluble when expressed at 25 °C. Together, these findings demonstrate that thioredoxin fusion protein and reduction of induction temperature from 37 °C to 25 °C enhance the solubility of SRPP and HRT2 in *E. coli*.

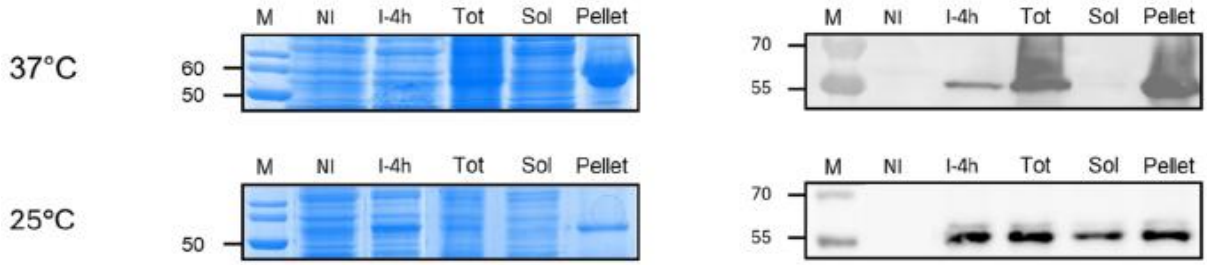

***Figure 15**: Expression and solubility analysis of HRT2-TrxA fusion protein in E. coli at 37 °C and 25 °C. SDS-PAGE (left panels) and Western blot (right panels) of protein extracts from E. coli BL21(DE3) cells transformed with pET30_TrxA_HRT2, before induction (NI) and 4 h after IPTG induction (I-4h). Protein solubility was assessed by analysing total (Tot), soluble (Sol), and insoluble (Pellet) fractions from bacteria grown at 25 °C and at 37°C.*

3.2.4 Co-expression of SRPP and HRT2 fusion proteins in *E. coli* at low temperature

To evaluate whether simultaneous expression of SRPP and HRT2 fusion proteins could improve their solubility, co-expression was performed in *E. coli* BL21(DE3) cells using the constructs pET32_SRPP and pET30_TrxA_HRT2. Given that expression at 25 °C had previously improved solubility when each protein was expressed individually, this temperature was selected for co-expression. Samples, obtained similarly to the above, were centrifuged, and the soluble and insoluble fraction was analyzed by SDS-PAGE followed by Coomassie blue staining and Western blot. As shown in Figure 16, both fusion proteins were successfully expressed; however, the majority of each remained predominantly in the insoluble fraction. Compared to individual expression systems, co-expression did not result in a noticeable enhancement in solubility, suggesting that the simultaneous production of both recombinant proteins may exceed the folding capacity of the bacterial host or may promote aggregation. These results indicate that co-expression at low temperature

alone is insufficient to improve solubility and may require further optimization, such as chaperone co-expression or other changes in induction strategy.

***Figure 16**: Co-expression of SRPP and HRT2 fusion proteins in E. coli at 25 °C: SDS-PAGE and Western blot analysis. Total protein extracts from E. coli BL21(DE3) cells co-transformed with pET32_SRPP and pET30_TrxA_HRT2 were collected before IPTG induction (NI) and 4 hours post-induction (I-4h). Protein fractions were separated into total (Tot), soluble (Sol), and insoluble (Pellet) components. The left panel shows Coomassie-stained SDS-PAGE gel, and the right panel shows Western blot detection of His-tagged proteins. Although both proteins were expressed, the majority accumulated in the insoluble fraction, indicating limited solubility under the tested conditions.*

3.2.5 Co-expression of SRPP and HRT2 in *E. coli* Arctic Express enhances protein solubility

To overcome the problem of low solubility in *E. coli* BL21(DE3), a genetically modified bacterial strain, *E. coli* Arctic Express, was employed to co-express HRT2 and SRPP from bicistronic expression vector pET30_SRPP_HRT2. Arctic Express was employed to enhance the solubility of target proteins by expressing cold-adapted chaperonins that facilitate protein folding at low temperatures. Cells were induced with IPTG and harvested at multiple time points (2 h, 5 h, 20 h, and 24 h post-induction). Protein expression and solubility of HRT2 and SRPP was analyzed by Coomassie blue staining and Western blot using anti-His and anti-V5 antibodies, respectively. Samples were fractionated into total, soluble, and insoluble fractions. As shown in Figure 17, both proteins were expressed over the entire course, with a consistent increase in band intensity between 5 h and 24 h. Importantly, Western blot analysis revealed a significant shift in protein distribution toward the soluble fraction compared to previous experiments using *E. coli* BL21(DE3). HRT2 (~34 kDa) and SRPP (~24 kDa) were clearly detectable in the soluble fraction, confirming that Arctic Express cells improve the solubility of both fusion-tagged proteins. These findings support the use of Arctic Express as a suitable expression host for enhancing the solubility of SRPP and HRT2, potentially increasing the probability of obtaining functionally active protein for downstream applications.

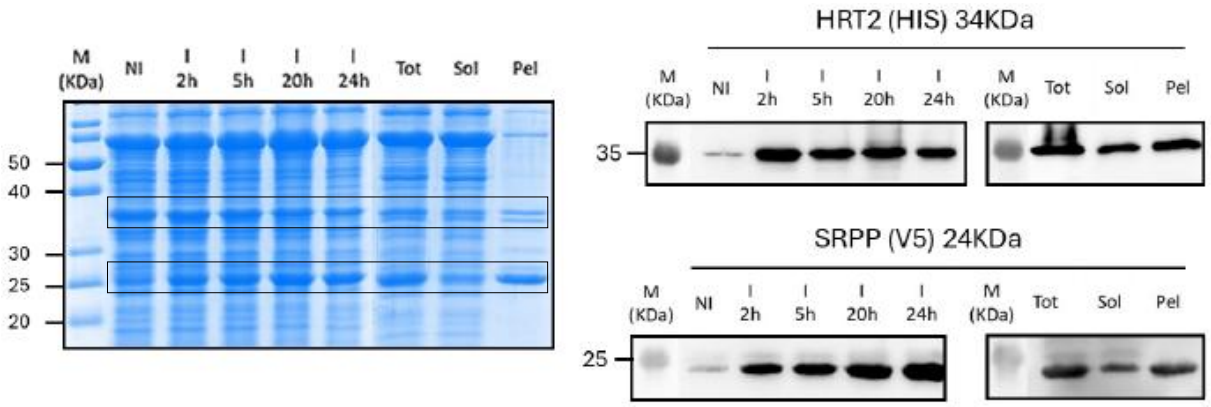

***Figure 17**: SDS-PAGE and Western blot analysis of SRPP and HRT2 co-expression in E. coli Arctic Express. E. coli Arctic Express cells were transformed with the pET30_SRPP_HRT2 construct and induced with IPTG. Samples were collected before induction (NI) and at multiple time points post-induction (2 h, 5 h, 20 h, and 24 h). Left panel: SDS-PAGE with Coomassie blue staining of total lysates. Right panels: Western blot analysis of HRT2 (top, anti-His) and SRPP (bottom, anti-V5) showing protein presence in total (Tot), soluble (Sol), and insoluble (Pel) fractions. Both proteins accumulate in the soluble fraction, indicating improved solubility in the Arctic Express strain.*

3.2.6 Preliminary characterization of the polymer extracted

Following the improved solubility and expression of SRPP and HRT2 proteins in *E. coli* Arctic Express, bacterial pellets were subjected to organic extraction to isolate any potentially synthesized polymeric material. The dried extracts were deposited on microscope slides (Figure 18C) and analyzed by infrared (IR) spectroscopy to investigate their chemical composition. Figure 17A presents the IR spectrum of the clean glass slide, which shows strong and characteristic absorbance in the 1200–600 cm^{-1} region, attributed to Si–O–Si stretching vibrations. These features overlap with potential polymeric signals, making this spectral region less informative for the interpretation of the deposited biological samples. IR spectra of five samples are shown in Figure 18B. Among these, only sample 3 displays clear and distinct spectral features. Notably, absorption bands above 3000 cm^{-1} are observed, which are consistent with C–H stretching vibrations typical of hydrocarbons, particularly those associated with cis-1,4-polyisoprene. Additionally, the region between 1600 and 1300 cm^{-1} shows bands compatible with C=C and C–C stretching modes of unsaturated carbon chains, supporting the hypothesis that the extract may contain isoprenoid-like material. In contrast, spectra from samples 2.1, 2.2 and 4 display prominent bands at 1618 cm^{-1} and 1520 cm^{-1}, corresponding to the Amide I and Amide II bands, respectively, which are indicative of protein contamination. These signals may obscure weaker polymeric signals and suggest incomplete separation of the expressed proteins during extraction. Due to the strong background absorbance from the glass and limited

sample quantity, definitive identification of polyisoprene was not achieved. Further analysis via nuclear magnetic resonance (NMR) spectroscopy would be required for conclusive structural characterization; however, the amount and solubility of the extracted material currently limit this approach.

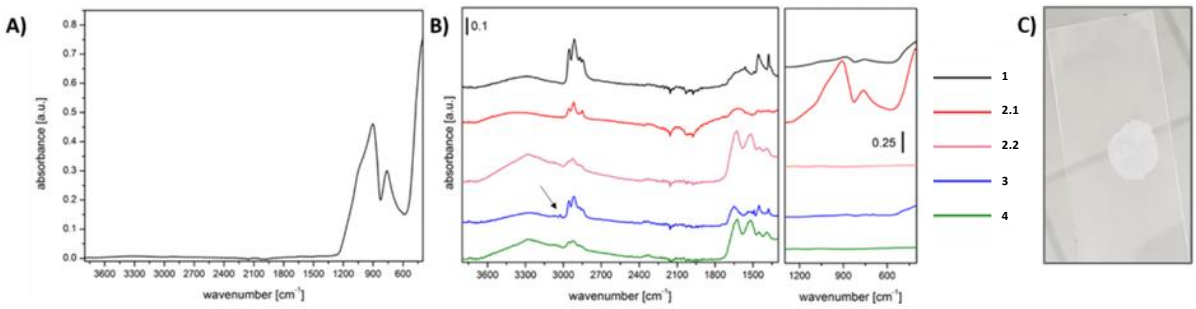

***Figure 18**: Preliminary IR analysis of bacterial extracts for the detection of polymeric material. (A) IR spectrum of the blank glass slide used for deposition, showing dominant Si–O–Si stretching features between 1200–600 cm⁻¹. (B) IR spectra of five extracted samples. Sample 2 was read twice at two different points on the slide. Sample 1: E. coli BL21(DE3) co-transformed with pET32_SRPP and pET30_TrxA_HRT2. Samples 2.1, 2.2 and 4: bacterial pellets from E. coli BL21(DE3) transformed with pET30_SRPP_HRT2 (grown at 37°C and 25°C respectively). Sample 3: E. coli Arctic Express expressing pET30_SRPP_HRT2 and exhibiting hydrocarbon-like IR bands suggestive of isoprenoid chains. Note the protein-related signals in samples 2 and 4 (Amide I and II). (C) Image of a dried extract deposited on a glass slide prior to IR analysis.*

DISCUSSION AND FUTURE PROSPECTIVE

The aim of this study is to develop a reliable electrospinning process for NR and to evaluate microbial biosynthesis of cis-1,4-polyisoprene as a sustainable alternative to electrospinning. Even though the results are encouraging, both approaches exhibit limitations, particularly in terms of scalability and technical feasibility.

The electrospinning phase of the study, carried out in collaboration with TissueGraft Srl, successfully produced nanofibrous scaffolds using NR blended with PVA, overcoming initial difficulties related to the incompatibility of the hydrophobic NR and hydrophilic PVA. Optimization strategies, including the addition of Triton X-100 as a surfactant and thermal crosslinking, proved essential for enhancing fiber homogeneity and structural integrity. Triton X-100 improved miscibility between polymer components by reducing bead formation and irregularities, while thermal treatment stabilized the scaffold, preventing disintegration during medium incubation. The biocompatibility of the thermally crosslinked NR/PVA scaffolds was validated by cell viability assays, which showed over 80% metabolic activity across almost all time points tested. Furthermore, direct cell adhesion experiments confirmed the material's suitability for biomedical applications such as tissue engineering and regenerative medicine by supporting cellular interactions. These results illustrate how the integration of scientific research and industrial know-how can drive the development of new solutions for regenerative medicine.

Looking forward, the demonstrated biocompatibility of these scaffolds paves the way for their functionalization with bioactive molecules, such as peptides, growth factors, or other molecules that promote tissue repair and regeneration. This can enhance their therapeutic use, particularly in chronic wound healing. Nevertheless, challenges remain, notably at high NR concentrations, where incompatibility causes disrupted fiber morphology. Its elasticity makes rubber an attractive candidate for biomaterials, particularly those requiring mechanical resilience and dynamic response. Understanding the mechanical properties of these scaffolds will be crucial to understanding their complete potential for biomedical use. Moreover, functionalization with bioactive molecules will be a promising approach to further enhance the therapeutic potential of the scaffold to offer an integrated solution to meet tissue engineering and regenerative medicine requirements.

In the second part of this work, we investigated the microbial biosynthesis of cis-1,4-polyisoprene, the principal component of NR, as a sustainable approach. Our

initial effort was directed to primarily engineer the solubility of the heterologously expressed *H. brasiliensis* proteins HRT2 and SRPP in *E. coli*, as poor solubility and aggregation as inclusion bodies are major challenges in the functional expression of exogenous proteins. While co-expression in Arctic Express strains significantly improved protein solubility thanks to the presence of cold-adapted chaperonins, these improvements did not translate into enhanced enzymatic activity. IR spectroscopy revealed hydrocarbon-like signals that might indicate polyisoprene, but the low amount and residual protein contamination limited definitive confirmation. Given the complexity of detection and the low yield, current literature exclusively reports the use of radioactive isotope techniques to assess IPP incorporation into the monomer and quantify the polymer length obtained. This method offers higher sensitivity, allowing more precise evaluation of the biosynthetic process (Krause et al., 2020). These results highlight the challenges associated with reconstructing this complex and not yet fully understood biosynthetic pathway in a heterologous host.

The complexity of biosynthetic machinery itself represents one of the fundamental limitations. There are several proteins involved in the synthesis of cis-1,4-polyisoprene in plants, which operate within specialized lipid-based structures called RPs. In the absence of these structures, bacteria cannot recreate the conditions necessary for effective biosynthesis. Moreover, while the two proteins expressed in this project (HRT2 and SRPP) are an integral part of the synthesis pathway, they are likely insufficient to replicate the full machinery. In the absence of the other proteins involved in the synthesis, probably the host cannot achieve the coordinated assembly and activity required for polymerization.

Another limitation concerns the incomplete understanding of the termination and regulation mechanisms of NR biosynthesis in plants. This gap in knowledge limits the enhancement of microbial host synthesis pathways. Further, eukaryotic organisms such as yeast may provide a suitable environment for establishing rubber biosynthetic complexes due to their intracellular organelles and lipid structures.

Despite these limitations, the research offers useful information on the limitations of microbial systems for polyisoprene production and identifies potential areas for future study. Metabolic engineering advances, the optimization of additional rubber biosynthetic proteins, or the generation of cell-free lipid scaffolds (Kuroiwa et al., 2022, 2024), could overcome some of the inherent constraints of bacterial systems.

In addition, the use of more sensitive analytical methods, like nuclear magnetic resonance (NMR) spectroscopy, can help in the characterization of polymer products if enough quantities of material are synthesized.

In conclusion, this study highlights the advantages and limitations of both electrospinning and microbial biosynthesis approaches for sustainable biomaterial development. The reproducibility and biocompatibility of electrospun NR/PVA scaffolds make them promising candidates for biomedical applications. Overall, these findings emphasize the importance of interdisciplinary collaboration to achieve the dual objectives of environmental sustainability and progress in biomaterial innovation.

APPENDIX

cells

MDPI

Article

Single-Nucleotide Polymorphisms of TAS2R46 Affect the Receptor Downstream Calcium Regulation in Histamine-Challenged Cells

Giulia Lecchi [1], Chiara Mocchetti [1], Davide Tunesi [1], Arianna Berto [1], Hari Baskar Balasubramanian [1], Sima Biswas [2], Angshuman Bagchi [2], Federica Pollastro [3], Luigia Grazia Fresu [1,*] and Maria Talmon [3,*]

[1] Department of Health Sciences, School of Medicine, University of Piemonte Orientale, Via Solaroli, 17, 28100 Novara, Italy
[2] Department of Biochemistry and Biophysics, University of Kalyani, Kalyani 741235, West Bengal, India
[3] Department of Pharmaceutical Sciences, University of Piemonte Orientale, Largo Donegani 2, 28100 Novara, Italy
* Correspondence: luigia.fresu@med.uniupo.it (L.G.F.); maria.talmon@med.uniupo.it (M.T.)

Abstract: Bitter taste receptors (TAS2Rs) expressed in extraoral tissues represent a whole-body sensory system, whose role and mechanisms could be of interest for the identification of new therapeutic targets. It is known that TAS2R46s in pre-contracted airway smooth muscle cells increase mitochondrial calcium uptake, leading to bronchodilation, and that several SNPs have been identified in its gene sequence. There are very few reports on the structure–function analysis of TAS2Rs. Thus, we delved into the subject by using mutagenesis and in silico studies. We generated a cellular model that expresses native TAS2R46 to evaluate the influence of the four most common SNPs on calcium fluxes following the activation of the receptor by its specific ligand absinthin. Then, docking studies were conducted to correlate the calcium flux results to the structural mutation. The analysed SNPs differently modulate the TAS2R46 signal cascade according to the altered protein domain. In particular, the SNP in the sixth transmembrane domain of the receptors did not modulate calcium homeostasis, while the SNPs in the sequence coding for the fourth transmembrane domain completely abolished the mitochondrial calcium uptake. In conclusion, these results indicate the fourth transmembrane domain of TAS2R46 is critical for the intrinsic receptor activity.

Keywords: bitter taste receptor; TAS2R; polymorphism; SNPs; calcium signalling

Citation: Lecchi, G.; Mocchetti, C.; Tunesi, D.; Berto, A.; Balasubramanian, H.B.; Biswas, S.; Bagchi, A.; Pollastro, F.; Fresu, L.G.; Talmon, M. Single-Nucleotide Polymorphisms of TAS2R46 Affect the Receptor Downstream Calcium Regulation in Histamine-Challenged Cells. *Cells* **2024**, *13*, 1204. https://doi.org/10.3390/cells13141204

Received: 8 May 2024
Revised: 2 July 2024
Accepted: 15 July 2024
Published: 16 July 2024

1. Introduction

Bitter taste receptors (TAS2Rs) are a family of G protein-coupled receptors which were first described in the oral cavity, exhibiting the ability to sense the bitter taste [1–3]. Afterwards, TAS2Rs were found to be distributed throughout the entire body, thus creating a whole-body sensory system [4]. However, the mechanisms behind their functionalities are not yet fully elucidated. Several studies have focused on TAS2Rs expressed in the respiratory systems as a putative alternative target for the treatment of asthma due to their well-established anti-inflammatory and bronchodilating activities [5–7]. Nevertheless, a stumbling block in the study of TAS2Rs is to precisely define their mechanism of action. It is established that the signalling cascade downstream of the bitter taste receptors can be divided into two steps. In all cell types the activation of TAS2Rs leads, first of all, to IP_3-dependent calcium release from the endoplasmic reticulum (ER), but then the fate of this cytosolic calcium differs depending on the bitter taste receptor subtype, the cellular localisation, the ligand, the characteristics of the cells constituting the contracted airway smooth muscle (ASM), and the bronchoconstrictor stimulus [5,6,8,9].

In recent years, we have focused on the identification of a specific inhibitor for bronchoconstriction, and can identify a highly specific agonist, absinthin, which is a sesquiterpene lactone molecule [10]. TAS2R46s are expressed at a lower level in comparison to the

other receptor subtypes from which they stand out due to their high sensitivity toward the bitter ligands [5], and this makes them relevant from a translational and pharmacological point of view. Indeed, absinthin is effective at micromolar concentrations, and the absinthin–TAS2R46 binding leads to anti-inflammatory action in bronchial epithelial cells [11] and to a modulation of the cytosolic calcium increased in ASM cells after histamine challenge [12]. In particular, absinthin acts through a striking calcium transient regulation, significantly reducing the cytosolic calcium rise induced by histamine while not reducing the ion flux through the plasma membrane [13] or decreasing Ca^{2+} efflux from the endoplasmic reticulum [13], but rather by increasing mitochondrial Ca^{2+} uptake [12].

From a structural point of view, TAS2Rs are characterised by seven transmembrane domains connected by three intracellular and three extracellular loops that are similar to class A GPCRs [14]. The binding with bitter ligands in the extracellular space and the intracellular signal transmission are critically influenced by the receptor core composed by the transmembrane domains [14,15]. Structure–function analysis identified the seventh transmembrane domain of TAS2R46 as responsible for the agonist selectivity [16]. For example, absinthin specifically binds to the receptor binding pocket through the allylic and homoallylic units that characterise its dimeric guaianolide structure [10], while, for the binding between TAS2R46s and strychnine, the involvement of both an orthosteric and an additional vestibular site have been demonstrated [17,18].

Since intracellular, extracellular, and transmembrane domains are pivotal in ligand binding and signal transmission, mutations in any amino acid of the total sequence of the receptor could affect both processes. TAS2R gene sequences are strongly characterised by the presence of polymorphisms as a result of a dynamic evolutionary adaptation to specific environments [4,19], and chimeric studies and genotypic–phenotypic association analysis showed that some of these polymorphisms alter bitter perception and the strength of the ligand binding [20]. Additionally, it has been identified that the SNPs in TAS2R38 sequences are responsible for the alterations of human taste perception, behavioural habits, and the incidence of some diseases [21,22] such as upper respiratory infection [23–25]. However, since few studies have been performed on the SNPs of the TAS2R46 gene [19,26,27], to deepen the knowledge of its structure and mechanism of action, we have selected four already-known SNPs in transmembrane domains (TM) four and six of the TAS2R46 sequence (Figure 1: TM6: rs2708381 (W250L); TM6: rs72477410 (I153V), rs72477411 (I147V), and rs200936852 (V141A); allele frequency > 0.1), and we have investigated their influence on absinthin binding and the consequent downstream receptor activity using both in silico and in vitro assays, respectively.

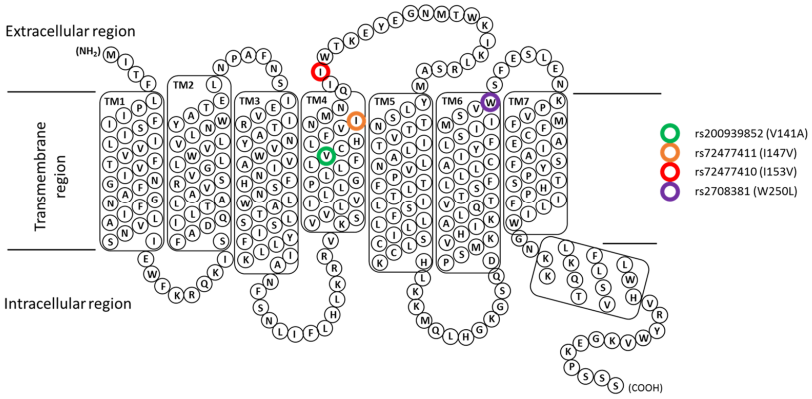

Figure 1. Schematic representation of the amino acid sequence of TAS2R46 with the SNPs considered in this study being highlighted. Snake plot representation of amino acid residues. TAS2R46 consists of a short N terminus (NH2), seven transmembrane domains (TM1-7), three extracellular loops, three intracellular loops, and a short C terminus (COOH). SNPs considered in the present study are marked by coloured circles: rs200939852 (V141A) in green; rs72477411 (I147L) in orange; rs72477410 (I153V) in red; rs2708381 (W250L) in purple.

2. Materials and Methods

2.1. Cell Culture

HeLa cells (ATCC; CCL-2) were maintained in Dulbecco's Modified Eagle Medium (DMEM, Sigma-Aldrich, Milan, Italy) supplemented with 10% heat-inactivated foetal bovine serum (FBS), 1% L-glutamine, and 1% antibiotic–antimycotic (all Thermo Fisher, Monza, Italy) at 37 °C under a 5% CO_2 humidified atmosphere.

2.2. In Vitro Mutagenesis and Generation of TAS2R46-Expressing HeLa Cells

The naïve sequence of the human TAS2R46 gene inserted in a pcDNA3.1-C-(k)DYK was purchased from GeneScript (Clone ID: OHu30358). The plasmid was already edited by in vitro site-directed mutagenesis to insert four selected SNPs of interest based on the allele frequency > 0.1: rs2708381, rs72477410, rs72477411, and rs200936852. The mutagenesis was carried out using the QuikChange Lightning Site-Directed Mutagenesis Kit (Agilent, Milano, Italy) following the manufacturer's instructions. The mutagenic primers (listed in Table 1) were designed using the web-based QuikChange Primer Design Program (www.agilent.com/genomics/qcpd; accessed on 22 June 2021). The amplification product was checked by Sanger LIGHTrun sequencing from Microsynth AG (Balgach, Switzerland). To generate the cellular models expressing the mutated receptors, 1.2×10^6 HeLa cells were plated in a 10 cm diameter Petri dish and transiently transfected using Lipofectamine 2000 (Invitrogen, Waltham, MA, USA), using 24 µg of each plasmid and 10 µL of Lipofectamine reagent for each dish.

Table 1. Primers for mutagenesis reactions.

Primer Name	Sequence	Tm (°C)
rs2708381 fw	5′-TTTTCCAGACTCTCAAAACTCWAAACTGACATGATTATGGACAG-3′	78.8
rs2708381 rev	5′-CTGTCCATAATCATGTCAGTTTWGAGTTTTGAGAGTCTGGAAAA-3′	78.8
rs72477410 fw	5′-TTCATATTCTTTTGTCCATACAATCTGATTCATGTTTATCACAAAAAGATGACAAACC-3′	79.5
rs72477410 rev	5′-GGTTTGTCATCTTTTTGTGATAAACATGAATCAGATTGTATGGACAAAAGAATATGAA-3′	79.5
rs72477411 fw	5′-TTGTCCATATAATCTGATTCATGTTTACCACAAAAAGATGACAAACCAAAAATAG-3′	78.6
rs72477411 rev	5′-CTATTTTTGGTTTGTCATCTTTTTGTGGTAAACATGAATCAGATTATATGGACAA-3′	78.6
rs200936852 fw	5′-TGTTTATCACAAAAAGATGACAAGCCAAAAATAGCAAAGGCCCCAA-3′	78.9
rs200936852 rev	5′-TTGGGGCCTTTGCTATTTTTGGCTTGTCATCTTTTTGTGATAAACA-3′	78.9

2.3. Calcium Imaging

HeLa cells were plated on a pre-coated glass coverslip with 0.1% polilysine. Cytosolic Ca^{2+} fluctuations were evaluated as previously described [12]. Briefly, cells were loaded with 5 µM Fura-2 AM in the presence of 0.02% Pluronic-127 and 10 µM sulfinpyrazone in Krebs–Ringer buffer (KRB) containing 2 mM CaCl2 (30 min, RT); then, they were incubated (20 min, RT) with KRB to allow for the de-esterification of the probe. For the measurements of the mitochondrial Ca^{2+}, the cells were loaded with Rhod-2AM in the presence of 0.2% Pluronic-127 in KRB containing 2 mM $CaCl_2$ (30 min, RT), and then they were incubated with KRB for 1 h to allow for the de-esterification. The basal calcium was monitored for about 50 s, and then the cells were challenged with the following stimuli, alone or combined: acetylcholine (100 µM; Sigma-Aldrich), absinthin (1, 10, and 100 µM; kindly provided by Dr. Pollastro), forskolin (10 µM; Sigma-Aldrich), and 8-pCPT-2′-O-Me-cAMP (10 µM; Sigma-Aldrich). The coverslips were mounted into an acquisition chamber and placed on the stage of a Leica DMI6000 epifluorescent microscope equipped with an S Fluor ×40/1.3 objective. Fura-2 AM was excited by alternating 340 nm and 380 nm using a Polychrome IV monochromator (Till Photonics, Gräfelfing, Germany), and the probe emission light was filtered through a 520/20 bandpass filter and collected by a cooled CCD camera (Hamamatsu, Japan). Rhod-2AM was excited at 552 nm and the

fluorescence emission was recorded at 580 nm. The fluorescence signals were acquired and processed using MetaFluor software 7.8 (Molecular Devices, San Jose, CA, USA). To quantify the differences in the amplitudes of the Ca^{2+} transients, the Fura-2AM and Rhod-2AM fluorescences were expressed relative to the fluorescence intensity at the stimulation time (ΔF/F0).

2.4. Model Building and Validations of Wild-Type and Mutant TAS2R46 Models

The Cryo_EM structures of the TAS2R46, represented by the codes 7XP4, 7XP5, and 7XP6 [18], are available in the Protein Data Bank (PDB) (https://www.rcsb.org/; accessed on 25 April 2024).

The details of the structures are as follows:

7XP4: TAS2R46 in apo state;
7XP5: TAS2R46 in ligand-free state;
7XP6: TAS2R46 in active state.

The 7XP6 had some missing residues; therefore, to perform the docking simulations, we filled in these missing residues and generated the final structure of the protein. The amino acid sequence of the protein was retrieved from UniProtKB (www.uniprot.org/; accessed on 25 April 2024), bearing the accession number P59540. The modelled structure of the protein, generated after incorporations of the missing residues, was subjected to energy minimisation in the Discovery Studio 2.5 (D.S 2.5) platform to remove any unwanted steric clashes following the smart minimisation protocol, which is a combination of the Steepest Descent and Conjugate Gradient approaches. The process of minimisation continued until the RMS gradient of the energy derivative reached the value of 0.01 kcal/mole. We then checked the amino acid dispositions in the model by using the SAVES6.0 server (https://saves.mbi.ucla.edu/; accessed on 26 April 2024).

Furthermore, we performed a second round of docking simulations with the 7XP6 without inserting the missing residues. In order to do so, we kept the coordinates of the atoms of the amino acid residues of the TAS2R46 protein only in the 7XP6, and we checked its stereochemical profiles with the help of Ramachandran plots [28]. We then used the Modloop server [29] to correct the loop segments of the protein, and the final structure was built after performing energy minimisation, following the same protocol as previously de-scribed. The mutant structures were built using the 'Build Mutant' protocol in D.S 2.5 and refined as per the same protocol mentioned before.

2.5. Molecular Docking Simulations

To understand the mode of binding interactions between the TAS2R46 (both the wild-type and mutant receptors) and the ligand absinthin, we used molecular docking simulations with the help of Autodock 4.2 [30]. The structure of the absinthin was retrieved from the PubChem database (https://pubchem.ncbi.nlm.nih.gov/; accessed on 25 April 2024), bearing the PubChem CID: 442138. Additionally, as a control run, we docked TAS2R46 with strychnine, bearing the PubChem CID: 441071. The chosen ligands were subjected to processing to make them suitable for the docking studies with the help of D.S 2.5. We used the flexible docking approach to carry out the molecular docking simulations. It was observed by Sandal et al. [17] and Xu et al. [18] that, along with the orthosteric agonist binding site, another extracellular binding site called the "vestibular" site is also present in the TAS2R46 receptor [17,18]. We then performed the directed docking simulation studies twice, one each for the wild-type and mutants, respectively, creating a box around the binding sites, as mentioned by the authors. The Lamarckian Genetic Algorithm (LGA) was used to perform the docking simulations. Based on the Autodock 4.2 scoring function, the best docking conformations of the protein–ligand complexes with the corresponding lowest binding free energy values were selected. Further interactions of the protein–ligand complexes were analysed by D.S 2.5 and ligplot (https://www.ebi.ac.uk/thornton-srv/software/LigPlus/; accessed on 28 April 2024). The same docking simulation approach was performed for the mutants as well.

2.6. Statistical Analysis

For the calcium imaging experiments, statistical analysis was performed by a parametric *t* test/one-way ANOVA or, otherwise, nonparametric alternatives were appropriately used, as reported in the figure captions. Data are presented as mean ± SEM of *n* cells in *n* independent experiments, as detailed in the figure legends. A p value < 0.05 was considered statistically significant.

3. Results

3.1. TAS2R46-HeLa Cells Efficiently Recapitulated the Calcium Movements Downstream of Receptor Activation

As previously demonstrated in the ASM cells, the binding between absinthin and TAS2R46 mediates the bronchodilation of histamine-challenged cells, driving the calcium shift from the ER to the mitochondria [12]. To ascertain the functional consequence on the receptor activity of the four mutations, wild-type hTAS2R46 and mutant receptors were expressed in HeLa cells, and mitochondrial and cytosolic calcium variations were quantitated in real time for about 50 s after the exposure of the cells to histamine and/or absinthin. First of all, we confirmed by immunofluorescence the goodness of the transfection (Figure S1); then, with a functional assay, we validated the TAS2R46-expressing HeLa cells as a good model to recap the downstream calcium modulation. Indeed, the non-transfected cells had no detectable calcium response either after treatment with absinthin alone or after co-treatment with histamine (Figure S2), while the wild-type TAS2R46-expressing cells showed a rapid increase in the cytosolic calcium concentration upon histamine challenge, which was promptly reversed by absinthin (Figure 2A), with a parallel significant increase in the mitochondrial calcium uptake (Figure 2B).

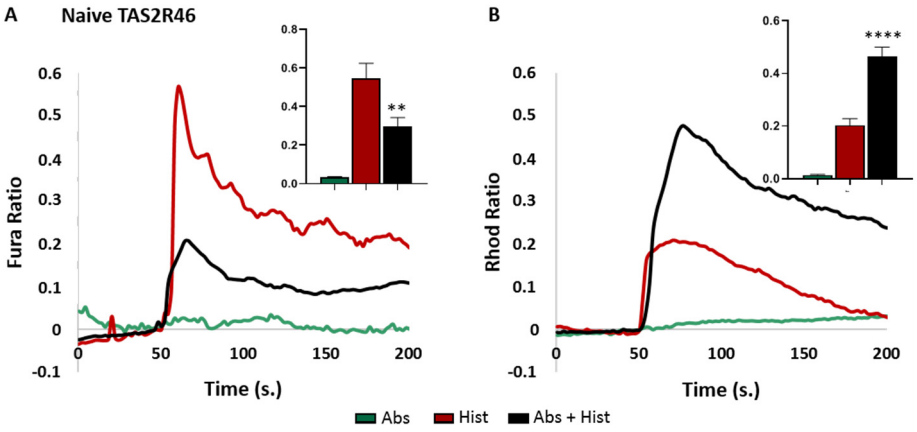

Figure 2. Cytosolic and mitochondrial Ca^{2+} analysis in HeLa cells expressing naive TAS2R46. Fura-2AM- and Rhod-2AM-loaded cells were stimulated with 10 µM of histamine (Hist) and 10 µM of absinthin (Abs) alone or combined. All data are illustrated as representative traces as well as histograms of the maximum peak (inset). (**A**) Cytosolic calcium transient in TAS2R46-expressing HeLa cells. Abs n = 33, Hist n = 31, and Abs+Hist n = 55 cells of 3 independent experiments. (**B**) Mitochondrial calcium analysis in TAS2R46-expressing HeLa cells. Abs n = 30 and Hist n = 59 cells of 3 independent experiments; Abs+Hist n = 134 cells of 4 independent experiments. Statistical analysis: Mann–Whitney U test; ** $p < 0.01$ and **** $p < 0.0001$ vs. Hist.

3.2. Effects of the Polymorphism on Downstream Signalling

As previously described in Figure 1, the amino acid mutations induced by each SNP are as follows: the rs2708381 polymorphism determines the mutation of the Trp250 into a Leu (W250L) or introduces a Stop codon in the sixth transmembrane domain, while the rs72477410, rs72477411, and rs200936852 polymorphisms lead to mis-sense variants in I153V, I147V, and V141A, respectively, in the fourth transmembrane domain. We therefore compared the signal transduction in native-receptor-expressing cells and those expressing

the SNPs to understand the impact a mutation may have on the ligand binding or activation of the downstream signalling pathway.

As shown in Figure 3, the response to the histamine/absinthin co-treatment of the W250L mis-sense variant in TM6 was superimposable to that of the wild-type.

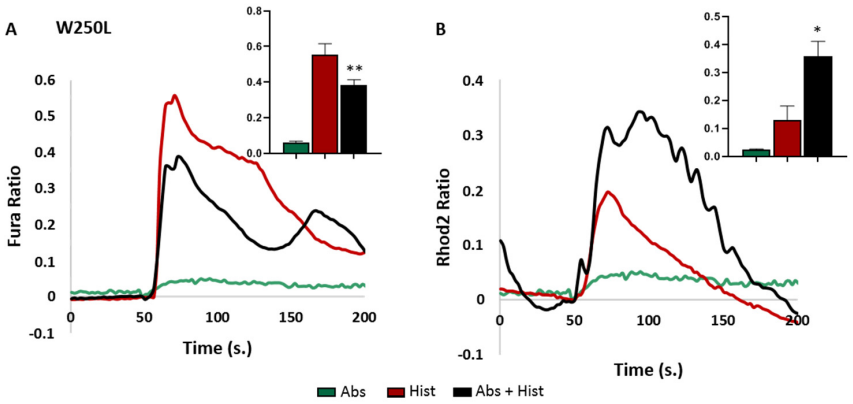

Figure 3. Cytosolic and mitochondrial Ca^{2+} analysis in HeLa cells expressing W250L-TAS2R46. Fura-2AM- and Rhod-2AM-loaded cells were stimulated with 10 µM of histamine (Hist) and 10 µM of absinthin (Abs) alone or combined. All data are illustrated as representative traces as well as histograms of the maximum peak (inset). (**A**) Cytosolic calcium transient in rs2708381 TAS2R46-expressing HeLa cells. Abs $n = 28$, Hist $n = 51$, and Abs+Hist $n = 73$ cells of 3 independent experiments. (**B**) Mitochondrial calcium analysis in rs2708381 TAS2R46-expressing HeLa cells. Abs $n = 24$, Hist $n = 26$, and Abs+Hist $n = 26$ cells of 3 independent experiments. Statistical analysis: Mann–Whitney U test; * $p < 0.05$ and ** $p < 0.01$ vs. Hist.

In contrast, mis-sense variants in I153V, I147V, and V141A in TM4 affected the receptor activity, with different consequences depending on the mutation site (Figure 4). Unexpectedly, we observed that, in I153V-HeLa cells, absinthin alone did not alter the basal cytosolic calcium level, while it did induce an increase in mitochondrial calcium (Figure 4A,B). Conversely, the other variants induced cytosolic calcium peaks (Figure 4C–F). Moreover, several of the SNPs also differentially affected the modulation of histamine calcium release. In fact, in I153V-HeLa cells, co-stimulation with absinthin and histamine significantly increased, rather than decreased, the calcium levels in the cytosol (Figure 4A), while no changes were recorded in the mitochondria compared with the stimulation of histamine alone (Figure 4B). In I147V-HeLa cells, absinthin was not able to revert the histamine-induced Ca^{2+} transient (Figure 4C), but the calcium uptake in the mitochondria was significantly lower in the cells stimulated with absinthin and histamine compared to histamine alone (Figure 4D). Finally, in the V141A-HeLa cells, absinthin synergised with histamine (Figure 4E), with no consequent effect recorded in the mitochondria (Figure 4F).

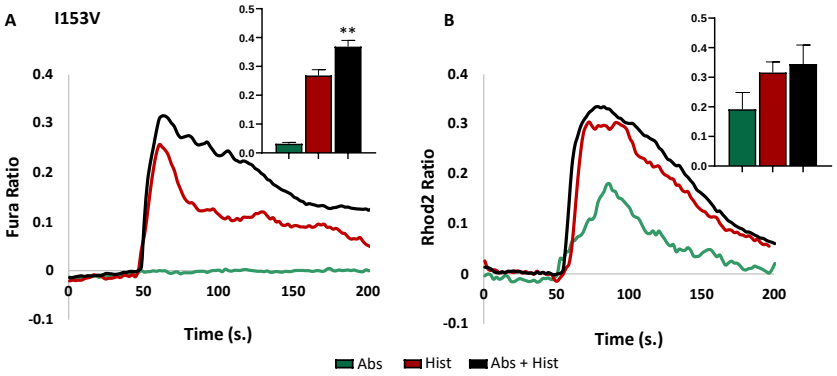

Figure 4. *Cont.*

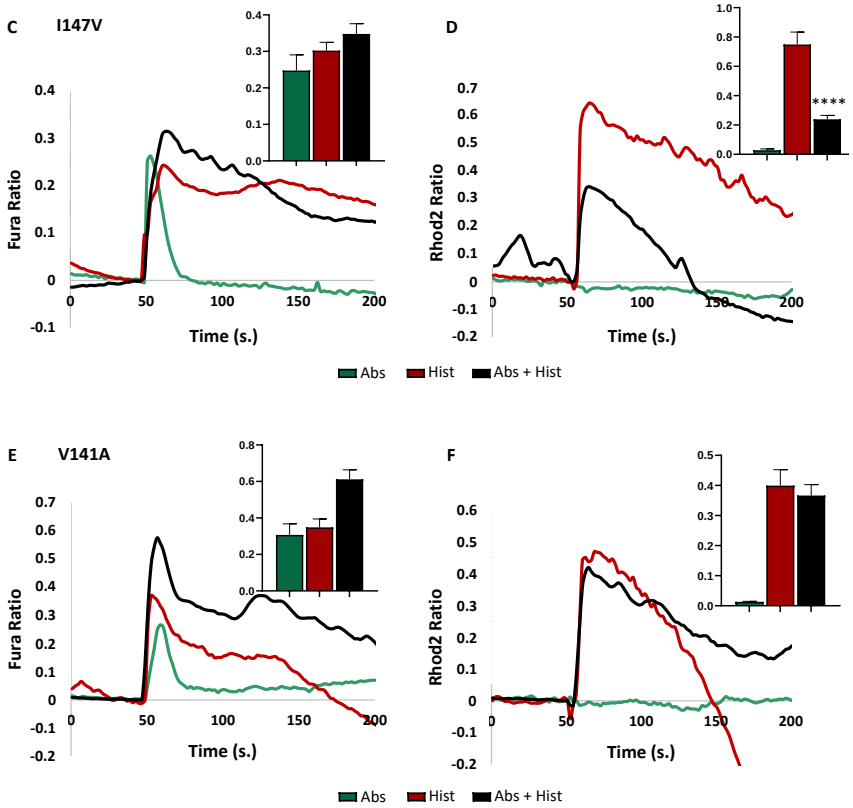

Figure 4. Cytosolic and mitochondrial Ca^{2+} analysis HeLa cells expressing I153V-, I147V-, and V141A-TAS2R46. Fura-2AM- and Rhod-2AM-loaded cells were stimulated with 10 μM of histamine (Hist) and 10 μM of absinthin (Abs) alone or combined. All data are illustrated as representative traces as well as histograms of the maximum peak (inset). (**A**) Cytosolic calcium transient in I153V-HeLa cells. Abs n = 47 cells of 3 independent experiments; Hist n = 81 and Abs+Hist n = 114 cells of 4 independent experiments. (**B**) Mitochondrial calcium analysis in I153V-HeLa cells. Abs n = 18, Hist n = 41, and Abs+Hist n = 29 cells of 3 independent experiments. (**C**) Cytosolic calcium transient in I147V-HeLa cells. Abs n = 46, Hist n = 38, and Abs+Hist n = 57 cells of 3 independent experiments. (**D**) Mitochondrial calcium analysis in I147V-HeLa cells. Abs n = 27, Hist n = 31, and Abs+Hist n = 48 cells of 3 independent experiments. (**E**) Cytosolic calcium transient in V141A-HeLa cells. Abs n = 38, Hist n = 36, and Abs+Hist n = 55 cells of 3 independent experiments. (**F**) Mitochondrial calcium analysis in V141A-HeLa cells. Abs n = 40, Hist n = 46, Abs+Hist n = 39 cells of 3 independent experiments. Statistical analysis: Mann–Whitney U test; ** $p < 0.01$ and **** $p < 0.0001$ vs. Hist.

3.3. EPAC Activation Rescued the Absinthin Effect Downstream of Mutated Receptors

The Exchange Protein Directly Activated by cAMP (EPAC) localises into the mitochondrial inner membrane and may control the mitochondrial calcium uniport (MCU) [31,32]. We have previously demonstrated that absinthin induces calcium shuttling into the mitochondria by activating the EPAC [12]. In naive HeLa cells, absinthin was ineffective against histamine-induced calcium rise, confirming that the effect on calcium modulation is TAS2R46-dependent (Figure S3) and, as previously demonstrated [12,33], the co-stimulation of histamine and forskolin (an adenylate cyclase activator) or the 8-pCPT-2-O-Me-cAMP (a selective EPAC activator) decreased the cytosolic calcium release (Figure S3). Then, in order to evaluate the interference of amino acid mutations in the fourth transmembrane (I153V, I147V, and V141A) domain on the cAMP-mediated signalling triggered by absinthin, we challenged transfected cells with forskolin and 8-pCPT-2-O-Me-cAMP (Figure 5). In line with Figure 4, we observed that absinthin was unable to counteract the histamine-induced cytosolic calcium release in transfected cells with the three variants (Figure 5A–C, right graphs). On the contrary, the addition of 8-pCPT-2-O-Me-cAMP, along with histamine and absinthin, caused a decrease in the cytosolic calcium peak and increased the mitochondrial

calcium (Figure 5), while the co-stimulation with forskolin showed an effect only in the I147V-HeLa cells, suggesting that the calcium modulation was mainly mediated by the EPAC. These data therefore corroborate the hypothesis that these mutations interfered with the trigger of the cAMP-EPAC signalling cascade induced by the binding of absinthin to TAS2R46.

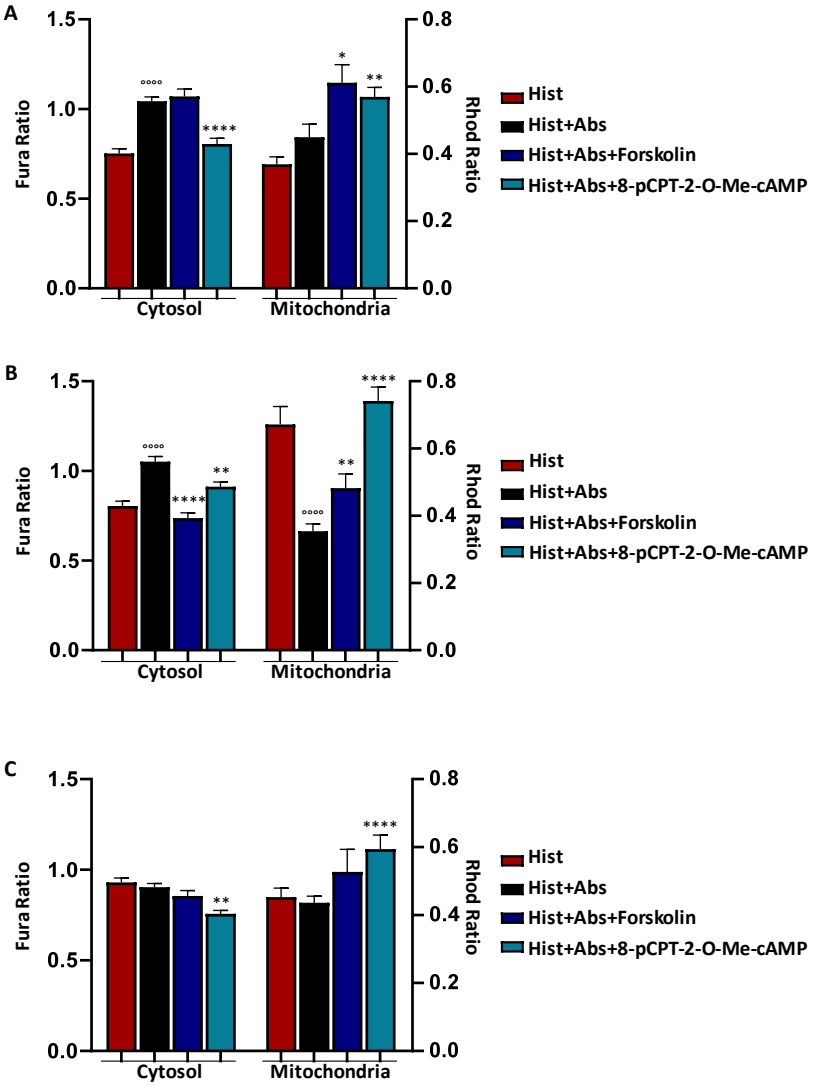

Figure 5. EPAC activation in HeLa cells expressing I153V-, I147V-, and V141A-TAS2R46. Fura-2AM- and Rhod-2AM-loaded cells were stimulated with 10 µM of histamine (Hist), 10 µM of absinthin (Abs), 10 µM of forskolin, and 10 µM of 8-pCPT-2-O-Me-cAMP. All data are illustrated as histograms showing the mean ± SEM of the maximum peak. (**A**) Cytosolic (Hist n = 219 cells; Hist+Abs n = 250; Hist+Abs+Forsk n = 175; Hist+Abs+8-pCPT-2-O-Me-cAMP n = 145) and mitochondrial (Hist n = 110 cells; Hist+Abs n = 109; Hist+Abs+Forsk n = 102; Hist+Abs+8-pCPT-2-O-Me-cAMP n = 133) calcium transient in I153V-HeLa cells. (**B**) Cytosolic (Hist n = 271 cells; Hist+Abs n = 219; Hist+Abs+Forsk n = 154; Hist+Abs+8-pCPT-2-O-Me-cAMP n = 254) and mitochondrial (Hist n = 71 cells; Hist+Abs n = 123; Hist+Abs+Forsk n = 59; Hist+Abs+8-pCPT-2-O-Me-cAMP n = 45) calcium transient in I147V-HeLa cells. (**C**) Cytosolic (Hist n = 336 cells; Hist+Abs n = 328; Hist+Abs+Forsk n = 281; Hist+Abs+8-pCPT-2-O-Me-cAMP n = 323) and mitochondrial (Hist n = 246 cells; Hist+Abs n = 204; Hist+Abs+Forsk n = 90; Hist+Abs+8-pCPT-2-O-Me-cAMP n = 205) calcium transient in V141A-HeLa cells. Statistical analysis: Mann–Whitney U test; °°°° $p < 0.0001$ vs. Hist; * $p < 0.05$, ** $p < 0.01$, and **** $p < 0.0001$ vs. Hist+Abs.

3.4. Structural Analysis

To understand whether the impairment of the downstream signal transduction was due to an alteration in the binding strength induced by the mutations, we performed two rounds of docking simulations. In the first round, we used the modelled structure of the TAS2R46 obtained after the insertions of the missing amino acid residues in the 7XP6. We made a structural comparison between the model and the 7XP6, and the RMSD of the backbone atoms was found to be 0.781Å (Figure 6). This would indicate that the model and the 7XP6 had similar structural organisations.

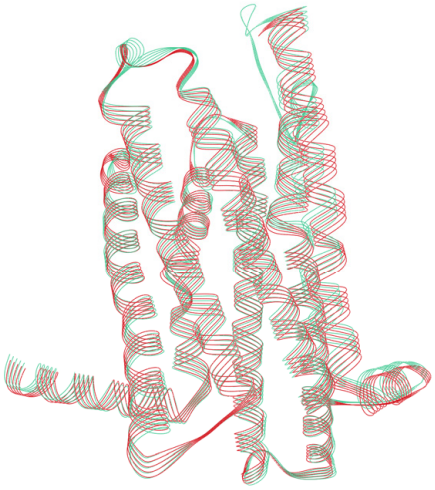

Figure 6. Structural comparison of the TAS2R46 model structure with 7XP6. The rust-red colour denotes the 7XP6 structure (Cryo_EM) and the sap-green colour denotes the modelled structure of TAS2R46.

We proceeded with a computational analysis based on the flexible docking simulations of absinthin with the wild-type (WT) and mutant TAS2R46 proteins both to the orthosteric (Figure 7) and vestibular sites (Figure 8), and compared the results with the binding interaction profile between strychnine and the WT receptor. We selected the best binding poses (Figures 7 and 8) with the lowest binding free energy values as obtained from Autodock 4.2.

As shown in Table 2, at the orthosteric site, the binding free energy values of absinthin with the wild-type (−10.91 kcal/mol) and the two mutant (W250L and I147V) structures of TAS2R46 (model) are similar. The energy values are slightly higher in the mutants I153V and V141A. Moreover, the binding interaction profiles are also different in the cases of these two mutants.

On the other hand, the binding free energy value of wild-type TAS2R46 (model) with strychnine is −8.68 kcal/mol. Thereafter, we went on to check the binding free energy value obtained after the docking of strychnine directly with the 7XP6, where the process of the insertions of the missing residues were not performed, and it was found to be −9.63 kcal/mol. In these two cases, similar patterns of binding interaction profiles between strychnine and TAS2R46 were also observed.

Interestingly, the patterns of the bindings in all of the complexes were somewhat similar, and the wild-type and mutant receptors shared a similar amino acid distribution in their zones of binding for the ligand absinthin. (Figure 7). However, in some cases their modes of bond formations were different. Similar trends in binding interactions were observed in both types of the aforementioned docking simulations.

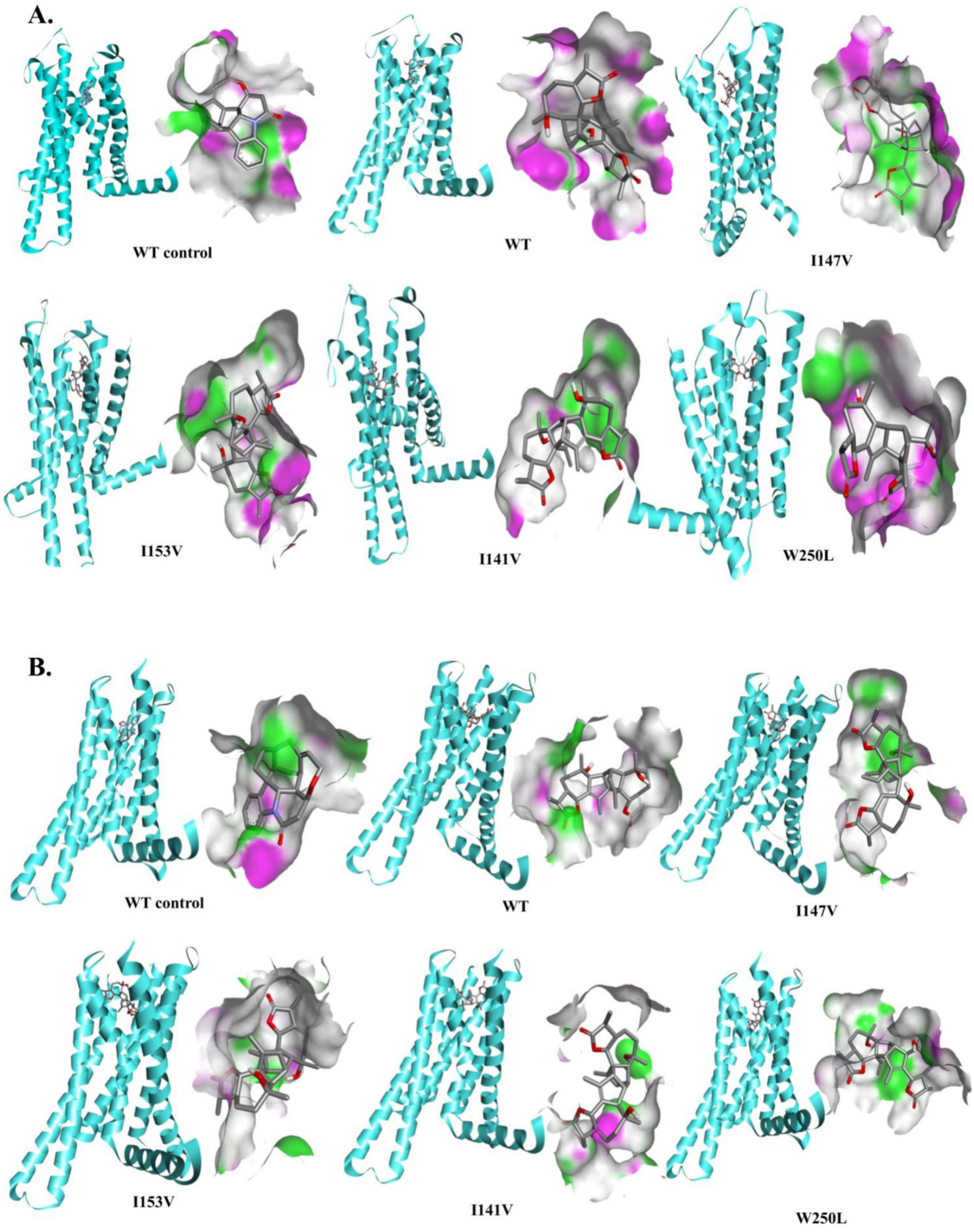

Figure 7. Structural analysis—Orthosteric site. (**A**) Modelled TAS2R46; (**B**) 7XP6: TAS2R46. WT control: structural analysis between the WT receptor and strychnine; WT, I147V, I153V, I141V, and W250L: structural analysis between TAS2R46 and absinthin. The binding interactions between the wild type and the mutant TAS2R46 proteins are presented as follows: the receptor is presented by secondary type while the ligand is shown in ball & stick. The interacting residues are presented in cloud form and depicted side-by-side.

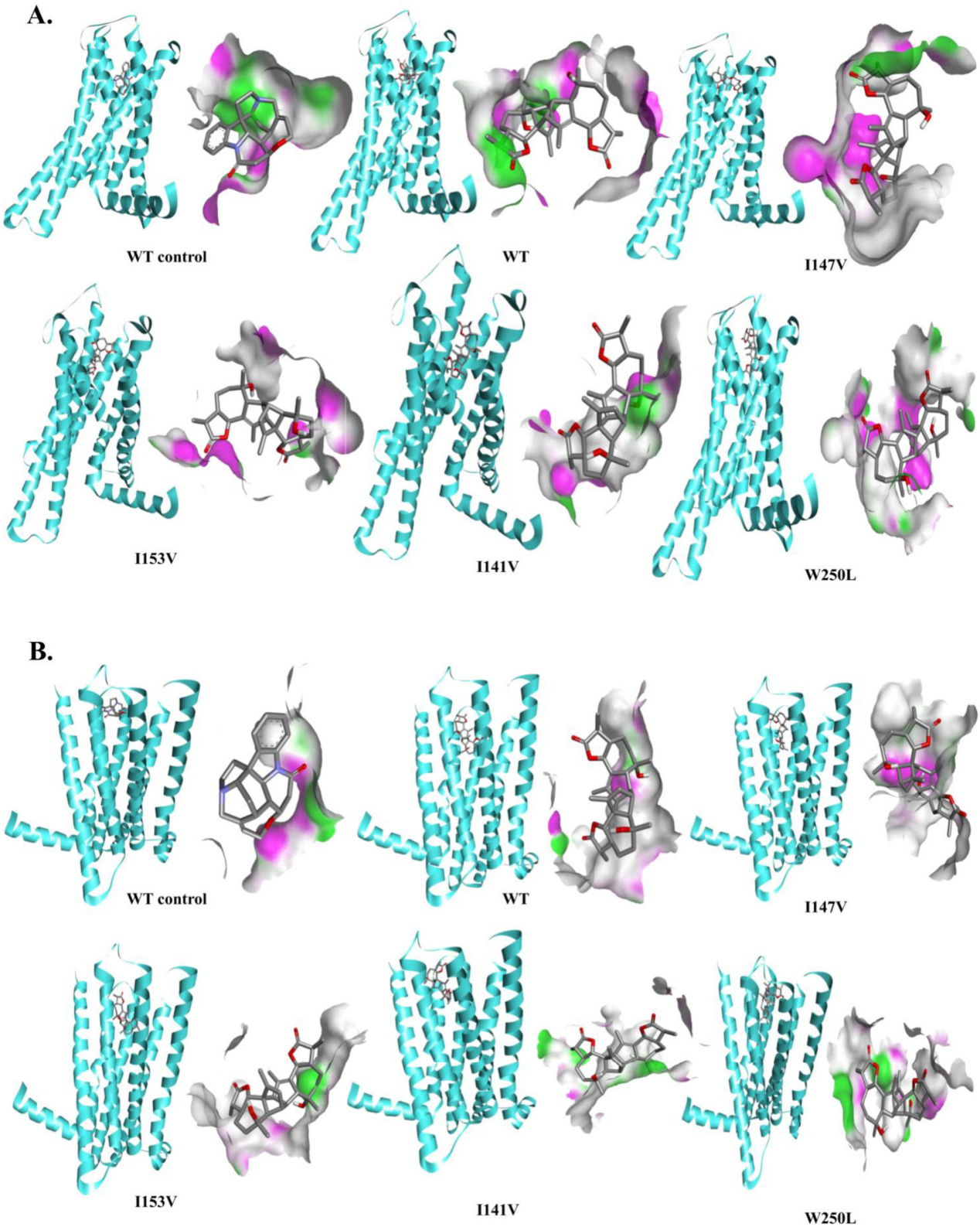

Figure 8. Structural analysis—Vestibular site. (**A**) Modelled TAS2R46; (**B**) 7XP6: TAS2R46. WT control: structural analysis between the WT receptor and strychnine; WT, I147V, I153V, I141V, and W250L: structural analysis between TAS2R46 and absinthin. The binding interactions between the wild type and the mutant TAS2R46 proteins are presented as follows: the receptor is presented by secondary type while the ligand is shown in ball & stick. The interacting residues are presented in cloud form and depicted side-by-side.

Table 2. Autodock binding free energy values of wild-type and mutant TAS2R46 proteins (model and 7XP6) based on their bindings onto the orthosteric site. Model: Modelled structure of TAS2R46 obtained after insertions of the missing residues in 7XP6.

Orthosteric Site		
Name of the Protein–Ligand Complex	**Binding Free Energy (kcal/mol)**	**Inhibition Constant (μM)**
Model_WT_strychnine	−8.68	0.43
Model_WT_absinthin	−10.91	0.01
Model_I147V_absinthin	−11.77	0.002
Model_I153V_absinthin	−12.59	0.0005
Model_V141A_absinthin	−12.54	0.0006
Model_W250L_absinthin	−11.01	0.008
7XP6_WT_strychnine	−9.63	0.087
7XP6_WT_absinthin	−12.10	0.001
7XP6_I147V_absinthin	−12.18	0.001
7XP6_I153V_absinthin	−11.40	0.004
7XP6_V141A_absinthin	−12.01	0.001
7XP6_W250L_absinthin	−10.77	0.012

Furthermore, we explored the binding interactions of absinthin to the vestibular binding site (Table 3). In this case, we found that the binding free energy values of the wild-type and mutant TAS2R46 proteins (model) were also similar, and that the mutant I147V showed a lower affinity than the wild-type protein. However, the binding affinity of strychnine was higher towards the orthosteric site (Figures S4 and S5). Surprisingly, when we docked strychnine in the vestibular site, the binding affinity was significantly lower than that of absinthin. Furthermore, strychnine interacted with different sets of amino acid residues (Figures S6 and S7). A possible reason behind this is the different chemical structure between the absinthin and strychnine, which therefore might lead the ligands to bind in different ways. Similar results were observed by performing both of the aforementioned docking simulations.

Table 3. Autodock binding free energy values of wild-type and mutant TAS2R46 proteins (model and 7XP6) based on their bindings onto the vestibular site. Model: Modelled structure of TAS2R46 obtained after insertions of the missing residues in 7XP6.

Vestibular Site		
Name of the Protein–Ligand Complex	**Binding Free Energy (kcal/mol)**	**Inhibition Constant (μM)**
7XP6_WT_strychnine	−5.21	152.25
7XP6_WT_absinthin	−8.16	1.04
7XP6_I147V_absinthin	−7.58	2.80
7XP6_I153V_absinthin	−9.82	0.63
7XP6_V141A_absinthin	−8.10	1.15
7XP6_W250L_absinthin	−8.35	0.76
Model_WT_strychnine	−8.01	1.34
Model_WT_absinthin	−9.60	0.09

Table 3. *Cont.*

Vestibular Site		
Name of the Protein–Ligand Complex	**Binding Free Energy (kcal/mol)**	**Inhibition Constant (μM)**
Model_I147V_absinthin	−7.26	4.77
Model_I153V_absinthin	−9.59	0.092
Model_V141A_absinthin	−8.12	1.12
Model_W250L_absinthin	−7.83	1.83

4. Discussion

The present report suggests the involvements of the fourth transmembrane domain (TM4) of TAS2R46 as the fundamental unit for the receptor activation by its ligand absinthin. A deeper understanding of the biology of the bitter taste receptor is a great challenge and is currently reliant on in silico and in vitro functional analyses. In fact, the TAS2Rs show a very low sequence and structural similarity with other GPCRs [14,34], which is why the TAS2Rs have been considered to belong to a distinct family [35] or have been grouped with frizzled receptors [36], but most of the studies classify them with the rhodopsin-like receptors (Class A GPCRs) [37–39]. TAS2R46, one of the 25 subtypes belonging to the bitter receptor family, has been studied by cryo-electron microscopy [18], computational analysis, and mutagenesis [16,17], which could help in deciphering its structure and biological response to ligands. However, most studies concern the binding between strychnine (a non-selective agonist for TAS2R and an antagonist of the glycine receptor) and TAS2R46, demonstrating that this receptor subtype is characterised by a particular structural rearrangement of TM3, TM4, and TM5 that leads to the formation of a pocket near the bilayer [18]. Furthermore, Sandal and colleagues identified a vestibular site involved in strychnine binding in addition to the classical orthosteric one [17]. Moreover, it is well reported that the domains critical to the receptor binding and activity vary depending on the bitter ligand [40].

In the present work, we investigated the behavioural binding of absinthin, a selective agonist for the bitter taste receptors of TAS2R46 [41], for which no affinity towards other receptors has been reported and whose ability to hamper calcium increase when triggered by a contraction stimulus (e.g., histamine) is well demonstrated [12]. We therefore focused on the binding interactions between TAS2R46 and absinthin by in silico and in vitro approaches, analysing the four most represented SNPs in the European population, to evaluate any changes in the signal transduction resulting from impaired ligand binding due to the mutations. Indeed, since the TAS2Rs share a high sequence homology among themselves, but show different affinities toward several ligands, a single amino acid substitution could determine a significant change in the receptor behaviour. As shown by our results, although the TM6 and TM7 have been previously demonstrated to be crucial for the ligand selectivity [16], the polymorphism affecting the 250th amino acid residue in TM6 did not alter the calcium modulation in histamine-challenged cells, demonstrating that, probably, this mutation could just reduce the affinity towards absinthin without interfering with the receptor activity. The docking study strengthened our observation, since the binding free energy values of wild-type TAS2R46 and the mutants affecting both TM6 and TM4 do not vary significantly, suggesting that the mutations do not induce drastic changes in the physico-chemical characteristics of the concerned amino acid residues involved in binding absinthin.

Interestingly, the in silico analysis demonstrated that absinthin binds with both the orthosteric and vestibular sites of the wild-type TAS2R46 with almost the same binding affinity, but the mutation I153V in the TM4 negatively affected the TAS2R46–absinthin interactions as compared to the wild-type. This might be due to the differences in the patterns of bond formations in both the orthosteric and vestibular sites of TAS246R in the case of the aforementioned mutant. The apparent consequence of this altered binding is an

altered intrinsic activity of absinthin manifested by the different modulation of calcium homeostasis. Moreover, in the mutant I147V, no significance changes were observed in both of the binding sites, but the mode of the bindings may have affected the calcium modulation due to an additional interaction with Asn65. Therefore, the results coming from the docking studies would complement the results from the in vitro experiments.

It is well established that, in GPCR class A, the structural core of the receptor composed of the seven transmembrane domains is highly conserved and crucial for both ligand binding and intracellular signal transduction [14,15]. Thus, it is conceivable that, as for other members of GPCR class A [37,40,42], the SNPs in the TM4 domain of TAS2R46 lead to a rearrangement of the receptor core, leading to an altered downstream transmission. Indeed, this may be the case since the stimulation of these cells with a specific EPAC activator is sufficient to rescue the absinthin/TAS2R46 effect on mitochondrial calcium uptake. This is in line with the already published results that highlighted the role of the EPAC in mediating TAS2R46 signalling in several cell types, such as smooth muscles [12], skeletal muscles [33], and the heart [32].

Based on our results, we can speculate that the TM4, even if it is not directly involved in ligand specificity [10], is fundamental for absinthin activity, but more functional studies (e.g., dose–response curves) must be conducted on mutated or chimeric receptors to respond to our hypothesis.

However, our preliminary results are helpful for the understanding of the structure and the biology of TAS2Rs, an almost stand-alone GPCR class, in order to validate these receptors as new potential targets for respiratory disease therapy.

Supplementary Materials: The following supporting information can be downloaded at: https://www.mdpi.com/article/10.3390/cells13141204/s1, Supplemental Material S1: Immunofluorescence; Figure S1: Immunofluorescence staining on transfected HeLa cells; Figure S2: Cytosolic and mitochondrial Ca^{2+} analysis in non-transfected HeLa cells; Figure S3: Cytosolic and mitochondrial Ca^{2+} analysis of non-transfected HeLa cells; Figure S4: Structural analysis; Figure S5: Interaction of modelled TAS2R46 with strychnine and absinthin in orthosteric site; Figure S6: Interaction of 7XP6 TAS2R46 with strychnine and absinthin in vestibular site; Figure S7: Interaction of modelled TAS2R46 with strychnine and absinthin in vestibular site.

Author Contributions: Conceptualisation, A.B. (Angshuman Bagchi) and L.G.F.; Funding acquisition, A.B. (Angshuman Bagchi) and M.T.; Investigation, G.L., C.M., D.T., A.B. (Arianna Berto), H.B.B., S.B., F.P. and M.T.; Writing—original draft, L.G.F. and M.T.; Writing—review and editing, A.B. (Angshuman Bagchi) and L.G.F. All authors have read and agreed to the published version of the manuscript.

Funding: This work was supported by research grants from the (1) Fondazione Roche per la Ricerca Indipendente 2020 to Maria Talmon; the (2) Department of Biotechnology, Government of India (Grant Sanction no.: BT/PR40162/BTIS/137/48/2022 and BT/PR40192/BTIS/137/69/2023), sanctioned to Angshuman Bagchi.

Institutional Review Board Statement: Not applicable.

Informed Consent Statement: Not applicable.

Data Availability Statement: The datasets analysed during the current study are not present in a database but are available from the corresponding author upon request.

Conflicts of Interest: The authors declare no conflicts of interest.

References

1. Lush, I.E.; Hornigold, N.; King, P.; Stoye, J.P. The Genetics of Tasting in Mice VII. Glycine Revisited, and the Chromosomal Location of *Sac* and *Soa*. *Genet. Res.* **1995**, *66*, 167–174. [CrossRef] [PubMed]
2. Adler, E.; Hoon, M.A.; Mueller, K.L.; Chandrashekar, J.; Ryba, N.J.P.; Zuker, C.S. A Novel Family of Mammalian Taste Receptors. *Cell* **2000**, *100*, 693–702. [CrossRef]
3. Bachmanov, A.A.; Beauchamp, G.K. Taste Receptor Genes. *Annu. Rev. Nutr.* **2007**, *27*, 389–414. [CrossRef]
4. Wooding, S.P.; Ramirez, V.A.; Behrens, M. Bitter Taste Receptors. *Evol. Med. Public Health* **2021**, *9*, 431–447. [CrossRef]

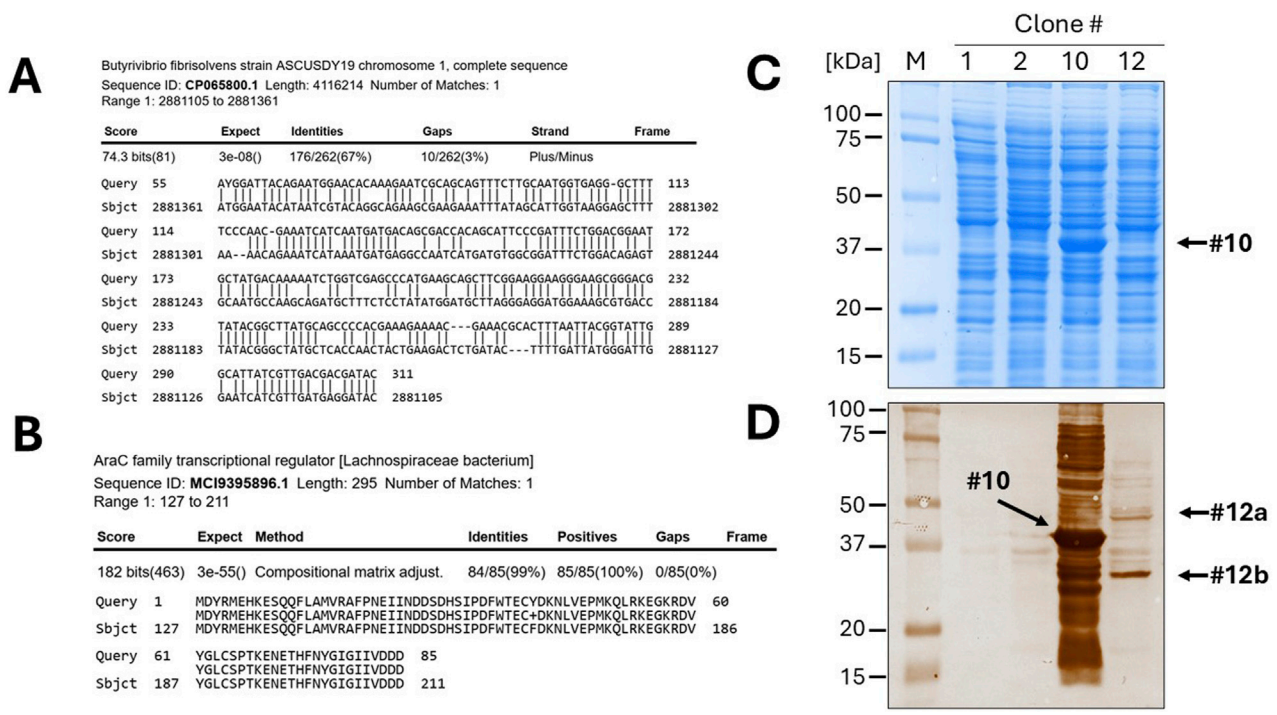

FIGURE 5
Identification of a novel, unannotated DNA sequence and expression of recombinant proteins. **(A)** The BLASTN analysis of clone 10 revealed only a 67% homology to the *Butyrivibrio fibrisolvens* genome. **(B)** After *in silico* translation and BLASTP, the DNA was identified as a fragment of a gene encoding a member of the AraC family of transcriptional regulator. Gel electrophoresis (SDS-PAGE) of bacterial lysates of the selected clones (1, 2, 10 and 12), followed by Coomassie blue staining **(C)** or Western blotting **(D)**, confirmed the efficient expression of the protein domains fused to β-lactamase.

4 Discussion

4.1 The value of functional metagenomics to life science education

How can undergraduate research projects in functional metagenomics provide valuable training and help meet curriculum standards, particularly in terms of preparing young scientists for the biological research workforce? Genetics, microbiology, biochemistry, and molecular biology are foundational courses in life science programs. Metagenomics illustrates how the genes of one organism are interconnected with those of others, as well as with the entire community, bridging basic sciences and advanced fields such as ecology, health sciences, and industrial biotechnology. This process highlights the importance of understanding the full diversity of life within a single environment and researching genes and organisms in their context. Since metagenomics spans multiple disciplines, it serves as an effective tool for teaching key themes and concepts that are integral to life science education.

By introducing students to functional metagenomics at the introductory level, with a focus on its practical applications, they can gain a clearer understanding of the fundamental concepts across various fields, the connections between them, and the broader impact of scientific advancements. Presenting functional metagenomics this way can inspire talented students to pursue careers in science by showing them that there are intriguing, unresolved questions they can contribute to answering. This approach fosters an experience of science as dynamic and ever evolving.

4.2 Functional metagenomics as a model for education-research integration

Students' research holds great potential to advance the field of functional metagenomics, given the vast amount of knowledge yet to be discovered. For example, many metagenomics projects involve collecting and analysing large numbers of samples to compare microbial communities from different sites with similar environmental conditions (Rebets et al., 2017; Zhang et al., 2021). Imagine a large-scale project with students from around the world, such as a global microbiome analysis. With a simple infrastructure of sampling kits and established processes, students could significantly expand the available data for functional metagenomic analysis. The development of effective data management systems, bioinformatics tools, technical innovations, and advancements in microbiology in the coming years could make student involvement in metagenomic sampling a viable option. Raising awareness and understanding of these opportunities within the biology research and teaching communities is the first step. It will be essential to create frameworks for engaging students in the study of microbial communities, their interactions with other organisms in various environments, and the practical applications of metagenomics.

5. Talmon, M.; Pollastro, F.; Fresu, L.G. The Complex Journey of the Calcium Regulation Downstream of TAS2R Activation. *Cells* **2022**, *11*, 3638. [CrossRef]
6. Nayak, A.P.; Shah, S.D.; Michael, J.V.; Deshpande, D.A. Bitter Taste Receptors for Asthma Therapeutics. *Front. Physiol.* **2019**, *10*, 884. [CrossRef]
7. An, S.S.; Liggett, S.B. Taste and Smell GPCRs in the Lung: Evidence for a Previously Unrecognized Widespread Chemosensory System. *Cell. Signal.* **2018**, *41*, 82–88. [CrossRef]
8. Dalesio, N.M.; Barreto Ortiz, S.F.; Pluznick, J.L.; Berkowitz, D.E. Olfactory, Taste, and Photo Sensory Receptors in Non-Sensory Organs: It Just Makes Sense. *Front. Physiol.* **2018**, *9*, 1673. [CrossRef]
9. Liggett, S.B. Bitter Taste Receptors on Airway Smooth Muscle as Targets for Novel Bronchodilators. *Expert Opin. Ther. Targets* **2013**, *17*, 721–731. [CrossRef]
10. Brockhoff, A.; Behrens, M.; Massarotti, A.; Appendino, G.; Meyerhof, W. Broad Tuning of the Human Bitter Taste Receptor hTAS2R46 to Various Sesquiterpene Lactones, Clerodane and Labdane Diterpenoids, Strychnine, and Denatonium. *J. Agric. Food Chem.* **2007**, *55*, 6236–6243. [CrossRef]
11. Talmon, M.; Bosso, L.; Quaregna, M.; Lopatriello, A.; Rossi, S.; Gavioli, D.; Marotta, P.; Caprioglio, D.; Boldorini, R.; Miggiano, R.; et al. Correction to Anti-Inflammatory Activity of Absinthin and Derivatives in Human Broncho-Epithelial Cells. *J. Nat. Prod.* **2020**, *83*, 2815–2816. [CrossRef]
12. Talmon, M.; Rossi, S.; Lim, D.; Pollastro, F.; Palattella, G.; Ruffinatti, F.A.; Marotta, P.; Boldorini, R.; Genazzani, A.A.; Fresu, L.G. Absinthin, an Agonist of the Bitter Taste Receptor hTAS2R46, Uncovers an ER-to-Mitochondria Ca^{2+}–Shuttling Event. *J. Biol. Chem.* **2019**, *294*, 12472–12482. [CrossRef] [PubMed]
13. Kulbacka, J.; Choromańska, A.; Rossowska, J.; Weżgowiec, J.; Saczko, J.; Rols, M.-P. Cell Membrane Transport Mechanisms: Ion Channels and Electrical Properties of Cell Membranes. In *Transport Across Natural and Modified Biological Membranes and its Implications in Physiology and Therapy*; Kulbacka, J., Satkauskas, S., Eds.; Advances in Anatomy, Embryology and Cell Biology; Springer International Publishing: Cham, Switzerland, 2017; Volume 227, pp. 39–58, ISBN 978-3-319-56894-2.
14. Di Pizio, A.; Levit, A.; Slutzki, M.; Behrens, M.; Karaman, R.; Niv, M.Y. Comparing Class A GPCRs to Bitter Taste Receptors. In *Methods in Cell Biology*; Elsevier: Amsterdam, The Netherlands, 2016; Volume 132, pp. 401–427, ISBN 978-0-12-803595-5.
15. Pallante, L.; Cannariato, M.; Androutsos, L.; Zizzi, E.A.; Bompotas, A.; Hada, X.; Grasso, G.; Kalogeras, A.; Mavroudi, S.; Di Benedetto, G.; et al. VirtuousPocketome: A Computational Tool for Screening Protein–Ligand Complexes to Identify Similar Binding Sites. *Sci. Rep.* **2024**, *14*, 6296. [CrossRef] [PubMed]
16. Brockhoff, A.; Behrens, M.; Niv, M.Y.; Meyerhof, W. Structural Requirements of Bitter Taste Receptor Activation. *Proc. Natl. Acad. Sci. USA* **2010**, *107*, 11110–11115. [CrossRef] [PubMed]
17. Sandal, M.; Behrens, M.; Brockhoff, A.; Musiani, F.; Giorgetti, A.; Carloni, P.; Meyerhof, W. Evidence for a Transient Additional Ligand Binding Site in the TAS2R46 Bitter Taste Receptor. *J. Chem. Theory Comput.* **2015**, *11*, 4439–4449. [CrossRef] [PubMed]
18. Xu, W.; Wu, L.; Liu, S.; Liu, X.; Cao, X.; Zhou, C.; Zhang, J.; Fu, Y.; Guo, Y.; Wu, Y.; et al. Structural Basis for Strychnine Activation of Human Bitter Taste Receptor TAS2R46. *Science* **2022**, *377*, 1298–1304. [CrossRef]
19. Ledda, M.; Kutalik, Z.; Souza Destito, M.C.; Souza, M.M.; Cirillo, C.A.; Zamboni, A.; Martin, N.; Morya, E.; Sameshima, K.; Beckmann, J.S.; et al. GWAS of Human Bitter Taste Perception Identifies New Loci and Reveals Additional Complexity of Bitter Taste Genetics. *Hum. Mol. Genet.* **2014**, *23*, 259–267. [CrossRef]
20. Roudnitzky, N.; Behrens, M.; Engel, A.; Kohl, S.; Thalmann, S.; Hübner, S.; Lossow, K.; Wooding, S.P.; Meyerhof, W. Receptor Polymorphism and Genomic Structure Interact to Shape Bitter Taste Perception. *PLoS Genet.* **2015**, *11*, e1005530. [CrossRef] [PubMed]
21. Chamoun, E.; Carroll, N.; Duizer, L.; Qi, W.; Feng, Z.; Darlington, G.; Duncan, A.; Haines, J.; Ma, D. The Guelph Family Health Study The Relationship between Single Nucleotide Polymorphisms in Taste Receptor Genes, Taste Function and Dietary Intake in Preschool-Aged Children and Adults in the Guelph Family Health Study. *Nutrients* **2018**, *10*, 990. [CrossRef]
22. Risso, D.S.; Kozlitina, J.; Sainz, E.; Gutierrez, J.; Wooding, S.; Getachew, B.; Luiselli, D.; Berg, C.J.; Drayna, D. Genetic Variation in the TAS2R38 Bitter Taste Receptor and Smoking Behaviors. *PLoS ONE* **2016**, *11*, e0164157. [CrossRef]
23. Risso, D.; Carmagnola, D.; Morini, G.; Pellegrini, G.; Canciani, E.; Antinucci, M.; Henin, D.; Dellavia, C. Distribution of TAS2R38 Bitter Taste Receptor Phenotype and Haplotypes among COVID-19 Patients. *Sci. Rep.* **2022**, *12*, 7381. [CrossRef] [PubMed]
24. Purnell, P.R.; Addicks, B.L.; Zalzal, H.G.; Shapiro, S.; Wen, S.; Ramadan, H.H.; Setola, V.; Siderovski, D.P. Single Nucleotide Polymorphisms in Chemosensory Pathway Genes GNB3, TAS2R19, and TAS2R38 Are Associated with Chronic Rhinosinusitis. *Int. Arch. Allergy Immunol.* **2019**, *180*, 72–78. [CrossRef] [PubMed]
25. Lee, R.J.; Xiong, G.; Kofonow, J.M.; Chen, B.; Lysenko, A.; Jiang, P.; Abraham, V.; Doghramji, L.; Adappa, N.D.; Palmer, J.N.; et al. T2R38 Taste Receptor Polymorphisms Underlie Susceptibility to Upper Respiratory Infection. *J. Clin. Investig.* **2012**, *122*, 4145–4159. [CrossRef]
26. Ryu, C.S.; Sakong, J.H.; Ahn, E.H.; Kim, J.O.; Ko, D.; Kim, J.H.; Lee, W.S.; Kim, N.K. Association Study of the Three Functional Polymorphisms (TAS2R46G>A, OR4C16G>A, and OR4X1A>T) with Recurrent Pregnancy Loss. *Genes Genom.* **2019**, *41*, 61–70. [CrossRef] [PubMed]
27. Dotson, C.D.; Zhang, L.; Xu, H.; Shin, Y.-K.; Vigues, S.; Ott, S.H.; Elson, A.E.T.; Choi, H.J.; Shaw, H.; Egan, J.M.; et al. Bitter Taste Receptors Influence Glucose Homeostasis. *PLoS ONE* **2008**, *3*, e3974. [CrossRef] [PubMed]
28. Eswar, N. Tools for Comparative Protein Structure Modeling and Analysis. *Nucleic Acids Res.* **2003**, *31*, 3375–3380. [CrossRef]

29. Fiser, A.; Sali, A. ModLoop: Automated Modeling of Loops in Protein Structures. *Bioinformatics* **2003**, *19*, 2500–2501. [CrossRef]
30. Morris, G.M.; Huey, R.; Lindstrom, W.; Sanner, M.F.; Belew, R.K.; Goodsell, D.S.; Olson, A.J. AutoDock4 and AutoDockTools4: Automated Docking with Selective Receptor Flexibility. *J. Comput. Chem.* **2009**, *30*, 2785–2791. [CrossRef]
31. Fazal, L.; Laudette, M.; Paula-Gomes, S.; Pons, S.; Conte, C.; Tortosa, F.; Sicard, P.; Sainte-Marie, Y.; Bisserier, M.; Lairez, O.; et al. Multifunctional Mitochondrial Epac1 Controls Myocardial Cell Death. *Circ. Res.* **2017**, *120*, 645–657. [CrossRef]
32. Wang, Z.; Liu, D.; Varin, A.; Nicolas, V.; Courilleau, D.; Mateo, P.; Caubere, C.; Rouet, P.; Gomez, A.-M.; Vandecasteele, G.; et al. A Cardiac Mitochondrial cAMP Signaling Pathway Regulates Calcium Accumulation, Permeability Transition and Cell Death. *Cell Death Dis.* **2016**, *7*, e2198. [CrossRef]
33. Talmon, M.; Massara, E.; Quaregna, M.; De Battisti, M.; Boccafoschi, F.; Lecchi, G.; Puppo, F.; Bettega Cajandab, M.A.; Salamone, S.; Bovio, E.; et al. Bitter Taste Receptor (TAS2R) 46 in Human Skeletal Muscle: Expression and Activity. *Front. Pharmacol.* **2023**, *14*, 1205651. [CrossRef]
34. Kooistra, A.J.; Mordalski, S.; Pándy-Szekeres, G.; Esguerra, M.; Mamyrbekov, A.; Munk, C.; Keserű, G.M.; Gloriam, D.E. GPCRdb in 2021: Integrating GPCR Sequence, Structure and Function. *Nucleic Acids Res.* **2021**, *49*, D335–D343. [CrossRef] [PubMed]
35. Horn, F. GPCRDB Information System for G Protein-Coupled Receptors. *Nucleic Acids Res.* **2003**, *31*, 294–297. [CrossRef]
36. Fredriksson, R.; Lagerström, M.C.; Lundin, L.-G.; Schiöth, H.B. The G-Protein-Coupled Receptors in the Human Genome Form Five Main Families. Phylogenetic Analysis, Paralogon Groups, and Fingerprints. *Mol. Pharmacol.* **2003**, *63*, 1256–1272. [CrossRef] [PubMed]
37. Cvicek, V.; Goddard, W.A.; Abrol, R. Structure-Based Sequence Alignment of the Transmembrane Domains of All Human GPCRs: Phylogenetic, Structural and Functional Implications. *PLoS Comput. Biol.* **2016**, *12*, e1004805. [CrossRef] [PubMed]
38. Di Pizio, A.; Niv, M.Y. Promiscuity and Selectivity of Bitter Molecules and Their Receptors. *Bioorg. Med. Chem.* **2015**, *23*, 4082–4091. [CrossRef]
39. Nordstrom, K.J.V.; Sallman Almen, M.; Edstam, M.M.; Fredriksson, R.; Schioth, H.B. Independent HHsearch, Needleman-Wunsch-Based, and Motif Analyses Reveal the Overall Hierarchy for Most of the G Protein-Coupled Receptor Families. *Mol. Biol. Evol.* **2011**, *28*, 2471–2480. [CrossRef]
40. Yang, L.; Liu, D.; Wüthrich, K. GPCR Structural Characterization by NMR Spectroscopy in Solution. *Acta Biochim. Biophys. Sin.* **2022**, *54*, 1207–1212. [CrossRef]
41. Brockhoff, A.; Behrens, M.; Roudnitzky, N.; Appendino, G.; Avonto, C.; Meyerhof, W. Receptor Agonism and Antagonism of Dietary Bitter Compounds. *J. Neurosci.* **2011**, *31*, 14775–14782. [CrossRef]
42. Balasubramanian, S. Sequence Variation in G-Protein-Coupled Receptors: Analysis of Single Nucleotide Polymorphisms. *Nucleic Acids Res.* **2005**, *33*, 1710–1721. [CrossRef]

frontiers | Frontiers in Bioengineering and Biotechnology

TYPE Methods
PUBLISHED 20 May 2025
DOI 10.3389/fbioe.2025.1602982

OPEN ACCESS

EDITED BY
Si-Yu Li,
National Chung Hsing University, Taiwan

REVIEWED BY
Michael J. Wolyniak,
Hampden–Sydney College, United States
Rachid Daoud,
Mohammed VI Polytechnic University, Morocco

*CORRESPONDENCE
Diego Cotella,
diego.cotella@uniupo.it

RECEIVED 30 March 2025
ACCEPTED 05 May 2025
PUBLISHED 20 May 2025

CITATION
Morra M, Marradi D, Gandini L, Ivagnes V, Ottolini G, Bovio A, Jabali G, Maraschi L, Dada IA, Chawanda TV, Gorla M, Tarasiuk O, Mocchetti C, Soluri MF, Boccafoschi F, Sblattero D and Cotella D (2025) A non-hypothesis-driven practical laboratory activity on functional metagenomics: "fishing" protein-coding DNA sequences from microbiomes. *Front. Bioeng. Biotechnol.* 13:1602982. doi: 10.3389/fbioe.2025.1602982

A non-hypothesis-driven practical laboratory activity on functional metagenomics: "fishing" protein-coding DNA sequences from microbiomes

Melissa Morra[1], Denise Marradi[1], Luca Gandini[1], Vittorio Ivagnes[1], Giulia Ottolini[1], Alessandro Bovio[1], Grace Jabali[1], Lorenzo Maraschi[1], Ifeoluwa Ayomide Dada[1], Tonderai Vitalis Chawanda[1], Martina Gorla[1], Olga Tarasiuk[1], Chiara Mocchetti[1], Maria Felicia Soluri[1,2], Francesca Boccafoschi[1], Daniele Sblattero[3] and Diego Cotella[1]*

[1]Department of Health Sciences, University of Eastern Piedmont, Novara, Italy, [2]Research Center on Autoimmune and Allergic Diseases (CAAD), University of Eastern Piedmont, Novara, Italy, [3]Department of Life Sciences, University of Trieste, Trieste, Italy

Practical laboratory of the most functional metagenomics courses focuses on activities aimed at providing specific skills in bioinformatics through the analysis of genomic datasets. However, sequence-based analyses of metagenomes should be complemented by function-based analyses, to provide evidential knowledge of gene function. A "true" functional metagenomic approach relies on the construction and screening of metagenomic libraries - physical libraries that contain DNA cloned from metagenomes of various origin. The information obtained from functional metagenomics will help in future annotations of gene function and serve as a complement to sequence-based metagenomics. Here, we describe a simple protocol for the construction of a metagenomic DNA library, optimized and tested by a team of undergraduate biotechnology students. This protocol is based on a technique developed in our laboratory and currently used for research. Using this protocol, libraries of protein domains can be quickly generated, from the DNA of any intron-less genome, such as those of bacteria or phages. Therefore, these libraries provide a valuable platform for training students in various validation tools, including computational methods - for example, metagenome assembly, functional annotation - and proteomics techniques, including protein expression and analysis. By varying the biological source and validation pipeline, this approach offers virtually limitless opportunities for innovative thesis research projects.

KEYWORDS

open reading frame, domainome, microbiome, course-based undergraduate research experience, synthetic biology

1 Introduction

Functional genomics is a discipline which, by combining Bioinformatics, Next-Generation Sequencing (NGS) and other Omics technologies, aims to assign functions and interactions to genes and their products of expression (Hieter and Boguski, 1997; Caudai et al., 2021). Several universities and research institutes offer hands-on courses on NGS and Bioinformatics as part of their advanced genomics-related courses.

Metagenomics has added a new level of complexity by allowing scientists to study the entire microbial population (or "microbiota") of a specific environment—like soil, the ocean, skin, or hot springs—at the genomic level. To give an example, the human gut microbiome (the collection of the genomes of all microorganisms living in the gut) records at least 3.3 million unique genes, 150 times more genes than our genome, because of a community of about 1,000 bacterial species that cohabit in our intestine (Qin et al., 2010). To provide knowledge of gene function, sequence-based analyses of metagenomes must be complemented by function-based analyses, for example, enzymatic assays (Wiltschi et al., 2020).

Incorporating functional metagenomics into university-level Life Science education offers advantages not only for students but also for researchers and their work. Research has shown that when researchers teach, it enhances their understanding, prompting students to ask new and often unexpected questions. This process can lead to fresh research directions and drive the development of innovative solutions to complex problems (Jurkowski et al., 2007). If the biology community can integrate functional metagenomics education with ongoing research advancements from the outset, students could play an active role in advancing the field. Teaching a new or emerging area of study is an excellent way to engage students in addressing key scientific questions and inspiring them to pose their own inquiries. In the case of functional metagenomics, even the simplest questions can yield profound insights. Answering these questions benefits both emerging scientists and established researchers. Many initiatives are currently underway to merge (meta) genomics research with education (Muth and Caplan, 2020; Ginnan and Bordenstein, 2023; Fuhrmeister et al., 2021; Heller et al., 2024).

The principle underlying Functional Metagenomics is to isolate DNA from microbial communities and to clone it into a suitable host (for example, *Escherichia coli*); each clone harbours a fragment (usually 25–40 kb in size) of the DNA isolate. Then, the metagenomic DNA library undergoes a screening process specifically designed to identify those clones with a desired activity - for example, antibiotic resistance, ability to catalyse a specific chemical reaction, bactericidal (Lam et al., 2015; Berini et al., 2017). This function-based approach enables the discovery of novel proteins whose functions would not be predicted based on DNA sequence alone.

Although seemingly simple, this procedure involves many steps, which makes the construction of metagenomic libraries laborious and time-consuming, requiring a high level of skills at the laboratory bench (Terrón-González et al., 2014; Lam et al., 2015). Moreover, this process has many other limitations such as the poor expression of correctly folded full-length proteins in heterologous hosts (Pouresmaeil and Azizi-Dargahlou, 2023). To simplify the production of metagenomic DNA libraries and to overcome the limitations associated, we have developed an approach aimed at "filtering" genomic DNA to generate expression libraries enriched in functional protein domains. This approach is based on the knowledge that >85% of the genome of prokaryotes is translated into proteins (Land et al., 2015) and that most proteins are organized into multiple domains, evolutionarily conserved, each of them contributing to a distinct function (Heger and Holm, 2003). Based on bioinformatic analyses indicating that the most common domain size is approximately 100 amino acids, any piece of prokaryotic DNA >150 nucleotides (50 amino acids) is likely to encode a protein domain (Tiessen et al., 2012). The recovery of functional open reading frames (ORFs) from bacterial DNA may therefore be a straightforward procedure (D'Angelo et al., 2011; Soluri et al., 2018). In brief, genomic DNA is randomly fragmented into short (250–1,000 nucleotides) fragments, cloned between a secretory leader sequence (a signal peptide) and the ß-lactamase gene in the pFILTER plasmid (Soluri et al., 2018), and transformed into *E. coli*. Transformed bacteria are then seeded on ampicillin-containing agar plates, and only those clones harbouring an ORF properly folded and in the correct frame with both the signal peptide and the ß-lactamase will grow under selective pressure (Figure 1). So, if the protein is functional, it can restore the activity of the gene which enables the *E. coli* to resist the ampicillin and grow. Such expression libraries of protein domains (the "*domainome*") will be useful for many purposes, including structural studies, antibody generation, protein/substrate binding analyses, domain shuffling for enzyme evolution and protein arrays (Gourlay et al., 2015; Antony et al., 2019; Soluri et al., 2020). Once the domainome libraries are transferred into systems like phage display for functional screening, they can be used to find protein domains that bind to specific targets (like proteins, DNA, sugars, fats, or enzyme substrates) or that have certain enzyme activities—if the right screening tools are available (Soluri et al., 2020; Puccio et al., 2020).

The whole process is called "interactome-seq" (Soluri et al., 2018; Puccio et al., 2020) and has been used in several research projects in our lab (Fasolo et al., 2019; Patrucco et al., 2015). Building these libraries takes less effort and time—usually under two weeks—compared to traditional large-insert metagenomic libraries, and the process is much easier (Lam et al., 2015).

Each year, two to four undergraduate biotechnology students (pursuing a bachelor's degree) carry out their internship for their thesis project in our lab. They usually spend one semester in the lab, earning a total of 6 credits or ECTS (European Credit Transfer and Accumulation System). We questioned whether this technique could be taught and learned quickly, and whether it would be suitable for simultaneously running several different, low-cost thesis projects. A group of students (eleven in total) from the bachelor's program in Biotechnology, assisted by their thesis mentors and older lab mates (master's and PhD students), have worked to optimize a protocol for the construction and analysis of metagenomics *domainome* libraries (Soluri et al., 2018).

As a result, a general laboratory activity has been defined, divided into a 3-week period, and organized according to the

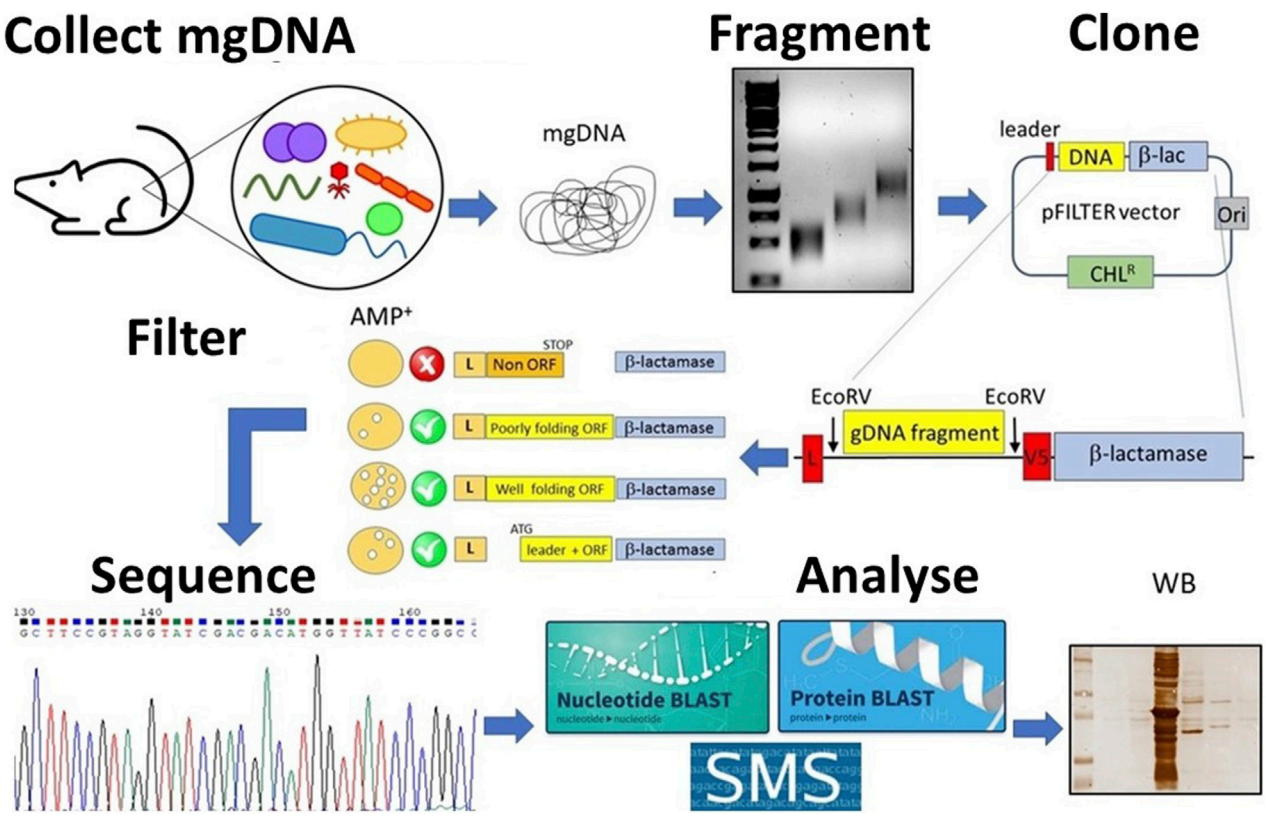

FIGURE 1
Schematic overview of the student's project. Metagenomic DNA (mgDNA) is extracted from an appropriate source (such as murine feces), then fragmented into a collection of 250–1,000 bp fragments and cloned into the pFILTER vector. *E. coli* cells are transformed with the ligation product and plated on ampicillin-containing media to carry out the "filtering" of open reading frames (ORFs). The resulting clones are sequenced and analyzed using computational tools (for example, BLAST, AlphaFold) as well as functional assays (for example, Western blotting, enzyme assays).

scheme summarized below. A detailed list of instruments, kits and reagents required is provided as Supplementary Material.

2 Course structure

2.1 Week 1. Metagenomic DNA preparation

Metagenomic DNA (mgDNA) can be directly extracted from environmental samples like soil, air, hot spring water, animal skin, faeces, toilet seats, or landfill soil (Bag et al., 2016). There are many kits and protocols available for this. To build one library, at least 10 μg of mgDNA is needed, which can be hard to get depending on the sample (Soluri et al., 2018). For instance, faeces—a rich source of microbes—can provide up to 10 μg of DNA from 100 mg of material (Claassen et al., 2013). As another option, microbes can be grown in suitable liquid or solid media, and mgDNA can be extracted after collecting the cells.

However, this step can introduce a bias in microbiota diversity, as the culture conditions (such as medium composition, incubation temperature, and oxygen concentration) will significantly influence microbial growth. As a result, the final composition of the microbial population will not accurately represent the true microbiome composition. This factor must be considered when discussing the results and drawing conclusions.

2.2 Week 2. Library construction

This part is the most technically challenging. The mgDNA must be randomly fragmented, for example, by mechanical (sonication, nebulization) or enzymatic (nuclease) means (Ribarska et al., 2022). The DNA fragments are then sorted by size, which can be obtained inexpensively by resolving the DNA by agarose gel electrophoresis, cutting a gel slice corresponding to the desired size range (250 bp–1,000 bp), and extracting the DNA from the gel (Soluri et al., 2018). Alternatively, a DNA sizing kit can be used. Purified DNA is then repaired, filled-in, and ligated into the pFILTER vector previously linearized with EcoRV (Soluri et al., 2018). This restriction enzyme creates blunt ends, so the digested plasmid needs to be dephosphorylated after cutting to prevent its self-circularization. The ligase reaction is then transformed into competent *E. coli* and the bacteria first seeded on agar plates containing chloramphenicol as selection. Chloramphenicol selection helps to recover all clones with a DNA insert, regardless of whether it contains a real ORF. Transformants grown on chloramphenicol plates are then transferred to ampicillin plates to "filter" for clones that contain a DNA insert placed in the correct reading frame (ORF), along with the signal peptide and the β-lactamase gene. In a typical experiment, chemical transformation by "heat shock" would provide <1,000 colony forming units (cfu), sufficient for a practical laboratory course or a small thesis work

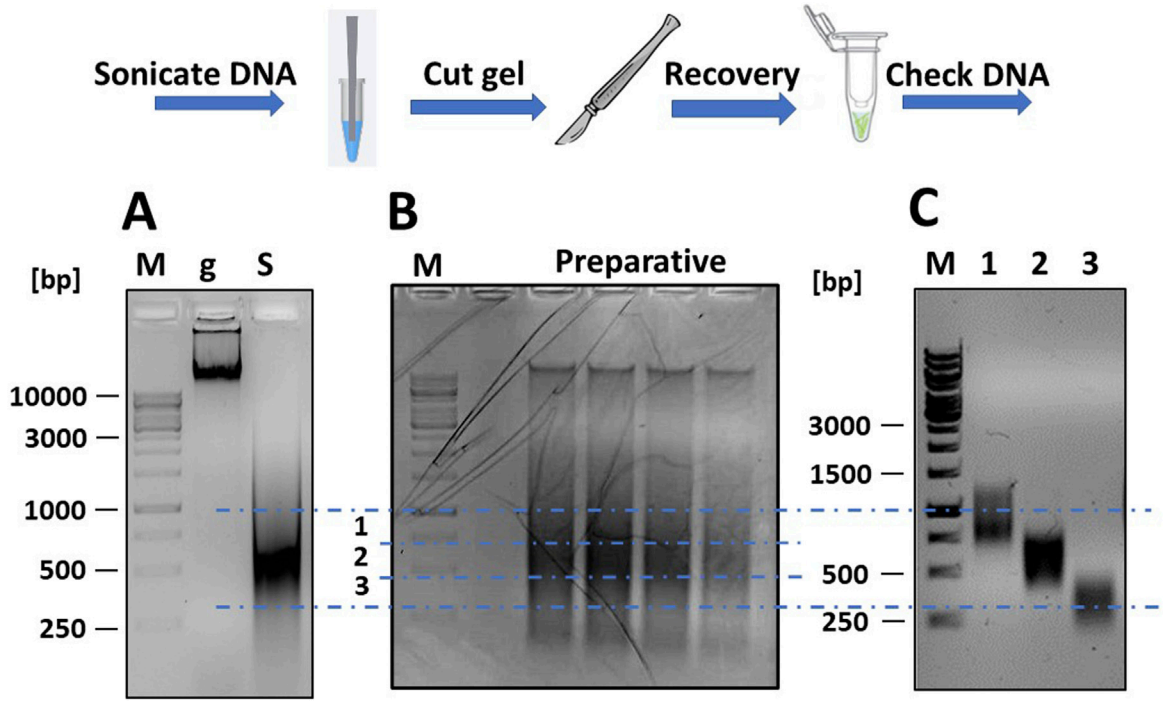

FIGURE 2
Fragmentation of mgDNA and purification of DNA into the desired size range. **(A)** Approximately 10 µg of mgDNA (lane "g") are fragmented into 250–1,000 bp fragments by sonication (lane "S") and checked by gel electrophoresis. **(B)** The sonicated DNA is loaded onto a preparative agarose gel, placed over a blue LED transilluminator, and the gel is cut into several DNA-containing slices of the desired size. **(C)** The pools of DNA fragments are purified from the agarose gel slices and checked again by gel electrophoresis (lane 1: range 250–500 bp; lane 2: range 500–750 bp; lane 3: range 750–1,000 bp; M: DNA ladders).

(von der Haar, 2019). If a higher complexity of the library is desired, for example, for projects involving the use of Next-Generation Sequencing (NGS) technologies, we suggest transforming the ligation products by electroporation (1.8 kV, time constant 4–5 ms), as it will easily yield $>10^6$ clones (Soluri et al., 2018).

2.3 Week 3 and beyond. Data analysis

This part gives more space to creativity. The simplest experiment students can perform is to randomly pick one or few colonies from the plate and sequence the cloned DNA fragment. The sequences will then be analysed using Nucleotide Blast (BLASTN) to identify the host organism, followed by *in silico* translation and analysis with Protein Blast (BLASTP) to confirm that the selected genomic fragment is protein-coding DNA (Camacho et al., 2009). At this stage, students can be guided to use various other tools, such as performing phylogenetic analyses (Jacques et al., 2023) or predicting protein solubility (Kyte and Doolittle, 1982) or 3D structure (Jumper et al., 2021), among others.

Since the DNA fragments cloned into pFILTER will be expressed as recombinant proteins fused to a V5 epitope tag for immunodetection, biochemical characterization can be performed using methods such as SDS-PAGE, Western blotting, or mass spectrometry. It will also be possible to sub-clone the DNA fragment into a plasmid suitable for the expression and purification of recombinant proteins for further characterization.

3 Representative results

Here we present some representative results of a thesis aimed at exploring a small library of metagenomic DNA from the intestinal microbiome, in search of DNA sequences encoding novel proteins. Most of the work was conducted by a single student (Morra, 2021), although all co-authors, with their previous work, contributed to the optimization of the whole procedure (Bovio, 2019; Ivagnes, 2019; Gandini, 2019; Ottolini, 2019; Marradi, 2020; Maraschi, 2024). A schematic overview of the student's project is provided in Figure 1. The mgDNA was extracted from murine faeces using a commercial kit (QIAGEN cat. 51804). Ten micrograms of mgDNA were randomly fragmented using a tip sonicator, applying a 15 s pulse and 10% maximum amplitude.

Fragmentation was verified by agarose gel electrophoresis, running two DNA samples taken before and after sonication, and results are shown in Figure 2A. The non-fragmented DNA appeared as an intense band that partially stuck in the well due to its large size. Following sonication, the DNA appeared as a diffuse smear, ranging in size from <200 to >3,000 bp.

The sonicated DNA was loaded onto a preparative gel (1% agarose in TAE buffer) for purification. After electrophoresis (45 min at 80 V), the gel was examined under a blue light LED transilluminator (Figure 2B). Using a scalpel and referencing the DNA ladders, the gel section containing DNA fragments between 250 and 1,000 bp was divided into three slices and excised. The blue light LED transilluminator was chosen for longer exposure times as

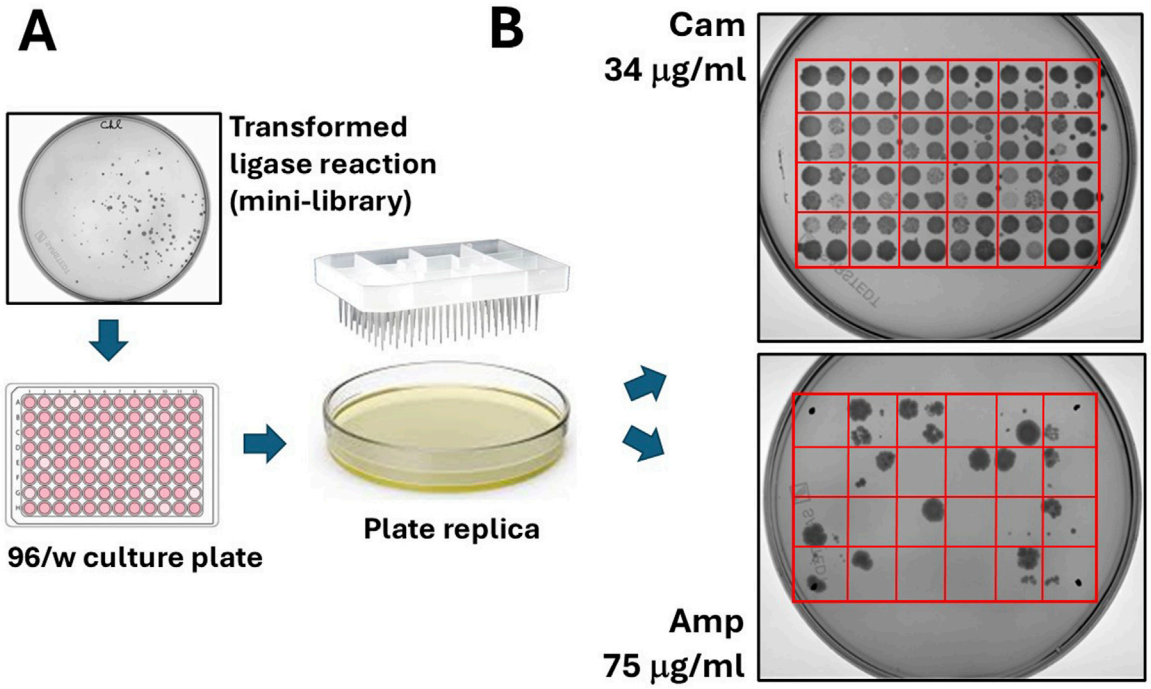

FIGURE 3
"Filtering" of open reading frames by selection on ampicillin. **(A)** Colonies grown on chloramphenicol agar plates are manually picked and seeded on 96/w plates. From here, colonies are replica plated on chloramphenicol and ampicillin agar dishes. **(B)** A typical result from the replica plating shows 96 colonies (100%) growing on chloramphenicol and much less (typically, only 5–10 colonies) growing on ampicillin.

it was safer for students and reduced the risk of DNA damage compared to a UV transilluminator. The DNA was then extracted from the gel using a commercial kit (Thermo Fisher Scientific cat. K0832) and re-checked by gel electrophoresis to confirm the correct size range of the DNA fragments (Figure 2C). The DNA was then repaired using a commercial kit for DNA blunting (NEB cat. E1201), as described (Soluri et al., 2018). The DNA fragments were then ligated into the linearized pFILTER vector with a T4 DNA ligase (Thermo Fisher Scientific cat. EL0014) and transformed into chemically competent *E. coli* DH5αF′ cells.

The bacteria were plated onto a 15 cm 2xTY/Cam agar plate (chloramphenicol 34 µg/mL) and incubated at 30°C overnight (O/N). Ninety-six colonies grown on chloramphenicol were selected and inoculated into a 96-well culture plate containing 100 µL of 2xTY/Cam medium. After incubating for 2 hours at 30°C, the colonies were transferred from the 96/w plate onto two 15 cm Petri dishes—one with 34 µg/mL chloramphenicol and the other with 75 µg/mL ampicillin. To do this, we used a 96-well pin replicator, depicted in Figure 3A. Plated colonies were grown O/N at 30°C. As shown in Figure 3B (upper-right panel), all colonies grew on chloramphenicol, while only some of them (around 10–15 clones) grew on ampicillin. We continued analysing 12 bacterial clones: four grown only on chloramphenicol (numbered 1–4), and 8 grown on ampicillin (numbered 5–12). The DNA inserts were amplified by colony PCR by using a pair of external primers and analysed by gel electrophoresis. The sequences of primers (pDAN_filter_sense/anti) are provided in the Supplementary Material. From the image of the gel presented in Figure 4A, it is possible to appreciate the presence of amplicons of different lengths ranging between 300 and 800 bp, suggesting that the various clones contain different DNA inserts.

The twelve clones were cultured in 2 mL of 2xTY medium with chloramphenicol for plasmid extraction, which was performed using a commercial plasmid DNA miniprep kit (Thermo Fisher Scientific cat. K0702). The inserts were then sequenced by Sanger sequencing using either the sense or antisense primer from the colony PCR. DNA traces (shown in Figure 4B) were visualized with the software Chromas version 2.6.6 (Technelysium Ltd.). The start and end of the DNA insert were identified in the obtained sequences, located adjacent to the consensus sequences recognized by EcoRV (GAT_ATC). The sequences were analysed using BLASTN to determine the species origin of the DNA fragments. Subsequently, the nucleotide sequences were *in silico* translated using the Sequence Manipulation Suite (SMS) version 2 (https://www.bioinformatics.org/sms2/). To identify the correct reading frame, the sequence was aligned with the known signal peptide (gca gca agc ggc gcg cat gcc, encoding Ala-Ala-Ser-Gly-Ala-His-Ala) and translated until the first stop codon. Visual confirmation of the inserts was possible by identifying the presence of the secretory leader sequence (L) upstream of the cloning site and the β-lactamase gene downstream, which served as reference markers for correct insert orientation and integration. Finally, BLASTP was used to analyse the resulting amino acid sequences. To provide a detailed illustration of the analysis conducted, the procedure performed for clone 10 is outlined below as an example. The colony PCR screening confirmed the presence of an insert approximately 200 bp in size, which appeared as a 300 bp amplicon on the gel due to the external

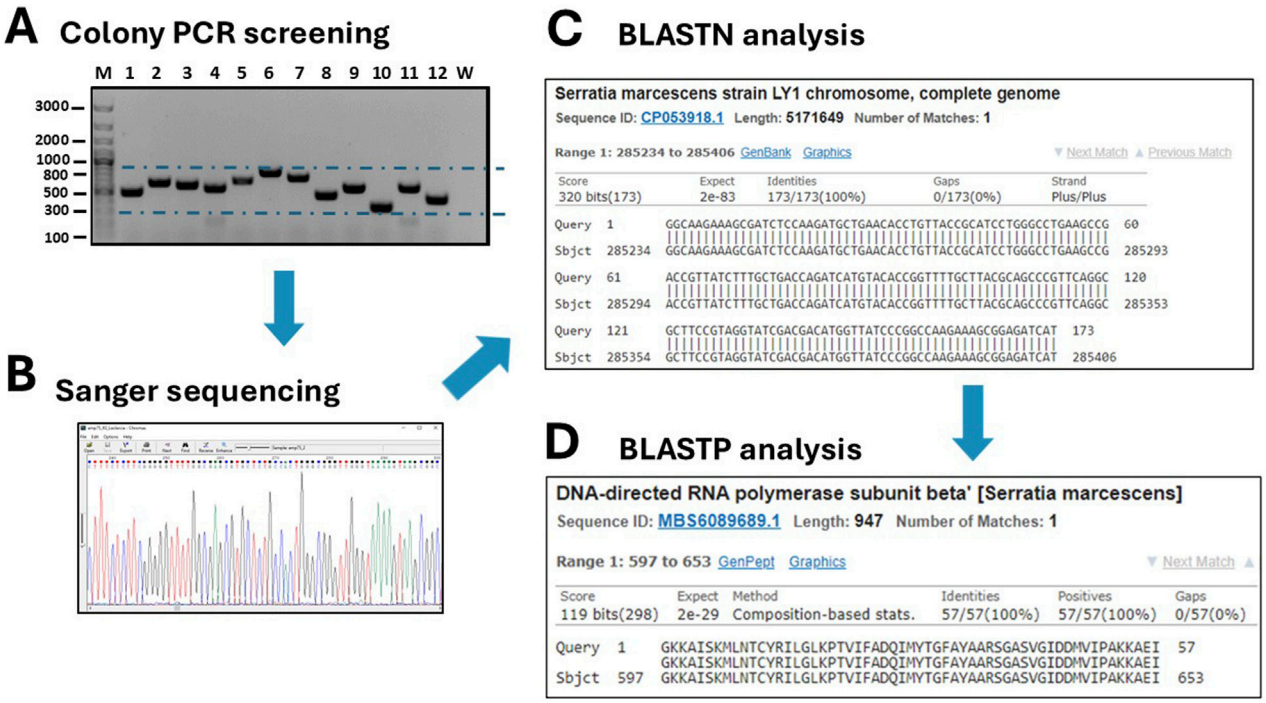

FIGURE 4
Screening of grown transformants. **(A)** A colony PCR is performed on several randomly picked clones (M: DNA ladders; W: negative control of PCR). **(B)** Positive clones are sequenced by Sanger sequencing and traces are visualized with the Chromas 2.6.6 software. **(C)** DNA sequences are analyses by BLASTN to identify the host organism. **(D)** After *in silico* translation, the sequences are further analyzed by BLASTP to confirm that they belong to true protein-coding genes or to identify a novel, putative protein.

primers used for PCR (Figure 4B). BLASTN analysis further revealed that a 173 bp segment of the insert was 100% homologous to the *Serratia marcescens* genome (Figure 4C). Although the sonication process was aimed at generating DNA fragments larger than 250 bp, shorter fragments may still be present due to the random nature of shearing and subsequent size selection limitations. Additionally, shorter fragments can sometimes be preferentially amplified or cloned, which may explain the presence of this 173 bp insert. The sequence was then translated *in silico* using the Sequence Manipulation Suite (SMS) tool, following the frame with β-lactamase. A BLASTP search of the amino acid sequence showed the closest match was a DNA-directed RNA polymerase from *S. marcescens* (Figure 4D). The results from clone 12 were particularly interesting. In this case, BLASTN analysis of a 262 bp fragment revealed partial homology (67%) with the genome of *Butyrivibrio fibrisolvens* (Figure 5A). This level of similarity suggests that the analyzed DNA fragment may originate from a microorganism that is phylogenetically related to the *Butyrivibrio* genus (class *Clostridia*), but whose genome may not yet be represented in current databases. Additionally, translation *in silico* of the predicted coding region showed 100% amino acid identity with an AraC-family transcriptional regulator from a *Lachnospiraceae* bacterium, also within the *Clostridia* class (Figure 5B). These findings support the possibility that the fragment is derived from a phylogenetically related, yet potentially unsequenced or underrepresented, microorganism. From this point, it is possible to perform some biochemical assays. An SDS-PAGE and, subsequently, a Western blot were carried out, shown in Figures 5C,D. Protein expression in sample 10 was notably high: a prominent band of approximately 37 kDa was clearly visible even on the Coomassie-stained gel, indicating strong expression (Figure 5C). Western blot analysis confirmed this observation, showing a very intense band at ~37 kDa, corresponding to the expected size of the expressed fusion protein. This size is consistent with the in-frame cloning of the 173 bp ORF (encoding ~58 amino acids, ~6 kDa) fused to the β-lactamase reporter (~32 kDa). Additional bands at higher molecular weights likely represent protein aggregates, while those at lower molecular weights may correspond to degradation products. Clone 12 also showed detectable expression by Western blotting, although at lower intensity compared to clone 10 (Figure 5D). In this case, two major bands were observed, with apparent sizes of ~45 kDa and ~35 kDa, respectively. The ORF length of 262 bp encodes a peptide of ~10 kDa, which, when fused to β-lactamase, results in a predicted fusion protein of ~42 kDa. Therefore, the upper band likely represents the full-length chimeric protein, while the lower band is consistent with a degradation product. Clones 1 and 2 were loaded as a negative control since they grew only on chloramphenicol but not on ampicillin and were therefore expected to be unable to produce a functional fusion protein. Sanger sequencing of these two clones showed that the DNA insert was not in the correct frame with the β-lactamase, confirming that the filtering process worked well in selecting protein-coding gene domains.

From there, the role of functional metagenomics in Life Science education can evolve and expand, adapting to the needs of both students and researchers.

Data availability statement

The raw data supporting the conclusions of this article will be made available by the authors, without undue reservation.

Author contributions

MM: Investigation, Methodology, Writing – review and editing. DM: Investigation, Methodology, Writing – review and editing. LG: Investigation, Methodology, Writing – review and editing. VI: Investigation, Methodology, Writing – review and editing. GO: Investigation, Methodology, Writing – review and editing. AB: Investigation, Methodology, Writing – review and editing. GJ: Investigation, Methodology, Writing – review and editing. LM: Investigation, Methodology, Writing – review and editing. ID: Supervision, Writing – review and editing. TC: Supervision, Writing – review and editing. MG: Supervision, Writing – review and editing. OT: Supervision, Writing – review and editing. CM: Resources, Supervision, Writing – review and editing. MS: Methodology, Resources, Writing – review and editing. FB: Resources, Supervision, Writing – review and editing. DS: Resources, Supervision, Writing – original draft. DC: Writing – original draft, Writing – review and editing.

Funding

The author(s) declare that financial support was received for the research and/or publication of this article. This work has been supported by intramural funding for teaching activities. CM acknowledges the funding by the EU–European Social Found - National Operational Program (NOP) Research and Innovation 2014–2020 (actions IV.4 and IV.5) - FSE-REACT EU, which supported her PhD scholarship. The authors acknowledge support from the Department of Health Sciences (DiSS) of the Università del Piemonte Orientale through the Article Processing Charge (APC) initiative.

Conflict of interest

The authors declare that the research was conducted in the absence of any commercial or financial relationships that could be construed as a potential conflict of interest.

Generative AI statement

The authors declare that no Generative AI was used in the creation of this manuscript.

Publisher's note

All claims expressed in this article are solely those of the authors and do not necessarily represent those of their affiliated organizations, or those of the publisher, the editors and the reviewers. Any product that may be evaluated in this article, or claim that may be made by its manufacturer, is not guaranteed or endorsed by the publisher.

Supplementary material

The Supplementary Material for this article can be found online at: https://www.frontiersin.org/articles/10.3389/fbioe.2025.1602982/full#supplementary-material

References

Antony, F., Deantonio, C., Cotella, D., Soluri, M. F., Tarasiuk, O., Raspagliesi, F., et al. (2019). High-throughput assessment of the antibody profile in ovarian cancer ascitic fluids. *Oncoimmunology* 8, e1614856. doi:10.1080/2162402X.2019.1614856

Bag, S., Saha, B., Mehta, O., Anbumani, D., Kumar, N., Dayal, M., et al. (2016). An improved method for high quality metagenomics DNA extraction from human and environmental samples. *Sci. Rep.* 6, 26775. doi:10.1038/srep26775

Berini, F., Casciello, C., Marcone, G. L., and Marinelli, F. (2017). Metagenomics: novel enzymes from non-culturable microbes. *FEMS Microbiol. Lett.* 364, fnx211. doi:10.1093/femsle/fnx211

Bovio, A. (2019). Utilizzo del vettore plasmidico pFILTER/TA per la selezione di domini proteici da DNA genomico batterico. Bachelor's thesis. Vercelli: Università del Piemonte Orientale.

Camacho, C., Coulouris, G., Avagyan, V., Ma, N., Papadopoulos, J., Bealer, K., et al. (2009). BLAST+: architecture and applications. *BMC Bioinforma.* 10, 421. doi:10.1186/1471-2105-10-421

Caudai, C., Galizia, A., Geraci, F., Le Pera, L., Morea, V., Salerno, E., et al. (2021). AI applications in functional genomics. *Comput. Struct. Biotechnol. J.* 19, 5762–5790. doi:10.1016/j.csbj.2021.10.009

Claassen, S., du Toit, E., Kaba, M., Moodley, C., Zar, H. J., and Nicol, M. P. (2013). A comparison of the efficiency of five different commercial DNA extraction kits for extraction of DNA from faecal samples. *J. Microbiol. Methods* 94, 103–110. doi:10.1016/j.mimet.2013.05.008

D'Angelo, S., Velappan, N., Mignone, F., Santoro, C., Sblattero, D., Kiss, C., et al. (2011). Filtering "genic" open reading frames from genomic DNA samples for advanced annotation. *BMC Genomics* 12 (Suppl. 1), S5. doi:10.1186/1471-2164-12-S1-S5

Fasolo, F., Patrucco, L., Volpe, M., Bon, C., Peano, C., Mignone, F., et al. (2019). The RNA-binding protein ILF3 binds to transposable element sequences in SINEUP lncRNAs. *FASEB J.* 33, 13572–13589. doi:10.1096/fj.201901618RR

Fuhrmeister, E. R., Larson, J. R., Kleinschmit, A. J., Kirby, J. E., Pickering, A. J., and Bascom-Slack, C. A. (2021). Combating antimicrobial resistance through student-driven research and environmental surveillance. *Front. Microbiol.* 12, 577821. doi:10.3389/fmicb.2021.577821

Gandini, L. (2019). Sviluppo di una piattaforma per il "filtering" di open reading frames da DNA genomico batterico. Bachelor's thesis. Vercelli: Università del Piemonte Orientale.

Ginnan, N., and Bordenstein, S. R. (2023). It is time to authenticate the Microbiome Sciences with accredited educational programs and departments. *PLOS Biol.* 21, e3002420. doi:10.1371/journal.pbio.3002420

Gourlay, L. J., Peano, C., Deantonio, C., Perletti, L., Pietrelli, A., Villa, R., et al. (2015). Selecting soluble/foldable protein domains through single-gene or genomic ORF filtering: structure of the head domain of Burkholderia pseudomallei antigen BPSL2063. *Acta Crystallogr. D. Biol. Crystallogr.* 71, 2227–2235. doi:10.1107/S1399004715015680

Heger, A., and Holm, L. (2003). Exhaustive enumeration of protein domain families. *J. Mol. Biol.* 328, 749–767. doi:10.1016/s0022-2836(03)00269-9

Heller, D. M., Sivanathan, V., Asai, D. J., and Hatfull, G. F. (2024). SEA-PHAGES and SEA-GENES: advancing virology and science education. *Annu. Rev. Virol.* 11, 1–20. doi:10.1146/annurev-virology-113023-110757

Hieter, P., and Boguski, M. (1997). Functional genomics: it's all how you read it. *Science* 278, 601–602. doi:10.1126/science.278.5338.601

Ivagnes, V. (2019). Ingegnerizzazione di un vettore plasmidico compatibile con il metodo "TA cloning" per il clonaggio e la selezione di librerie di open reading frames. Bachelor's thesis. Vercelli: Università del Piemonte Orientale.

Jacques, F., Bolivar, P., Pietras, K., and Hammarlund, E. U. (2023). Roadmap to the study of gene and protein phylogeny and evolution—a practical guide. *PLOS ONE* 18, e0279597. doi:10.1371/journal.pone.0279597

Jumper, J., Evans, R., Pritzel, A., Green, T., Figurnov, M., Ronneberger, O., et al. (2021). Highly accurate protein structure prediction with AlphaFold. *Nature* 596, 583–589. doi:10.1038/s41586-021-03819-2

Jurkowski, A., Reid, A. H., and Labov, J. B. (2007). Metagenomics: a call for bringing a new science into the classroom (while it's still new). *CBE Life Sci. Educ.* 6, 260–265. doi:10.1187/cbe.07-09-0075

Kyte, J., and Doolittle, R. F. (1982). A simple method for displaying the hydropathic character of a protein. *J. Mol. Biol.* 157, 105–132. doi:10.1016/0022-2836(82)90515-0

Lam, K. N., Cheng, J., Engel, K., Neufeld, J. D., and Charles, T. C. (2015). Current and future resources for functional metagenomics. *Front. Microbiol.* 6, 1196. doi:10.3389/fmicb.2015.01196

Land, M., Hauser, L., Jun, S. R., Nookaew, I., Leuze, M. R., Ahn, T. H., et al. (2015). Insights from 20 years of bacterial genome sequencing. *Funct. Integr. Genomics* 15, 141–161. doi:10.1007/s10142-015-0433-4

Maraschi, L. (2024). Costruzione di una libreria di domini proteici espressi dal genoma di SARS-CoV-2. Bachelor's thesis. Vercelli: Università del Piemonte Orientale.

Marradi, D. (2020). Utilizzo della tecnica "orf filtering" per lo studio e caratterizzazione di nuove specie batteriche. Bachelor's thesis. Vercelli: Università del Piemonte Orientale.

Morra, M. (2021). Sviluppo di una piattaforma per il "filtering" di Open Reading Frames da DNA metagenomico. Bachelor's thesis. Vercelli: Università del Piemonte Orientale.

Muth, T. R., and Caplan, A. J. (2020). Microbiomes for all. *Front. Microbiol.* 11, 593472. doi:10.3389/fmicb.2020.593472

Ottolini, G. (2019). "Filtering" di Open Reading Frames da campioni di DNA genomico per annotazioni avanzate. Bachelor's thesis. Vercelli: Università del Piemonte Orientale.

Patrucco, L., Peano, C., Chiesa, A., Guida, F., Luisi, I., Boria, I., et al. (2015). Identification of novel proteins binding the AU-rich element of alpha-prothymosin mRNA through the selection of open reading frames (RIDome). *RNA Biol.* 12, 1289–1300. doi:10.1080/15476286.2015.1107702

Pouresmaeil, M., and Azizi-Dargahlou, S. (2023). Factors involved in heterologous expression of proteins in *E. coli* host. *Arch. Microbiol.* 205, 212. doi:10.1007/s00203-023-03541-9

Puccio, S., Grillo, G., Consiglio, A., Soluri, M. F., Sblattero, D., Cotella, D., et al. (2020). InteractomeSeq: a web server for the identification and profiling of domains and epitopes from phage display and next generation sequencing data. *Nucleic Acids Res.* 48, W200–W207. doi:10.1093/nar/gkaa363

Qin, J., Li, R., Raes, J., Arumugam, M., Burgdorf, K. S., Manichanh, C., et al. (2010). A human gut microbial gene catalogue established by metagenomic sequencing. *Nature* 464, 59–65. doi:10.1038/nature08821

Rebets, Y., Kormanec, J., Luzhetskyy, A., Bernaerts, K., and Anné, J. (2017). Cloning and expression of metagenomic DNA in streptomyces lividans and subsequent fermentation for optimized production. *Methods Mol. Biol.* 1539, 99–144. doi:10.1007/978-1-4939-6691-2_8

Ribarska, T., Bjørnstad, P. M., Sundaram, A. Y. M., and Gilfillan, G. D. (2022). Optimization of enzymatic fragmentation is crucial to maximize genome coverage: a comparison of library preparation methods for Illumina sequencing. *BMC Genomics* 23, 92. doi:10.1186/s12864-022-08316-y

Soluri, M. F., Puccio, S., Caredda, G., Edomi, P., D'Elios, M. M., Cianchi, F., et al. (2020). Defining the *Helicobacter pylori* disease-specific antigenic repertoire. *Front. Microbiol.* 11, 1551. doi:10.3389/fmicb.2020.01551

Soluri, M. F., Puccio, S., Caredda, G., Grillo, G., Licciulli, V. F., Consiglio, A., et al. (2018). Interactome-seq: a protocol for domainome library construction, validation and selection by phage display and next generation sequencing. *J. Vis. Exp.*, 56981. doi:10.3791/56981

Terrón-González, L., Genilloud, O., and Santero, E. (2014). "Potential and limitations of metagenomic functional analyses," in *Metagenomics, methods, applications and perspectives* (New York: Nova Publishers), 1–43.

Tiessen, A., Pérez-Rodríguez, P., and Delaye-Arredondo, L. J. (2012). Mathematical modeling and comparison of protein size distribution in different plant, animal, fungal and microbial species reveals a negative correlation between protein size and protein number, thus providing insight into the evolution of proteomes. *BMC Res. Notes* 5, 85. doi:10.1186/1756-0500-5-85

von der Haar, T. (2019). *Preparation and transformation of competent* E. coli *cells (CCMB80 method).* doi:10.17504/protocols.io.hayb2fw

Wiltschi, B., Cernava, T., Dennig, A., Galindo Casas, M., Geier, M., Gruber, S., et al. (2020). Enzymes revolutionize the bioproduction of value-added compounds: from enzyme discovery to special applications. *Biotechnol. Adv.* 40, 107520. doi:10.1016/j.biotechadv.2020.107520

Zhang, L., Chen, F., Zeng, Z., Xu, M., Sun, F., Yang, L., et al. (2021). Advances in metagenomics and its application in environmental microorganisms. *Front. Microbiol.* 12, 766364. doi:10.3389/fmicb.2021.766364

ACKNOWLEDGEMENTS

I would first like to thank Professor Diego Cotella for granting me the opportunity to conduct my doctoral research under his supervision. His support was crucial in developing my competencies and advancing my research.

This research was carried out in collaboration with the spin-off TissueGraft, and I am particularly grateful to Professor Francesca Boccafoschi for the opportunity and to Dr. Elena Canciani and Dr. Manuela Rizzi for their valuable support throughout the project.

would also like to thank the Pharmacology Laboratory, particularly Professor Luigia Grazia Fresu, for her guidance, and Maria, Lara and Giulia for their availability. Furthermore, I would like to thank Professor Giovanni Battista Giovenzana and Professor Ivana Miletto for their contributions to the chemical characterization aspects of this research.

Their guidance and collaboration have been instrumental throughout this doctoral work, and I am grateful to all those who contributed to this research.

BIBLIOGRAPHY

Adeli, H., Khorasani, M. T., & Parvazinia, M. (2019). Wound dressing based on electrospun PVA/chitosan/starch nanofibrous mats: Fabrication, antibacterial and cytocompatibility evaluation and in vitro healing assay. *International Journal of Biological Macromolecules*, *122*, 238–254. https://doi.org/10.1016/j.ijbiomac.2018.10.115

Andler, R. (2020). Bacterial and enzymatic degradation of poly(*cis*-1,4-isoprene) rubber: Novel biotechnological applications. *Biotechnology Advances*, *44*, 107606. https://doi.org/10.1016/j.biotechadv.2020.107606

Andrade, K. L., Ramlow, H., Floriano, J. F., Acosta, E. D., Faita, F. L., & Machado, R. A. F. (2023). Latex and natural rubber: Processing techniques for biomedical applications. *Brazilian Journal of Chemical Engineering*, *40*(4), 913–927. https://doi.org/10.1007/s43153-023-00317-y

Anton, F. (1934). *Process and apparatus for preparing artificial threads* (United States Patent No. US1975504A). https://patents.google.com/patent/US1975504A/en

Asawatreratanakul, K., Zhang, Y.-W., Wititsuwannakul, D., Wititsuwannakul, R., Takahashi, S., Rattanapittayaporn, A., & Koyama, T. (2003). Molecular cloning, expression and characterization of cDNA encoding cis-prenyltransferases from Hevea brasiliensis. *European Journal of Biochemistry*, *270*(23), 4671–4680. https://doi.org/10.1046/j.1432-1033.2003.03863.x

Berthelot, K., Lecomte, S., Estevez, Y., & Peruch, F. (2014). *Hevea brasiliensis* REF (Hev b 1) and SRPP (Hev b 3): An overview on rubber particle proteins. *Biochimie*, *106*, 1–9. https://doi.org/10.1016/j.biochi.2014.07.002

Bouvier, F., Rahier, A., & Camara, B. (2005). Biogenesis, molecular regulation and function of plant isoprenoids. *Progress in Lipid Research*, *44*(6), 357–429. https://doi.org/10.1016/j.plipres.2005.09.003

Chang, M. C. Y., & Keasling, J. D. (2006). Production of isoprenoid pharmaceuticals by engineered microbes. *Nature Chemical Biology*, *2*(12), 674–681. https://doi.org/10.1038/nchembio836

Chappell, J., Wolf, F., Proulx, J., Cuellar, R., & Saunders, C. (1995). Is the Reaction Catalyzed by 3-Hydroxy-3-Methylglutaryl Coenzyme A Reductase a Rate-Limiting Step for Isoprenoid Biosynthesis in Plants? *Plant Physiology*, *109*(4), 1337–1343. https://doi.org/10.1104/pp.109.4.1337

Chen, F.-M., & Liu, X. (2016). Advancing biomaterials of human origin for tissue engineering. *Progress in Polymer Science*, *53*, 86–168. https://doi.org/10.1016/j.progpolymsci.2015.02.004

Collins-Silva, J., Nural, A. T., Skaggs, A., Scott, D., Hathwaik, U., Woolsey, R., Schegg, K., McMahan, C., Whalen, M., Cornish, K., & Shintani, D. (2012). Altered levels of the *Taraxacum kok-saghyz* (Russian dandelion) small rubber particle protein, TkSRPP3, result in qualitative and quantitative changes in rubber metabolism. *Phytochemistry*, *79*, 46–56. https://doi.org/10.1016/j.phytochem.2012.04.015

Cooley, J. F. (1902). *Apparatus for electrically dispersing fluids* (United States Patent No. US692631A). https://patents.google.com/patent/US692631A/en

Cordoba, E., Salmi, M., & León, P. (2009). Unravelling the regulatory mechanisms that modulate the MEP pathway in higher plants. *Journal of Experimental Botany*, 2933–2943. https://doi.org/10.1093/jxb/erp190

Cornish, K. (2001). Similarities and differences in rubber biochemistry among plant species. *Phytochemistry*, *57*(7), 1123–1134. https://doi.org/10.1016/S0031-9422(01)00097-8

Cornish, K. (2017). Alternative Natural Rubber Crops: Why Should We Care? *Technology & Innovation*, *18*(4), 244–255. https://doi.org/10.21300/18.4.2017.245

Cornish, K., Castillón, J., & Scott, D. J. (2000). Rubber Molecular Weight Regulation, in Vitro, in Plant Species that Produce High and Low Molecular Weights in Vivo. *Biomacromolecules*, *1*(4), 632–641. https://doi.org/10.1021/bm000034z

Cornish, K., Wood, D. F., & Windle, J. J. (1999). Rubber particles from four different species, examined by transmission electron microscopy and electron-paramagnetic-resonance spin labeling, are found to consist of a homogeneous rubber core enclosed by a contiguous, monolayer biomembrane. *Planta*, *210*(1), 85–96. https://doi.org/10.1007/s004250050657

da Costa, B. M. T., Keasling, J. D., & Cornish, K. (2005). Regulation of Rubber Biosynthetic Rate and Molecular Weight in Hevea brasiliensis by Metal Cofactor. *Biomacromolecules*, *6*(1), 279–289. https://doi.org/10.1021/bm049606w

Dai, X., Nie, W., Shen, H., Machens, H.-G., Böker, K., Taheri, S., Lehmann, W., Shen, Y., & Schilling, A. F. (2024). Electrospinning based biomaterials for biomimetic fabrication, bioactive protein delivery and wound regenerative repair. *Regenerative Biomaterials*, *12*, rbae139. https://doi.org/10.1093/rb/rbae139

Ducluzeau, A.-L., Wamboldt, Y., Elowsky, C. G., Mackenzie, S. A., Schuurink, R. C., & Basset, G. J. C. (2012). Gene network reconstruction identifies the authentic trans-prenyl diphosphate synthase that makes the solanesyl moiety of ubiquinone-9 in Arabidopsis. *The Plant Journal*, *69*(2), 366–375. https://doi.org/10.1111/j.1365-313X.2011.04796.x

European Commission. (2020, September 3). *Critical Raw Materials Resilience: Charting a Path towards greater Security and Sustainability*. Brussels. https://eur-lex.europa.eu/legal-content/EN/TXT/?uri=celex:52020DC0474

Gemeinder, J. L. P., Barros, N. R. D., Pegorin, G. S., Singulani, J. D. L., Borges, F. A., Arco, M. C. G. D., Giannini, M. J. S. M., Almeida, A. M. F., Salvador, S. L. D. S., & Herculano, R. D. (2021). Gentamicin encapsulated within a biopolymer for the treatment of *Staphylococcus aureus* and *Escherichia coli* infected skin ulcers. *Journal of Biomaterials Science, Polymer Edition*, *32*(1), 93–111. https://doi.org/10.1080/09205063.2020.1817667

George, K. W., Thompson, M. G., Kim, J., Baidoo, E. E. K., Wang, G., Benites, V. T., Petzold, C. J., Chan, L. J. G., Yilmaz, S., Turhanen, P., Adams, P. D., Keasling, J. D., & Lee, T. S. (2018). Integrated analysis of isopentenyl pyrophosphate (IPP) toxicity in isoprenoid-producing *Escherichia coli*. *Metabolic Engineering*, *47*, 60–72. https://doi.org/10.1016/j.ymben.2018.03.004

Gervaso, F., Sannino, A., & Peretti, G. M. (2017). The biomaterialist's task: Scaffold biomaterials and fabrication technologies. *Joints*, *01*, 130–137. https://doi.org/10.11138/jts/2013.1.3.130

Guerra, N. B., Sant'Ana Pegorin, G., Boratto, M. H., de Barros, N. R., de Oliveira Graeff, C. F., & Herculano, R. D. (2021). Biomedical applications of natural rubber latex from the rubber tree Hevea brasiliensis. *Materials Science and Engineering: C*, *126*, 112126. https://doi.org/10.1016/j.msec.2021.112126

Herculano, R. D., dos Santos, T. O., de Barros, N. R., Pegorin Brasil, G. S., Scontri, M., Carvalho, B. G., Mecwan, M., Farhadi, N., Kawakita, S., Perego, C. H., Carvalho, F. A., dos Santos, A. G., Guerra, N. B., Floriano, J. F., Mussagy, C. U., Tirpáková, Z., Khorsandi, D., Peirsman, A., Nguyen, H. T., … Jucaud, V. (2023). *Aloe vera*-loaded natural rubber latex dressing as a potential complementary treatment for psoriasis. *International Journal of Biological Macromolecules*, *242*, 124779. https://doi.org/10.1016/j.ijbiomac.2023.124779

Hillebrand, A., Post, J. J., Wurbs, D., Wahler, D., Lenders, M., Krzyzanek, V., Prüfer, D., & Gronover, C. S. (2012). Down-Regulation of Small Rubber Particle Protein Expression Affects Integrity of Rubber Particles and Rubber Content in Taraxacum brevicorniculatum. *PLOS ONE*, *7*(7), e41874. https://doi.org/10.1371/journal.pone.0041874

Hirooka, K., Bamba, T., Fukusaki, E., & Kobayashi, A. (2003). Cloning and kinetic characterization of Arabidopsis thaliana solanesyl diphosphate synthase. *The Biochemical Journal*. https://portlandpress.com/biochemj/article-abstract/370/2/679/40023/Cloning-and-kinetic-characterization-of

Hu, X., Liu, S., Zhou, G., Huang, Y., Xie, Z., & Jing, X. (2014). Electrospinning of polymeric nanofibers for drug delivery applications. *Journal of Controlled Release*, *185*, 12–21. https://doi.org/10.1016/j.jconrel.2014.04.018

Kharel, Y., & Koyama, T. (2003). Molecular analysis of cis-prenyl chain elongating enzymes. *Natural Product Reports*, *20*(1), 111–118. https://doi.org/10.1039/B108934J

Kim, J.-H., Wang, C., Jang, H.-J., Cha, M.-S., Park, J.-E., Jo, S.-Y., Choi, E.-S., & Kim, S.-W. (2016). Isoprene production by Escherichia coli through the exogenous mevalonate pathway with reduced formation of fermentation byproducts. *Microbial Cell Factories*, *15*(1), 214. https://doi.org/10.1186/s12934-016-0612-6

Kim, S. W., & Keasling, J. D. (2001). Metabolic engineering of the nonmevalonate isopentenyl diphosphate synthesis pathway in Escherichia coli enhances lycopene production. *Biotechnology and Bioengineering*. https://doi.org/10.1002/1097-0290(20000220)72:4<408::aid-bit1003>3.0.co;2-h

Krause, T., Reichelt, M., Gershenzon, J., & Schmidt, A. (2020). Analysis of the isoprenoid pathway intermediates, dimethylallyl diphosphate and isopentenyl diphosphate, from crude plant extracts by liquid chromatography tandem mass spectrometry. *Phytochemical Analysis*, *31*(6), 770–777. https://doi.org/10.1002/pca.2941

Krupp, T., Dos Santos, B. D., Gama, L. A., Silva, J. R., Arrais-Silva, W. W., de Souza, N. C., Américo, M. F., & de Souza Souto, P. C. (2019). NATURAL RUBBER - PROPOLIS MEMBRANE IMPROVES WOUND HEALING IN SECOND-DEGREE BURNING MODEL Krupp, T., Dos Santos, B. D., Gama, L. A., Silva, J. R., Arrais-Silva, W. W., de Souza, N. C., Américo, M. F., & de Souza Souto, P. C. *International Journal of Biological Macromolecules*, *131*, 980–988. https://doi.org/10.1016/j.ijbiomac.2019.03.147

Kuroiwa, F., Nishino, A., Mandal, Y., Honzawa, M., Suenaga-Hiromori, M., Suzuki, K., Takani, Y., Miyagi-Inoue, Y., Yamaguchi, H., Yamashita, S., Takahashi, S., & Tozawa, Y. (2022). Reconstitution of prenyltransferase activity on nanodiscs by components of the rubber synthesis machinery of the Para rubber tree and guayule. *Scientific Reports*, *12*(1), 3734. https://doi.org/10.1038/s41598-022-07564-y

Kuroiwa, F., Suda, H., Yabuki, M., Atsuzawa, K., Yamaguchi, H., Toyota, M., Kaneko, Y., Yamashita, S., Takahashi, S., & Tozawa, Y. (2024). Cell-free translation system with artificial lipid-monolayer particles as a unique tool for characterizing lipid-monolayer binding proteins. *Bioscience, Biotechnology, and Biochemistry*, *88*(5), 555–560. https://doi.org/10.1093/bbb/zbae026

Lee, & Kim. (2016). *Method for producing natural rubber by using recombinant microorganism* (World Intellectual Property Organization Patent No. WO2016204503A1). https://patents.google.com/patent/WO2016204503A1/en

Li, D., & Xia, Y. (2004). Electrospinning of Nanofibers: Reinventing the Wheel? *Advanced Materials*, *16*(14), 1151–1170. https://doi.org/10.1002/adma.200400719

Lichtenthaler, H. K. (2000). Non-mevalonate isoprenoid biosynthesis: Enzymes, genes and inhibitors. *Biochemical Society Transactions*, *28*(6). https://antlia.med.unipmn.it:2184/11171208/?dopt=Abstract

Lima, A. F., Pegorin, G. S., Miranda, M. C. R., Cachaneski-Lopes, J. P., Silva, W. M., Borges, F. A., Guerra, N. B., Herculano, R. D., & Batagin-Neto, A. (2021). Ibuprofen-loaded biocompatible latex membrane for drug release: Characterization and molecular modeling. *Journal of Applied Biomaterials & Functional Materials*. https://doi.org/10.1177/22808000211005383

Liu, C. L., Dong, H. G., Zhan, J., Liu, X., & Yang, Y. (2019). Multi-modular engineering for renewable production of isoprene via mevalonate pathway in Escherichia coli. *Journal of Applied Microbiology*, *126*(4), 1128–1139. https://doi.org/10.1111/jam.14204

Liu, G., Gu, Z., Hong, Y., Cheng, L., & Li, C. (2017). Electrospun starch nanofibers: Recent advances, challenges, and strategies for potential pharmaceutical applications. *Journal of Controlled Release*, *252*, 95–107. https://doi.org/10.1016/j.jconrel.2017.03.016

Liu, H., Wang, Y., Tang, Q., Kong, W., Chung, W. J., & Lu, T. (2014). MEP pathway-mediated isopentenol production in metabolically engineered Escherichia coli Liu, H., Wang, Y., Tang, Q., Kong, W., Chung, W. J., & Lu, T. *Microbial Cell Factories*, *13*(1), 135. https://doi.org/10.1186/s12934-014-0135-y

Liu, H., Wei, L., Ba, L., Yuan, Q., & Liu, Y. (2022). Biopolymer production in microbiology by application of metabolic engineering. *Polymer Bulletin*, *79*(8), 5773–5794. https://doi.org/10.1007/s00289-021-03820-9

Martin, V. J. J., Pitera, D. J., Withers, S. T., Newman, J. D., & Keasling, J. D. (2003). Engineering a mevalonate pathway in Escherichia coli for production of terpenoids. *Nature Biotechnology*, *21*(7), 796–802. https://doi.org/10.1038/nbt833

Meng, X., Song, Q., Ye, J., Wang, L., & Xu, F. (2017). Characterization, Function, and Transcriptional Profiling Analysis of 3-Hydroxy-3-methylglutaryl-CoA Synthase Gene (GbHMGS1) towards Stresses and Exogenous Hormone Treatments in Ginkgo biloba. *Molecules*, *22*(10), Article 10. https://doi.org/10.3390/molecules22101706

Mooibroek, H., & Cornish, K. (2000). Alternative sources of natural rubber. *Applied Microbiology and Biotechnology*, *53*(4), 355–365. https://doi.org/10.1007/s002530051627

Oh, S. K., Han, K. H., Ryu, S. B., & Kang, H. (2000). Molecular Cloning, Expression, and Functional Analysis of a cis-Prenyltransferase from Arabidopsis thaliana Oh, S. K., Han, K. H., Ryu, S. B., & Kang, H. *Journal of Biological Chemistry*. https://doi.org/10.1074/jbc.M002000200

Panichpakdee, J., Larpkiattaworn, S., Nuchchapong, S., Naruepai, B., Leekrajang, M., & Somwongsa, P. (2019a). Electrospinning of natural rubber latex-blended polyvinyl alcohol. *Materials Today: Proceedings*, *17*, 2020–2027. https://doi.org/10.1016/j.matpr.2019.06.250

Panichpakdee, J., Larpkiattaworn, S., Nuchchapong, S., Naruepai, B., Leekrajang, M., & Somwongsa, P. (2019b). Electrospinning of natural rubber latex-blended polyvinyl alcohol. *Materials Today: Proceedings*, *17*, 2020–2027. https://doi.org/10.1016/j.matpr.2019.06.250

Pinto, M. F., Quevedo, B. V., Asami, J., Komatsu, D., Hausen, M. de A., & Duek, E. A. de R. (2023). Electrospun Membrane Based on Poly(L-co-D,L lactic acid) and Natural Rubber Containing Copaiba Oil Designed as a Dressing with Antimicrobial Properties. *Antibiotics*, *12*(5), Article 5. https://doi.org/10.3390/antibiotics12050898

Priya, P., Venkatachalam, P., & Thulaseedharan, A. (2007). Differential expression pattern of rubber elongation factor (REF) mRNA transcripts from high and low yielding clones of rubber tree (Hevea brasiliensis Muell. Arg.). *Plant Cell Reports*, *26*(10), 1833–1838. https://doi.org/10.1007/s00299-007-0402-z

Qian, C., Xin, T., Xiao, W., Zhu, H., Zhang, Q., Liu, L., Cheng, R., Wang, Z., Cui, W., & Ge, Z. (2020). Vascularized silk electrospun fiber for promoting oral mucosa regeneration. *NPG Asia Materials*, *12*(1), 1–16. https://doi.org/10.1038/s41427-020-0221-z

Rosa, S. de S. R. F., Rosa, M. F. F., Fonseca, M. A. M., Luz, G. V. da S., Avila, C. F. D., Domínguez, A. G. D., Dantas, A. G. D., & Richter, V. B. (2019). Evidence in Practice of Tissue Healing with Latex Biomembrane: Integrative Review. *Journal of Diabetes Research*, *2019*, 7457295. https://doi.org/10.1155/2019/7457295

Sharkey, T. D., Yeh, S., Wiberley, A. E., Falbel, T. G., Gong, D., & Fernandez, D. E. (2005). Evolution of the Isoprene Biosynthetic Pathway in Kudzu. *Plant Physiology*, *137*(2), 700–712. https://doi.org/10.1104/pp.104.054445

Silva, T. H., Alves, A., Ferreira, B. M., Oliveira, J. M., Reys, L. L., Ferreira, R. J. F., & Reis, R. L. (2012). Materials of marine origin: A review on polymers and ceramics of biomedical interest. *International Materials Reviews*. https://journals.sagepub.com/doi/abs/10.1179/1743280412Y.0000000002

Surmacz, L., Plochocka, D., Kania, M., Danikiewicz, W., & Swiezewska, E. (2014). *Cis*-Prenyltransferase AtCPT6 produces a family of very short-chain polyisoprenoids *in planta*. *Biochimica et Biophysica Acta (BBA) - Molecular and Cell Biology of Lipids*, *1841*(2), 240–250. https://doi.org/10.1016/j.bbalip.2013.11.011

van Beilen, J. B., & Poirier, Y. (2007a). Establishment of new crops for the production of natural rubber. *Trends in Biotechnology*, *25*(11), 522–529. https://doi.org/10.1016/j.tibtech.2007.08.009

van Beilen, J. B., & Poirier, Y. (2007b). Guayule and Russian Dandelion as Alternative Sources of Natural Rubber. *Critical Reviews in Biotechnology*, *27*(4), 217–231. https://doi.org/10.1080/07388550701775927

Wang, D., Sun, Y., Chang, L., Tong, Z., Xie, Q., Jin, X., Zhu, L., He, P., Li, H., & Wang, X. (2018). Subcellular proteome profiles of different latex fractions revealed washed solutions from rubber particles contain crucial enzymes for natural rubber biosynthesis. *Journal of Proteomics*, *182*, 53–64. https://doi.org/10.1016/j.jprot.2018.05.002

Whited, G. M., Feher, F. J., Benko, D. A., Cervin, M. A., Chotani, G. K., McAuliffe, J. C., LaDuca, R. J., Ben-Shoshan, E. A., & Sanford, K. J. (2010). TECHNOLOGY UPDATE: Development of a gas-phase bioprocess for isoprene-monomer production using metabolic pathway engineering. *Industrial Biotechnology*, *6*(3), 152–163. https://doi.org/10.1089/ind.2010.6.152

Wood, D. F., & Cornish, K. (2000). Microstructure of Purified Rubber Particles. *International Journal of Plant Sciences*, *161*(3), 435–445. https://doi.org/10.1086/314269

Wright, L. P., Rohwer, J. M., Ghirardo, A., Hammerbacher, A., Ortiz-Alcaide, M., Raguschke, B., Schnitzler, J. P., Gershenzon, J., & Phillips, M. A. (2014). Deoxyxylulose 5-Phosphate Synthase Controls Flux through the Methylerythritol 4-Phosphate Pathway in Arabidopsis. *Plant Physiology*. https://academic.oup.com/plphys/article/165/4/1488/6113203

Yamashita, S., Mizuno, M., Hayashi, H., Yamaguchi, H., Miyagi-Inoue, Y., Fushihara, K., Koyama, T., Nakayama, T., & Takahashi, S. (2018). Purification and characterization of small and large rubber particles from Hevea brasiliensis. *Bioscience, Biotechnology, and Biochemistry*, *82*(6), 1011–1020. https://doi.org/10.1080/09168451.2017.1401913

Yamashita, S., & Takahashi, S. (2020). Molecular Mechanisms of Natural Rubber Biosynthesis. *Annual Review of Biochemistry*, *89*(Volume 89, 2020), 821–851. https://doi.org/10.1146/annurev-biochem-013118-111107

Yamashita, S., Yamaguchi, H., Waki, T., Aoki, Y., Mizuno, M., Yanbe, F., Ishii, T., Funaki, A., Tozawa, Y., Miyagi-Inoue, Y., Fushihara, K., Nakayama, T., & Takahashi, S. (2016). Identification and reconstitution of the rubber biosynthetic machinery on rubber particles from Hevea brasiliensis. *eLife*, *5*, e19022. https://doi.org/10.7554/eLife.19022

Yan, B., Zhang, Y., Li, Z., Zhou, P., & Mao, Y. (2022). Electrospun nanofibrous membrane for biomedical application. *SN Applied Sciences*, *4*(6), 172. https://doi.org/10.1007/s42452-022-05056-2

Yang, C., Gao, X., Jiang, Y., Sun, B., Gao, F., & Yang, S. (2016). Synergy between methylerythritol phosphate pathway and mevalonate pathway for isoprene production in Escherichia coli Yang, C., Gao, X., Jiang, Y., Sun, B., Gao, F., & Yang, S. *Metabolic Engineering,*. https://doi.org/10.1016/j.ymben.2016.05.003

Yarin, A. L., Koombhongse, S., & Reneker, D. H. (2001). Bending instability in electrospinning of nanofibers. *Journal of Applied Physics*, *89*(5), 3018–3026. https://doi.org/10.1063/1.1333035

Zhao, L., Chang, W., Xiao, Y., Liu, H., & Liu, P. (2013). Methylerythritol Phosphate Pathway of Isoprenoid Biosynthesis. *Annual Review of Biochemistry*, *82*, 497. https://doi.org/10.1146/annurev-biochem-052010-100934

Zhao, Y., Yang, J., Qin, B., Li, Y., Sun, Y., Su, S., & Xian, M. (2011). Biosynthesis of isoprene in Escherichia coli via methylerythritol phosphate (MEP) pathway Zhao, Y., Yang, J., Qin, B., Li, Y., Sun, Y., Su, S., & Xian, M. *Applied Microbiology and Biotechnology*, *90*(6), 1915–1922. https://doi.org/10.1007/s00253-011-3199-1